UNIVERSITÉ DE STRASBOURG

ÉCOLE DOCTORALE ED222

THÈSE présentée par :

Roman AKASOV

soutenue le : **07 mars 2017**

pour obtenir le grade de : **Docteur de l'université de Strasbourg**

Discipline/ Spécialité : **biotechnologie**

co-tutelle

TITRE de la thèse

Novel 3D *in vitro* models based on multicellular tumor spheroids to test anticancer drugs and drug delivery vehicles

THÈSE dirigée par :

Dr. Thierry VANDAMME	Professeur, université de Strasbourg
Dr. Elena MARKVICHEVA	Professeur, Shemyakin & Ovchinnikov Institute of Bioorganic Chemistry, Rus. Acad. Sci

RAPPORTEURS :

Dr. Denis PONCELET	Professeur, Université de Nantes
Dr. Natalia KLYACHKO	Professeur, Lomonosov Moscow State University

Modèle de 1ère page de résumé de Thèse de Doctorat

UNIVERSITE DE STRASBOURG

ECOLE DOCTORALE DES SCIENCES CHIMIQUES

RESUME DE LA THESE DE DOCTORAT

Discipline : Chimie

Spécialité (facultative) : Sciences pharmaceutiques

Présentée par : Presented by : Roman Akasov
(*Nom Prénom du candidat)*

Titre : Novel 3D in vitro models based on multicellular tumor spheroids to test anticancer drugs and drug delivery vehicles (Nouveaux modèles 3D in vitro à base de sphéroïdes multicellulaires tumoraux pour tester des substances anticancéreuses et des vecteurs de délivrance de médicaments)

Unité de Recherche : UMR 7199 CNRS
(N° et Nom de l'Unité) Laboratoire de Conception et d'Application de Molécules Bioactives

Directeur de Thèse : Thierry Vandamme, PhD, Professeur
(Nom Prénom – Grade)

Co-Directeur de Thèse (s'il y a lieu) : Elena Markvicheva, PhD, Dr. Sci, Professeur
(Nom Prénom – Grade)

Localisation : 74 route du Rhin, 67400 Illkirch, Unité CNRS 7199, Faculté de Pharmacié, Université de Stracbourg.

16/10 Miklukho-Maklaya, 117997, Moscou, Russie. Shemyakin-Ovchinnikov Institut de chimie bioorganique.

Thèse confidentielle ☑ NON ☐ OUI

RESUMÉ

- Introduction

Le développement de nouvelles formulations anticancéreuses est un défi prioritaire en biomédecine. Environ 10.000 composés ayant une activité antitumorale sont testés chaque année [1]. De plus, plusieurs particules nano- et micrométriques ont été proposées comme systèmes de délivrance (liposomes, nanoémulsions, microcapsules polyélectrolytiques, particules métalliques, etc.). Ces systèmes de délivrance protègent les médicaments d'une dégradation prématurée tout comme ils peuvent les vectoriser vers des tumeurs. Toutefois, seulement 6,7% de préparations antitumorales entrent en phase clinique I et font l'objet d'une approbation par la FDA [2]. C'est environ deux fois moins que le taux habituel rencontré avec d'autres principes actifs (non antitumoraux). Ces chiffres confirment la faible valeur pronostique des méthodes d'essai *in vitro* en tant que techniques d'évaluations *in vitro* pour des principes actifs antitumoraux.

Pour sélectionner les formulations les plus prometteuses, des modèles *in vitro* basés sur des cultures cellulaires bidimensionnelles en monocouches (2D) sont couramment employés. Ces modèles ont cependant leurs limites et c'est la raison pour laquelle des systèmes *in vitro* tridimensionnels (3D) sont développés afin de mimer les tumeurs solides [3]. L'utilisation de cellules en culture 2D conduit celles-ci à une exposition à des concentrations uniformes en oxygène et en éléments nutritifs alors que dans les tumeurs solides les cellules sont exposées à des conditions de gradient des facteurs essentiels. De plus, la chimiothérapie peut être facilement délivrée aux cellules cibles dans le cas de cultures de cellules sous forme de monocouches alors qu'*in vivo* les principes actifs doivent pénétrer/diffuser au travers de plusieurs couches de cellules. En conclusion, la croissance de cellules dans des cultures 3D permet de mieux appréhender la réalité d'un traitement comparé à celle observée dans le cas de mise en œuvre de cultures cellulaires sous forme d'une monocouche [4]. Les imperfections mentionnées ci-dessus quant à l'utilisation de monocouches cellulaires ont comme conséquence une sensibilité réduite aux agents chimiothérapeutiques lorsque des cultures cellulaires 3D sont envisagées comparées à la culture de monocouches cellulaires.

Les sphéroïdes multicellulaires tumoraux (SMT) sont des agrégats 3D sphériques denses qui pourraient imiter les tumeurs solides de petites tailles et simuler les interactions cellule-cellule ainsi que le microenvironnement cellulaire [5]. Les SMT ont été décrits pour la première fois dans les années soixante-dix par Sutherland [6] et

utilisés depuis dans l'étude de la biologie des tumeurs, de l'impact des rayonnements sur les cellules, de l'influence de la photodynamique et des chimiothérapies. Plusieurs techniques ont été proposées pour former des SMT, telle que l'agrégation spontanée, les flacons tournants, des systèmes de culture cellulaire mis en rotation, des systèmes à base de gouttes pendantes, des systèmes de plateaux avec de faibles adhésions et la microencapsulation dans des microcapsules de polyélectrolytes [7]. Cependant, bon nombre des techniques mentionnées ci-dessus présentent des difficultés de mise en pratique et ce, dû à un manque de rapidité, de reproductibilité, de simplicité et de rendement. Une nouvelle approche permettant de former des sphéroïdes tumoraux comme résultat d'une auto-aggrégation en présence de peptides, contenant un motif RGD (L-arginine, glycine, et L-acide aspartique) a été proposée dans cette dissertation doctorale en tant que solution possible à ce problème.

Le but de la thèse de doctorat était de développer une technique permettant une très bonne reproductibilité pour la formation de SMT et de démontrer la possibilité d'utilisation de ces sphéroïdes 3D comme modèles *in vitro*.

Plus spécifiquement, les approches suivantes ont été réalisées:

1. Etudier l'agrégation cellulaire induite par RGD en utilisant des lignées cellulaires de différentes caractéristiques et origines.
2. Evaluer les propriétés des sphéroïdes (forme, taille, viabilité cellulaire) en fonction des conditions d'agrégation cellulaire induites par RGD.
3. Mettre en place une technique de co-culture de cellules tumorales et normales sous forme de sphéroïdes formés en tant que résultat d'une agrégation cellulaire induite par du RGD.
4. Proposer de nouveaux composés avec une activité antitumorale potentielle et différentes particules nano- et micrométriques destines à la délivrance de substances antitumorales.
5. Démontrer l'intérêt des sphéroïdes tumoraux induits par du RGD en tant que modèle 3D *in vitro* pour tester l'efficacité de composés antitumoraux et de différents vecteurs nano- et micrométriques chargés de substances antitumorales.

- Résultats et discussions

1. Agrégation cellulaire induite par le RGD en tant qu'outil pour former des sphéroïdes tumoraux multicellulaires

Une nouvelle approche simple a été proposée pour former des sphéroïdes constitués de cellules tumorales basés sur des auto-assemblages cellulaires. Pour

atteindre cet objectif, cinq composés contenant du RGD ont été synthétisés (tableau 1). Une liaison covalente de bromure de 4-carboxybutyl-triphénylphosphonium (TPP) sous forme cationique aux peptides est supposée faciliter l'auto-assemblage dû à l'augmentation des interactions électrostatiques.

Tableau 1. Caractéristiques des composés contenant du RGD

Abréviation	**Structure composée**	**Masse moléculaire**
cyclo-RGDfK	cyclique Arg-Gly-Asp-D-Phe-Lys	603
cyclo-RGDfK(TPP)	cyclique Arg-Gly-Asp-D-Phe-Lys modifié avec du bromure de 4-carboxybutyltriphenylphosphonium	1029
RGDF	linéaire Arg-Gly-Asp-Phe	494
TPP-RGDF	linéaire Arg-Gly-Asp-Phe modifié avec du bromure de 4-carboxybutyltriphenylphosphonium	919
$(TPP)_2$-KRGDF	linéaire lys-Arg-Gly-Asp-Phe modifié avec du bromure de 4-carboxybutyltriphenylphosphonium	1472

L'auto-assemblage a été induit par l'addition d'un peptide cyclique Arg-Gly-Asp-D-Phe-Lys (cyclo-RGDfK) modifié avec du TPP directement ajouté à la monocouche de culture cellulaire. 16 lignées cellulaires de différentes origines (humaine, souris) et de divers types (carcinome, mélanome, gliome et cellules normales) ont été étudiées. 12 d'entre elles pouvaient former des SMT en présence de 10-100 μM de cyclo-RGDfK (TPP) après 2 ou 3 jours d'incubation (Table 2). Cette observation est d'un grand intérêt, puisque des peptides de types RGD habituellement linéaires sont connus pour empêcher la formation d'agrégats de cellules lorsqu'ils sont ajoutés au milieu [8]. Au contraire, les protéines naturelles de la matrice extracellulaire (MEC) favorisent l'auto-agrégation de cellules et promeuvent la formation compacte de sphéroïdes [9]. Ainsi, suite à ces observations, nous avons pu conclure que le cyclo-RGDfK (TPP) peut imiter les protéines naturelles de la matrice extracellulaire en termes d'agrégation cellulaire voire de l'augmenter.

Tableau 2. Génération de sphéroïdes induits par l'utilisation de peptides cycliques de types RGD dans des cultures monocouches, 72 heures d'incubation, DMEM + 10% FBS.

Lignées cellulaires	**La minimale concentration du peptide, μM**	
	cyclo-RGDfK	cyclo-RGDfK(TPP)
U-87 MG	25	10
M-3	25	10
HCT-116	50	10

PANC1-GemR	50	10
PANC1	50	25
MCF-7	50	25
MCF-7 TMX	50	25
HepG2	50	25
A-375	50	25
L-929	100	25
BNL-CL2	100	50

Il est intéressant de noter que 9 des 12 lignées cellulaires ont donné lieu à la formation de sphéroïdes tumoraux bien définis de formes rondes et denses. Ces lignées cellulaires sont mentionnées dans le tableau 2 en caractères gras. Les micrographies d'une de ces lignées cellulaires (glioblastome humain U-87 MG) sont donnés à la figure 1 (rangée supérieure). Trois autres lignées cellulaires (A-375, PANC1, PANC1-GemR) ont donné lieu à la formation d'agrégats moins réguliers. Ces lignées cellulaires sont mentionnées dans le tableau 2 avec une police de caractères en italiques. Les micrographies d'une de ces lignées cellulaires (mélanome humain A-375) sont données à la figure 1 (rangée inférieure). Seulement 4 lignées cellulaires (A-172, HaCaT, HOS, MCF-7 ADR) parmi les 16 lignées étudiées n'ont pas donné lieu à la formation de sphéroïdes en présence des peptides cyclos-RGDfK.

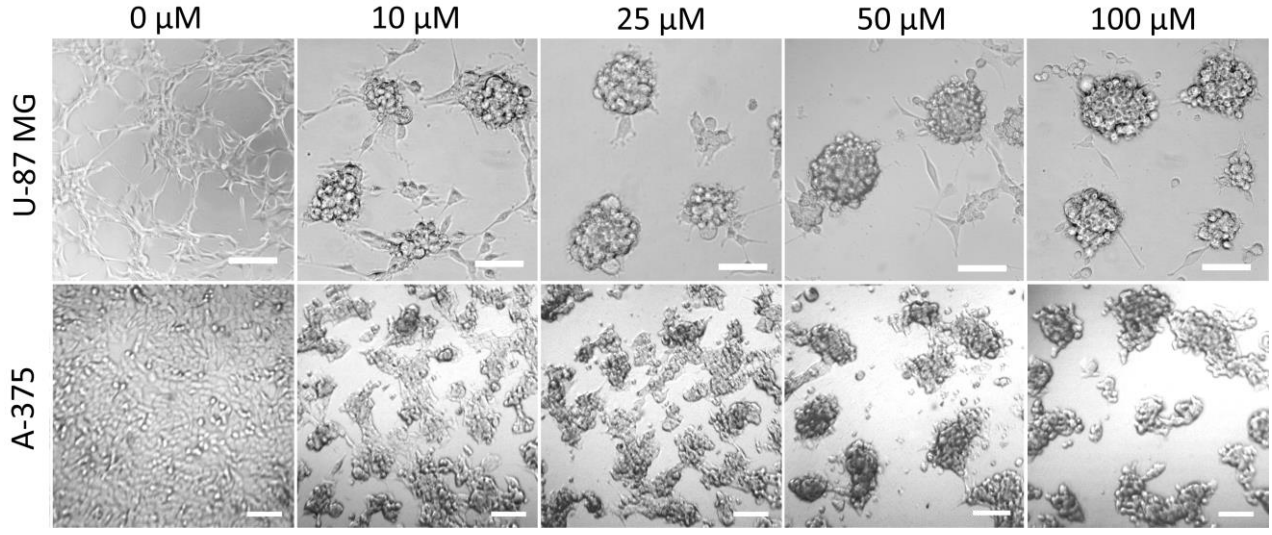

Figure 1. Auto-agrégation dépendante du temps d'incubation des cellules humaines de glioblastome U-87 MG et humaines de mélanome A-375 en présence du peptide cyclo-RGDfK (TPP) dans un milieu DMEM (Dulbecco's Modified Eagle Medium) supplémenté avec 10% de sérum fœtal de bovin (SFB), 72 h. Les cellules (culture sous forme de monocouche) sans traitement de peptide (0 µM) ont été employées comme contrôles.

Les images ont été obtenues par microscopie optique et la barre d'échelle représente 100 µm.

Le mécanisme de l'effet d'auto-assemblage est probablement lié à des intégrines favorisant les interactions cellule-cellule et les interactions de la cellule-matrice. Auparavant, le rôle de l'intégrine α5β1 dans l'agrégation cellulaire induite par la fibronectine a été démontrée [10]. Nous avons utilisé le ligand K34c (10 µM) qui est fortement sélectif pour l'intégrine α5β1 [11] comme inhibiteur concurrent de la cyclo-RGDfK (TPP). En effet, de petites concentrations de K34c (10 µM) ont empêché l'agrégation cellulaire induite normalement par RGD et ce fait a permis de confirmer notre hypothèse quant à la participation d'intégrines dans l'auto-assemblage cellulaire (Figure 2). De plus, le rôle de la sialylation de surface cellulaire a été étudié quant à l'agrégation induite par RGD. Les résidus d'acides sialiques (AS) sont souvent liés aux récepteurs cellulaires, comprenant des intégrines, et changent leurs fonctions biochimiques. Pour examiner le rôle des acides sialiques sur la formation de sphéroïdes, nous avons réalisé une inhibition en utilisant de la lectine dans des cultures pour lesquelles des monocouches de cellules MCF-7 ont été traitées avec diverses lectines ciblant les AS ainsi que le peptide (TPP) cyclo-RGDfK. Les expérimentations réalisées ont permis de constater qu'un traitement préparatoire des cellules MCF-7 avec une dose-dépendante de lectines ciblant les AS réduit sensiblement la formation de sphéroïdes. En revanche, des lectines ne ciblant pas les AS n'ont exercé aucun effet inhibiteur sur l'agrégation causée par RGD. Ces résultats ont été confirmés grâce à une analyse immunologique et de viabilité cellulaire, indiquant clairement la participation de AS dans la formation de sphéroïdes.

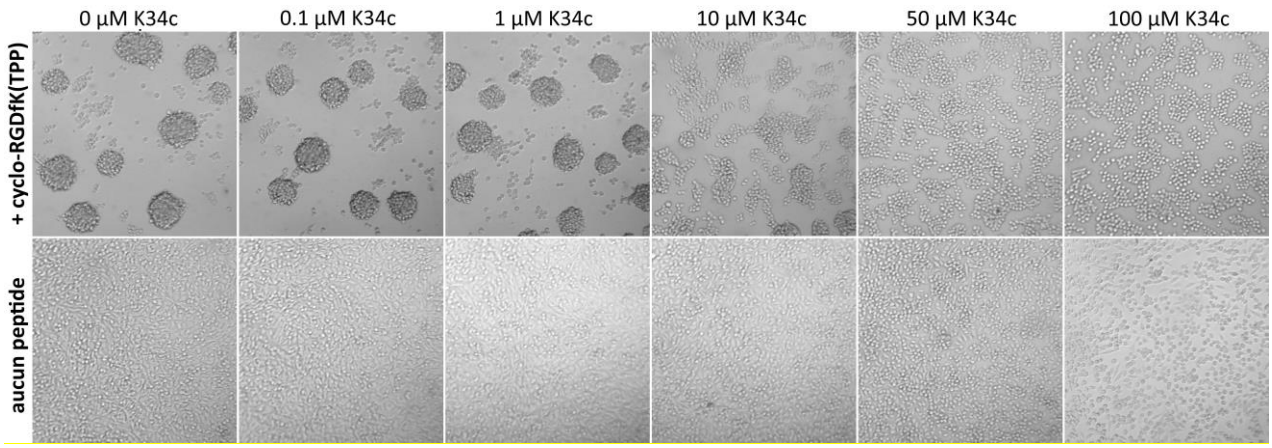

Figure 2. Inhibition de l'agrégation cellulaire induite par RGD en presence du composé K34c. Cellules M-3 de mélanomes de souris, 25 µM de cyclo-RGDfK(TPP), 72 heures.

Nous avons utilisé le test au MTT pour vérifier la cytotoxicité des peptides cycliques de type RGD. Les experimentations ont permis d'observer que l'incubation avec des peptides de types RGD ont pour conséquence une légère décélération de croissance jusqu'à 70-80% comparé au contrôle. Cependant, l'analyse de mortalité basée sur le marquage à l'aide de la calcéine AM et PI n'a indiqué aucune mort cellulaire pour le cyclo-RGDfK et pour le cyclo-RGDfK (TPP). De plus, il est important de noter que l'effet de décélération de croissance s'est produit à 10 µM et 50 µM de cyclo-RGDfK (TPP) pour les lignées cellulaires M-3 et le MCF-7, ce qui est en bonne concordance avec les concentrations minimales en peptide nécessaires pour les formations de sphéroïdes multicellulaires tumoraux (STM) (tableau 2). Par conséquent, la décélération de croissance cellulaire pourrait se produire du fait de la présence de cellules "au repos" au centre des sphéroïdes mais pas en raison de la cytotoxicité causée par RGD. Après le remplacement du milieu de culture contenant des peptides RGD par un milieu frais, on a observé la désagrégation des sphéroïdes et le ré-attachement des cellules au fond des boîtes de culture avec une prolifération cellulaire. Ainsi, nous n'avons indiqué aucune cytotoxicité du peptide pour les cellules dans les concentrations utilisées par le RGD pour donner lieu à la formation de sphéroïdes dans une gamme de concentration allant de 1 à 100 µM

Les expérimentations ont également permis de conclure que plus les cellules sont malignes moins la quantité de peptides était nécessaire pour donner lieu à la formation de sphéroïdes. Ainsi, les cellules U-87 MG et les cellules mélanome M-3, caractérisées et connues comme variétés cellulaires « fortement agressives » et métastatiques donnent facilement lieu à la production de sphéroïdes [12]. Dans notre étude, pour réaliser la génération de sphéroïdes à partir de ces lignées cellulaires, seule une concentration minimale de 10 µM en peptide s'est révélée être nécessaire. Pour la génération de sphéroïdes à base de cellules MCF-7 qui sont considérées comme des cellules cancéreuses du carcinome de sein non-agressives [13], la concentration de cyclo-RGDfK(TPP) nécessaire était de 25 µM. Enfin, pour réaliser la formation d'agrégats de cellules d'hépatocytes non tumoraux de type BNL.CL2, seulement une concentration de 50 µM de cyclo-RGDfK (TPP) a été nécessaire. Une taille moyenne de 50-150 µm de sphéroïdes a pu être obtenue avec une distribution étroite, dépendant de la lignée cellulaire, de la composition du sérum ainsi que du temps d'incubation. De plus, une corrélation a pu être établie entre l'importance du caractère malin des cellules et la taille moyenne des sphéroïdes obtenus: plus le caractère malin cellulaire était important plus la taille des sphéroïdes générés était importante (Figure 3).

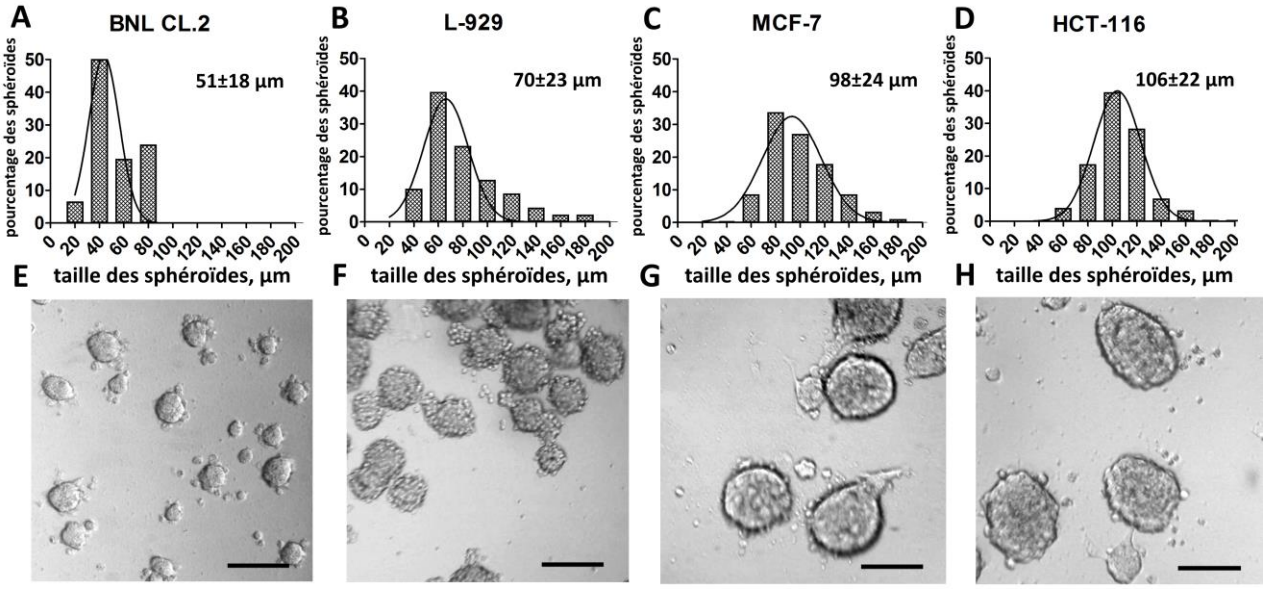

Figure 3. Distribution de tailles de sphéroïdes (A-D) et images obtenues par microscopie électronique à balayage de sphéroïdes (E-H) de cellules tumorales et de cellules normales dans du DMEM supplémenté avec 10% de sérum bovin foetal après 72 h d'incubation avec 50 µM de peptide RGDfK (TPP). La barre d'échelle est équivalente à 100 µm.

L'incubation à long terme en présence des peptides de type RGD conduit à l'augmentation de la taille des sphéroïdes. Ainsi, la taille moyenne des sphéroïdes multicellaires tumoraux réalisés à partir de cellules MCF-7 a augmenté d'un facteur 3 allant de 103±21 µm (2 jours d'incubation) à 293±66 µm (8 jours d'incubation) (figure 4). Cependant, l'augmentation de taille a été accompagnée par une agrégation entre les sphéroïdes. En conséquence, nous avons dénombré moins de sphéroïdes (pas plus de 5-10 après 8 jours d'incubation) avec un indice plus élevé de multidispersion. C'est la raison pour laquelle nous avons choisi les sphéroïdes âgés de trois jours comme outil pour étudier les substances antitumorales.

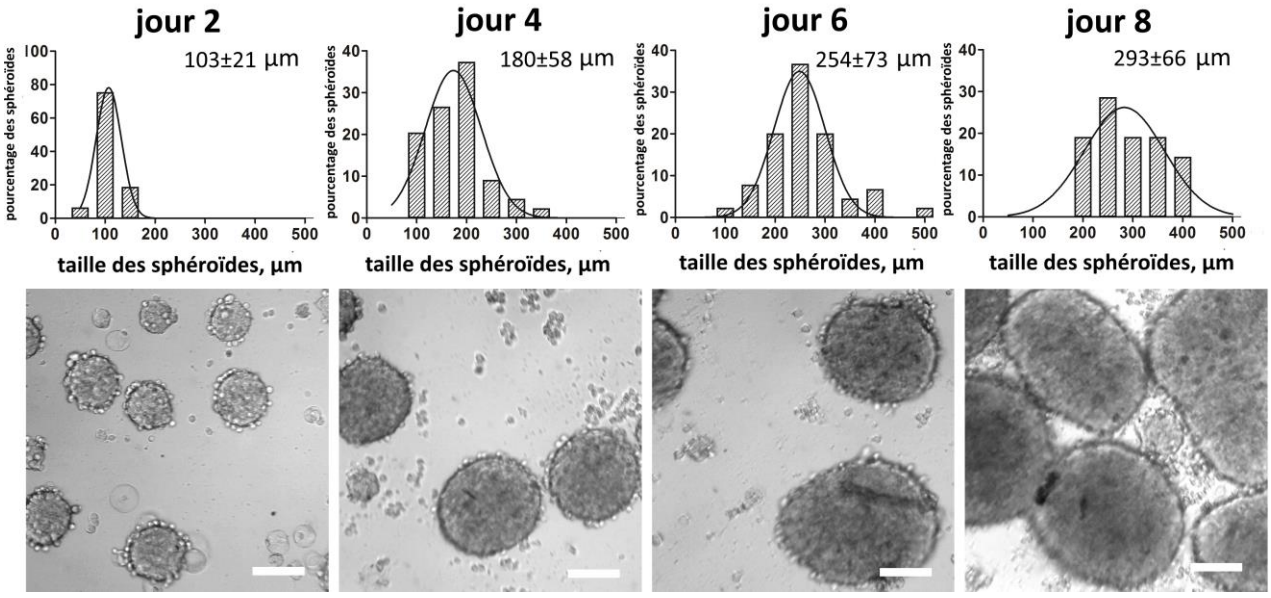

Figure 4. Augmentation de la taille moyenne de sphéroïdes à base de MCF-7 en fonction du temps d'incubation. DMEM+10% FBS, 50 µM cyclo-RGDfK(TPP). La barre d'échelle est équivalente à 100 µm.

2. Techniques de Co-culture basées sur la formation de sphéroïdes tumoraux induits par RGD

Il est bien connu que les tumeurs solides ainsi que les cellules malignes, impliquent des fibroblastes hôtes, des cellules endothéliales ainsi que des cellules immunitaires interagissant l'une avec l'autre ainsi qu'avec les facteurs microenvironmentaux pour conduire à la progression tumorale [7]. La contribution de cellules stromales dans le développement de cancers et de résistance aux principes actifs a été démontrée pour le cancer du sein, le gliome et le mélanome [14,15]. L'utilisation à la fois de tissus normaux et tumoraux pourrait permettre de classer les formulations selon leur rapport efficacité / sécurité. Pour réaliser ces conditions *in vitro*, deux nouveaux modèles de co-culture 3D ont été développés de manière à fournir une structure bien identifiée de type « cœur-écorce ». Les deux modèles ont pu être facilement fabriqués en utilisant le peptide RGD cyclique de manière à induire l'auto-assemblage cellulaire. La première approche consiste en l'association du peptide RGD avec la technique de recouvrement liquide, alors que la seconde est basée sur la co-encapsulation de sphéroïdes tumoraux (obtenus au préalable par traitement du peptide RGD) et des cellules normales dans des microcapsules de polyélectrolytes (figure 5).

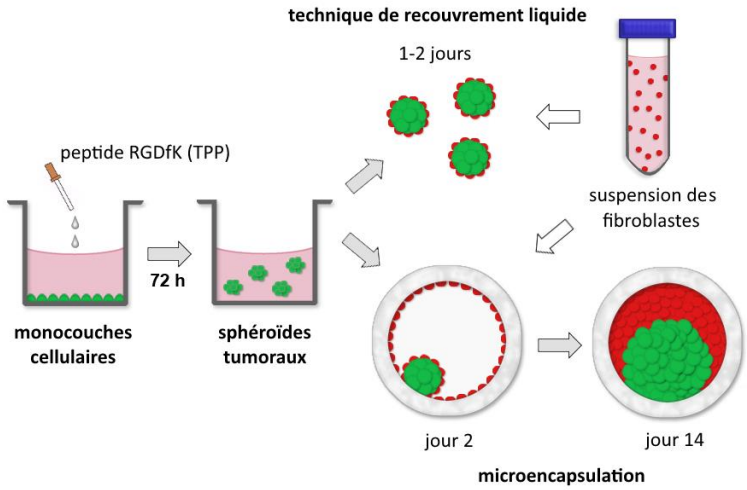

Figure 5 : Schéma de préparation de deux modèles de co-culture 3D *in vitro* utilisant le peptide RGD pour induire la formation de sphéroïdes d'une part tumoraux et d'autre part de cellules normales.

Pour produire des sphéroïdes de co-culture selon la première approche, les cellules ont été mises en culture durant 1-2 jours. Par la suite, les fibroblastes L-929 ont été étalés sur la surface des sphéroïdes du mélanome M-3 formant une structure complexe de type noyau-écorce (figure 6). Les cellules M-3 et L-929 ont été facilement distinguées par microscopie confocale par le marquage cellulaire avec des colorants DiO et DiI, respectivement.

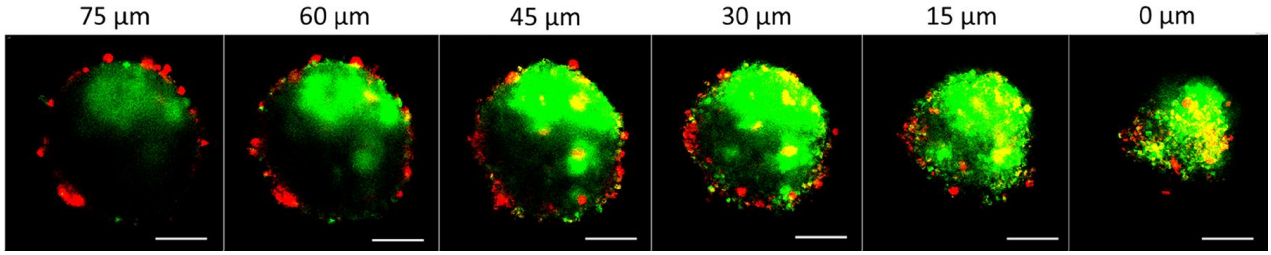

Figure 6. Images confocales de sphéroïdes tumoraux de cellules de mélanomes (DIO marquées en vert et de fibroblastes uniques L-929 (DIL-marqués en rouge) après 24 heures d'incubation. DMEM+10% FBS, 50 µM cyclo-RGDfK(TPP). La barre d'échelle représente 50 µm; une étape de formation à 15 µm, "0 µm" représente le bas du sphéroïde.

Le Dr. Elena Markvicheva [16] a proposé par le passé la microencapsulation de cellules dans des microcapsules semi-perméables constituées d'alginate-chitosan. Dans les travaux de recherches proposés dans le cadre de la dissertation doctorale, cette technique a été proposée cette pour la Co-culture des sphéroïdes tumoraux et des cellules normales dans des microcapsules. Pour fabriquer des sphéroïdes de co-culture dans des microcapsules, une mise en culture sur un long terme de 2 semaines s'est

révélé être nécessaire. Comme observé à la figure 7, les sphéroïdes M-3 ont maintenu leur structure, alors que les cellules L-929 se développaient à la fois sur la surface intérieure de la membrane de polyélectrolytes et sur la surface des sphéroïdes tumoraux. Bien que la seconde technique soit plus compliquée, elle permet néanmoins de fabriquer des sphéroïdes de taille souhaitée (200–650 µm) [17]. Les deux modèles de co-culture 3D *in vitro* ont pu être utilisés pour étudier les interactions cellule-cellule ainsi que de pouvoir tester de nouveaux principes actifs anticancéreux et de nouveaux vecteurs de médicaments.

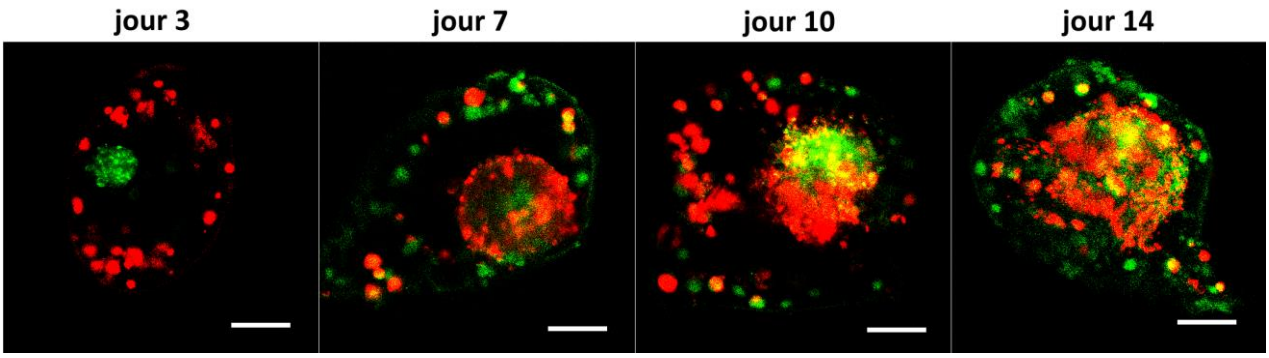

Figure 7. Images confocales de sphéroïdes tumoraux obtenus à partir de cellules de mélanomes M-3 (DIO marquées en vert) et de fibroblastes uniques L-929 (DIL marquées en rouge) dans des microcapsules. DMEM+10% FBS, la barre d'échelle représente 50 µm.

3. Shéroïdes tumoraux pour tester de nouvelles péparations antitumorales

Les sphéroïdes ont été employés pour tester trois principes actifs de faibles poids moléculaires modèles, à savoir la doxorubicine (DOX), la curcumine (CUR), et le temozolomide TMZ), qui sont connus pour posséder différents mécanismes d'action anticancéreux. Ces expérimentations ont permis de mettre en évidence que la DOX et la CUR étaient moins efficaces au contact de sphéroïdes cellulaires comparé à des cellules cultivées sous forme de monocouches. Pour visualiser la mort cellulaire dans les sphéroïdes, du TMZ non fluorescent a été utilisé dans le dénombrement de la mortalité. La figure 8 permet d'observer qu'un ajout de TMZ à des concentrations allant de 10-150 mM a eu comme conséquence d'induire la mort cellulaire accompagnée d'une destruction de surface des sphéroïdes ainsi qu'une réduction de la taille des sphéroïdes. Une augmentation de la concentration de TMZ (>200 mM) a conduit à la désintégration des sphéroïdes suivie par la formation d'agrégats irréguliers (<50 µm). La figure 8 permet également d'observer qu'en l'absence de traitement avec un principe actif toutes les cellules sont maintenues en vie dans les sphéroïdes.

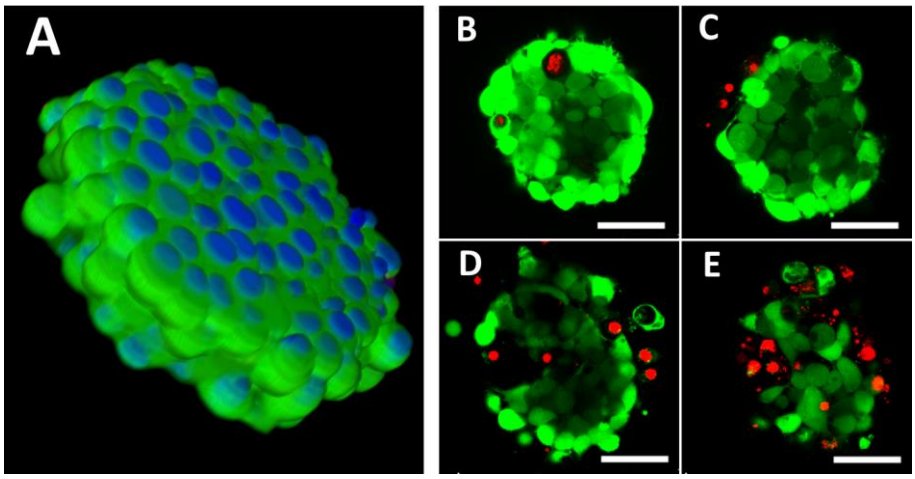

Figure 8. Images confocales de sphéroïdes multicellulaires tumoraux de cellules humaines de glioblastome U-87 MG : visualisation 3D d'une section transversale d'un sphéroïde (A) et dénombrement de mortalité (B-E). Les noyaux des cellules sont marqués avec le colorant Hoechst 33342 (en bleu), les cellules vivantes sont marquées avec de la calcéine AM (en vert) et les cellules mortes sont marquées avec de l'iodure de propidium (IP) (en rouge). L'observation de la section transversale des sphéroïdes n'ayant subi aucun traitement de principe actif (A) a été obtenue grâce à l'utilisation d'un microscope confocal permettant le traitement des images alors que le dénombrement des cellules mortes (B-E) a été réalisé en traitant les sphéroïdes durant 24 heures d'incubation avec du TMZ à différentes concentrations (10 mM, 50 mM, 100 mM et 150 mM). La barre d'échelle représente 50 µm.

3.1. Evaluations de nouveaux composés dérivés de la doxorubicine

Pour surmonter la multirésistance aux différents principes actifs anticancéreux, situation souvent rencontrée dans le cas des tumeurs, nous avons synthétisé cinq dérivés de doxorubicine (DOX) et parmi lesquels deux d'entre eux ont été modifiés de manière non covalente avec de l'albumine sérique humaine (ASH) (Tableau 3). L'évaluation de leur efficacité a été réalisée en utilisant deux lignées cellulaires tumorales, à savoir d'une part des cellules humaines de l'adénocarcinome du sein MCF-7 (type sauvage) et d'autre part des cellules résistantes (MCF-7/ADR) à la doxorubicine. De plus, les cellules MCF-7 ont été encapsulées dans des microcapsules d'alginate-chitosan et les sphéroïdes multicellulaires tumoraux (STM) produits ont été utilisés comme modèle 3D *in vitro* pour étudier la cytotoxicité des dérivés de la DOX.

Tableau 3. Dérivés de la doxorubicine (structures and poids moléculaires).

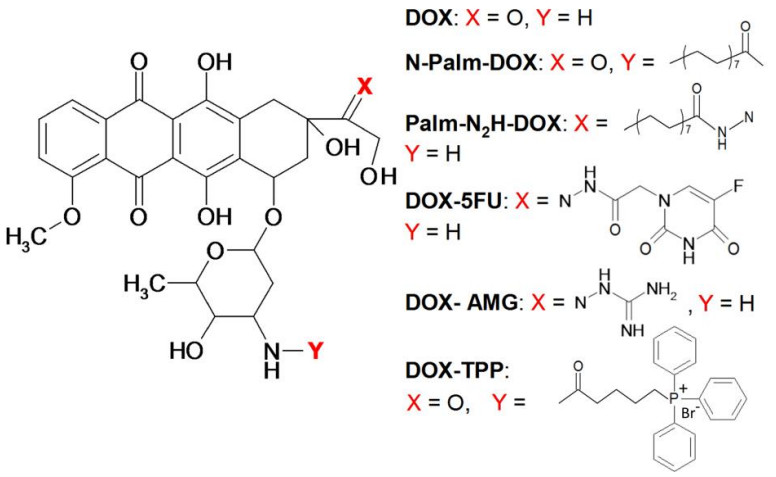

Dérivés	P.M.
N-Palm-DOX	781,94
Palm-N_2H-DOX	795,97
DOX-5FU	727,66
DOX-AMG	599,60
DOX-TPP	888,93
HSA-N-Palm-DOX	~ 65000
HSA-Palm-N_2H-DOX	~ 65000

En raison de leurs structures 3D les sphéroïdes tumoraux présentaient une résistance plus importante à la chimiothérapie comparée à celle observée en utilisant une culture conventionnelle de cellules sous forme de monocouche (tableau 4). En termes de cytotoxicité, les expérimentations ont permis de mettre en évidence que tous les dérivés de DOX étaient moins efficaces à l'égard des sphéroïdes multicellulaires tumoraux (SMT) à base de MCF-7/ADR et de MCF-7. Cependant, certains dérivés de DOX étaient plus actifs par leurs taux d'accumulation à l'intérieur des cellules. A titre d'exemple, la DOX attachée de manière covalente à l'acide palmitique (conjugué de DOX-N2H-Palm) s'est accumulée à des concentrations quatre fois plus importantes dans des cellules de type MCF-7/ADR comparé à l'accumulation observée avec de la DOX conventionnelle (Figure 9). De plus, en présence de sérum dans le milieu de culture, l'accumulation du conjugué de DOX-N2H-Palm était 10 fois plus importante que celle de la DOX conventionnelle.

Tableau 4. Valeurs IC_{50} des dérivés de DOX dans les sphéroïdes tumoraux.

Dérivé	IC_{50}, µM	
	48 h	72 h
DOX	26.2	8.0
Palm-N_2H-DOX	37.7	23.0
N-Palm-DOX	86.2	43.0
DOX-5FU	93.1	74.8
DOX-AMG	171.1	97.2
DOX-TPP	183.2	101.1

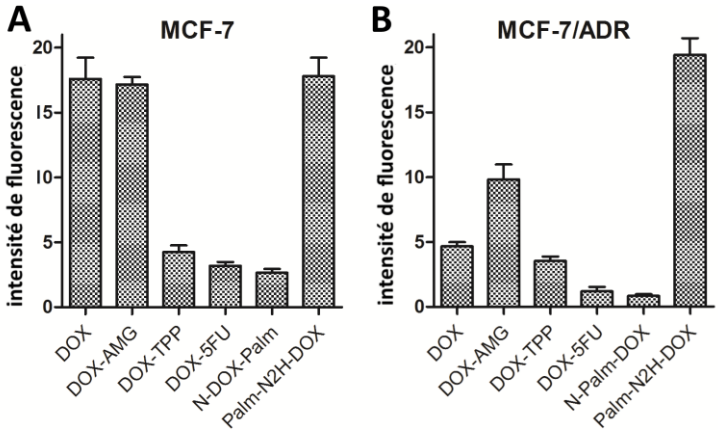

Figure 9. Accumulation des dérivés de DOX dans des cellules de MCF-7 et de MCF-7/ADR, 30 min d'incubation. Données de cytométrie de flux, 20,000 coups dans chaque échantillon.

Sur la base de ces résultats, deux complexes non-covalents de dérivés à base d'acide palmitique de DOX avec ASH ont été obtenus et leurs efficacités ont été étudiées en termes de solubilité dans l'eau et de cytotoxicité. Les valeurs IC50 du composé HSA-Palm-N2H-DOX sur des cellules MCF-7/ADR sont respectivement de 39,9 µM, 30,1 µM et 16,8 µM après 24 h, 48 h et 72 h. Ce sont les valeurs d'IC50 les plus faibles observées parmi tous les dérivés permettant de conclure que parmi tous les dérivés, les composés à base de HAS peuvent être les plus intéressants pour les recherches futures.

3.2. Micelles chargées avec de la curcumine

La curcumine (CUR), un composant actif principal du safran des indes (*Curcuma longa*), est un composé polyphénolique de faible poids moléculaire naturel avec une activité anticancéreuse prononcée. La curcumine empêche la prolifération, l'invasion, l'angiogenèse et la métastase des tumeurs par l'interaction avec de multiples cellules exprimant les protéines responsables de ces activités [18]. Toutefois, l'utilisation de la curcumine est limitée en raison de sa faible biodisponibilité et de sa faible solubilité en milieu aqueux. De ces faits, le développement de nouvelles formulations pour assurer la mise à disposition de la curcumine est très important. L'immobilisation de la curcumine dans des systèmes nanométriques de délivrance de principes actifs permet de surmonter ces limites. L'état de l'art dans ce domaine est décrit dans de nombreux articles scientifiques de revues [19]. Cependant, la plupart des systèmes de délivrances

proposés sont basés sur l'encapsulation physique de la curcumine dans des vecteurs de médicaments alors que la conjugaison covalente est une nouvelle approche. A travers les travaux de recherches de cette dissertation doctorale, des conjugués de curcumine ont été proposés avec des copolymères à blocs biodégradables de Pluronic pour la délivrance du principe actif. Au total, 4 conjugués ont été synthétisés. Cependant, presque tous ces composes ont été caractérisés par une faible encapsulation de curcumine. Seul le composé MC-17 (conjugué de CUR avec Pluronic F-68) contenait environ 4% en poids de CUR alors que 9 % en poids étaient le maximum qui pouvait être attaint. De ce fait, seul le conjugué MC-17 a été choisi pour poursuivre les recherches *in vitro*. Les experimentations ont permis de mettre en avant que le composé MC-17 se dissout aisément en milieu aqueux à des concentrations allant jusqu'à 600 µM (au moins) et qu'il donne lieu à la formation de micelles avec des tailles moyennes allant de 100 à 600 nanomètres selon d'une part la concentration en MC-17 et d'autre part selon la température (tableau 5). Des micelles avec une taille moyenne d'environ 100 nanomètres (1 mg/ml, 25°C) ont été réalisées pour mettre en place les essais sur les cultures cellulaires en 2D et en 3D. La technique d'agrégation cellulaire causée par la présence de RGD a été mise à profit pour obtenir des sphéroïdes tumoraux dans le cadre de ces recherches.

Tableau 5. Tailles moyennes des micelles MC-17 en fonction de la concentration de CUR-F68 et de la température du PBS (pH 7,4).

MC-17 concentration, mg/ml	Température (°C)	Taille moyennee, nm	IPD
0.01	25	273.3	0,46
0.1	25	254.6	0,31
1	25	107.3	0,57
0.01	37	603.8	0,50
0.1	37	401.9	0,37
1	37	292.7	0,37

Les experimentations ont permis de mettre en évidence que les micelles étaient moins efficaces à l'égard des cellules sauvages de types MCF-7 et d'U-87 MG comparées au CUR libre, mais plus toxiques vis-à-vis des cellules résistantes MCF-7/ADR (tableau 6). Une efficacité plus élevée des micelles contenant MC-17 à l'égard des cellules de types MCF-7/ADR pourrait être expliquée par une accumulation cellulaire en MC-17 plus élevée, due au passage facilité au travers des protéines de MDR. Toutefois, les données de cytometrie de flux n'ont pas permis de confirmer cette proposition. D'autre part, il a pu

être démontré que les micelles contenant du MC-17 étaient localisées dans des organelles cellulaires (lysosomes ou mitochondries), alors que la CUR libre était accumulée dans le cytoplasme. La littérature scientifique mentionne que la formulation de DOX avec du Pluronic P85 peut surmonter la résistance multidrogue chez des cellules de type MCF-7/ADR par leur localisation dans les mitochondries [20].

Tableau 6.Valeurs IC_{50} de micelles MC-17 et de CUR libre dans des cultures cellulaires sous forme de monocouche (2D).

	IC_{50}, µM					
	CUR			**MC-17**		
	24 h	**48 h**	**72 h**	**24 h**	**48 h**	**72 h**
U-87 MG	38.1	36.3	30.2	159.0	141.5	55.0
MCF-7	29.1	9.2	5.4	110	48	21.5
MCF-7/ADR	90.6	52.3	59.8	33.7	18	16.4

Malheureusement, les micelles contenant du MC-17 ne peuvent pas vaincre la résistance médicamenteuse présente dans les sphéroïdes tumoraux et étaient moins efficaces à l'égard des sphéroïdes multicellulaires tumoraux constitués des cellules MCF-7 et U-87 MG comparées à la curcumine libre (tableau 7). Le taux d'accumulation de micelles MC-17 était également plus faible que le taux de CUR libre (données de cytometrie de flux). Il aurait été intéressant de tester les micelles contenant du MC-17 en utilisant des sphéroïdes multicellulaires tumoraux constitués de cellules de type MCF-7/ADR. Néanmoins, cette lignée cellualire ne donne pas lieu à la formation de sphéroïdes multicellualires tumoraux par la technique d'agrégation cellulaire induite par le peptide RGD.

Tableau 7. Valeurs d'IC_{50} de micelles MC-17 et de CUR libre dans des cultures cellulaires de sphéroïdes tumoraux (3D).

	IC_{50}, µM					
	CUR			**MC-17**		
	24 h	**48 h**	**72 h**	**24 h**	**48 h**	**72 h**
U-87 MG	157.5	123.0	94.1	454.7	360.0	197.4
MCF-7	167.8	135.3	126.1	494.2	339.8	224.3

3.3 Microréservoirs de polysaccharides chargés avec de la thymoquinone

La thymoquinone (TQ) est le composant actif principal de l'huile essentielle de *Nigella sativa*. Ce composé est décrit pour ses effets anti-inflammatoires et anticancéreux dus à l'inhibition à la fois des métastases tumorales et à l'angiogenèse [21]. Du fait de l'instabilité de la TQ en milieu aqueux, et en particulier à un pH alcalin, l'encapsulation

dans des véhicules de délivrance de principes actifs doit permettre de protéger la TQ contre la dégradation. Récemment, une nouvelle classe des microréservoirs à base de chitosane (CS) et de gomme xanthane (XG) et obtenus par un ultrasonication à basse fréquence a été développée par le Dr. Borodina [22]. Cette technique est basée sur une cavitation acoustique apparaissant pendant l'ultrasonication et induisant la production de radicaux libres fortement réactifs, principalement OH• et H•. Les radicaux réagissent avec des parties de polymères situées à l'interface entre la phase dispersée et le milieu dispersant, conduisant à la réticulation et à la formation d'une structure stable. En conséquence, la phase d'huileuse s'émulsionne spontanément dans la phase polymère aqueuse en donnant la formation d'une couche polymère réticulée à la surface des gouttelettes émulsionnées. Dans le cadre des recherches de cette thèse doctorale, des microréservoirs (MRs) constitués de chitosane/gomme xanthane ont été suggérés pour assurer la délivrance de principes actifs lipophiles anticancéreux. Pour ce faire, la TQ a été dissoute dans l'huile de soja et encapsulée dans les microréservoirs constitués de chitosane/gomme xanthane ayant un diamètre moyen de 0,5 µm (TQ-MC-0,5) et de 2 µm (TQ-MC-2) en faisant varier le rapport huile/eau (1:150 et 1:30, respectivement).

Tableau 8. Valeurs moyennes de tailles et de potentiels ζ des microréservoirs en fonction du rapport d'huile/eau

sample	oil/water ratio	size, nm	ζ-potential, mV
MC-0.5	1/150	512±80	-55
TQ-MC-0.5		530±50	-50
MC-2	1/30	2051±200	-52
TQ-MC-2		1952±250	-48

La capture des MRs par des cellules de mélanomes de souris M-3 a été évaluée à la fois sur des monocouches cellulaires (2D) et sur des sphéroïdes multicellulaires tumoraux (3D) par microscopie confocale, cytométrie de flux et fluorimétrie. Afin de visualiser les réservoirs micrométriques, un rouge de Nile lipophile a été encapsulé dans le cœur huileux des microcapsules. La cytotoxicité plus élevée de l'échantillon TQ-MC-0.5 que celle de l'échantillon TQ-MC-2 était en parfaite corrélation avec une accumulation plus élevée de MC-0.5 plus élevée dans les cellules. Dans la culture cellulaire 3D de sphéroïdes multicellulaires tumoraux à la fois les préparations à base de MC-0.5 et de MC-2 se sont avérés pénétrer dans les sphéroïdes de manière dépendante du temps, avec toutefois une profondeur différente. Ainsi, on a observé que le MC-0.5 était présent dans la couche externe des sphéroïdes après 1 heure d'incubation alors qu'après 4 heures ils atteignaient déjà les cellules au centre des sphéroïdes (figures 10 A, B). Quant

à l'échantillon MC-2, la profondeur de pénétration était plus faible comparée à celle de MC-0.5, particulièrement après 4 h (figure 10 D, E). De plus, les niveaux de fluorescence de l'échantillon MC-0.5 étaient deux fois plus élevés comparés à celui de l'échantillon MC-2 après 8 et 24 heures d'incubations (figure 10 F). De ces expérimentations il a pu être conclu que les vecteurs MC-0.5 étaient plus prometteurs que les vecteurs MC-2 en raison d'une capture cellulaire plus élevée dans les deux modèles 2D et 3D. Ces expérimentations ont également permis d'observer un effet antitumoral également supérieur ainsi qu'une toxicité non spécifique inférieure pour MC-0.5.

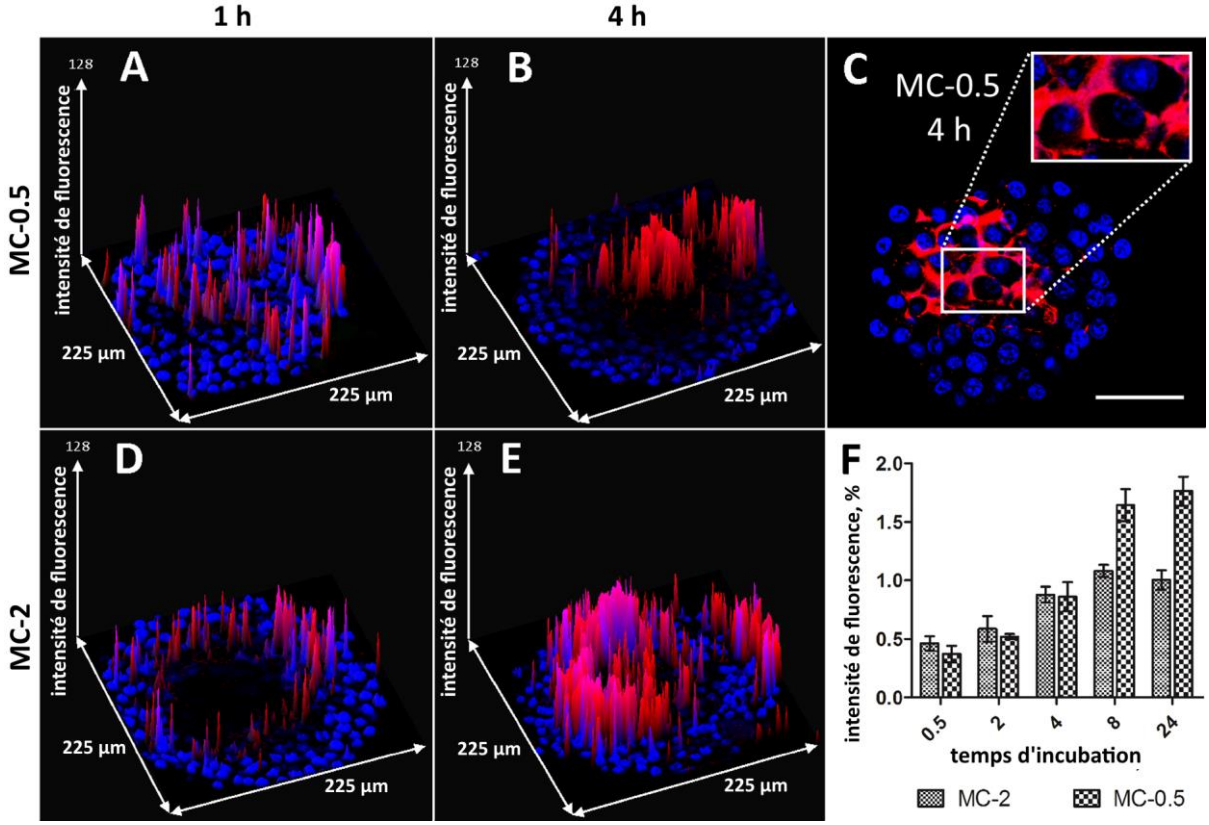

Figure 10.Distribution (A−E) et accumulation (F) des microcapsules chargées de rouge de nile dans des sphéroïdes tumoraux constitués de cellules tumorales M-3 : tracés des surfaces des sphéroïdes traités avec des échantillons VM-0.5 (A−C) et VM-2 (D, E) après 1 et 4 h d'incubation et données de fluorimétrie de la capture des MRs par les cellules constitutives des sphéroïdes (F). Les noyaux des cellules ont été marqués avec le colorant Hoechst (bleu). Les données de fluorimétrie sont exprimées en pour cent d'intensité de fluorescence comparée à celle obtenue avec des MRs dans la suspension du milieu de culture

3.4 Nanoémulsions chargées avec du rouge de Nile 668

Excepté pour la délivrance de principes actifs antitumoraux, des véhicules nano- et micrométriques pourraient également être utilisés pour le diagnostique et la visualisation

in vivo de tumeurs. Des colorants fluorescents ainsi que des agents de contraste iodés pourraient être utilisés à cet effet. Dans le cadre des recherches effectuées dans cette thèse de recherche, le colorant rouge de Nile modifié 668 a été mis en oeuvre car il est plus lumineux et plus stable comparé au rouge de Nile classique [23]. Ce colorant a été encapsulé dans des émulsions nanoparticulaires formulées suivant une méthode basée sur la nanoémulsification spontanée comme décrite précédemment [24]. Ainsi, des nanoemulsions (NEs) ayant une phase interne avec une dimension particulière comprise dans une gamme de taille allant de 30-200 nanomètres ont été préparées. Tous les gouttelettes des nanoémulsions ont été recouvertes d'une couche externe pégylée qui a permis une stabilisation forte au niveau de l'interface non seulement huile/eau, mais également de manière à permettre une fonctionnalisation extérieure très efficace des gouttelettes de lipides, conférant ainsi de la furtivité. Dans ce cas, les NEs ont donné lieu à la formation d'une dispersion stable des substances antitumorales fortement concentrées et encapsulées dans des nanogouttes lipidiques recouvertes de polyéthylèneglycol. La pénétration des NEs obtenues et chargées avec un colorant NR668 a été examinée en utilisant diverses lignées cellulaires. Les macrophages (à l'exception des autres cellules) se sont avérés capables de réaliser la capture des gouttelettes des nanoémulsions. De plus, la capture des NEs par les macrophages était fonction du diamètre moyen des gouttelettes de phase interne des nanoémulsions. Celles qui sont caractérisées par une taille de 100 nm montraient une accumulation cellulaire plus importante comparée à celles ayant un diamètre moyen de 55 nm.

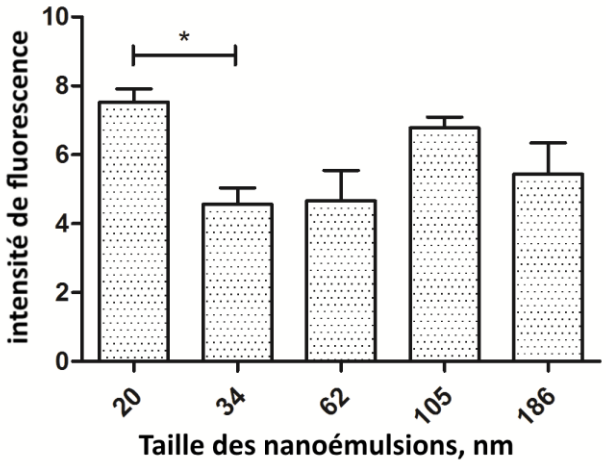

Figure 11. Accumulation de nanoémulsions dans des sphéroïdes multicellulaires tumoraux après 4 heures d'incubation. L'importance de la fluorescence a été évaluée en traitant les images confocales

avec un programme Image J. U=0.0571
(Test statistique U Mann–Whitney).
L'interaction des NEs avec les sphéroïdes multicellulaires tumoraux induits par le RGD a également été observée par microscopie confocale. Malgré l'absence de différences significatives parmi les différentes tailles de NEs (figure 11), l'accumulation préférée de NEs de 20 nanomètres doit néanmoins être mentionné (U=0.0571 dans le test statistique U de Mann-Whitney). L'utilisation de Cremophor® au lieu du Kolliphor® pour la réalisation des NEs influence également faiblement légèrement au niveau de l'accumulation (7,6±1,4 contre 4,6±0,5, respectivement, pour des NEs de 30 nanomètres, 4 h d'incubation).

D'autre part, une corrélation claire entre l'accumulation de NEs et le moment de l'incubation a été trouvée (figure 12). De plus, pendant les 4 premières heures, l'accumulation de NEs dans les sphéroïdes multicellulaires tumoraux constitués de MCF-7 était plus importante que dans ceux constitués de U-87 MG (figure 13). Cependant, cette différence pourrait être expliquée avec les différences de tailles des sphéroïdes multicellulaires tumoraux des deux lignées cellulaires (98±24 µm pour MCF-7 comparé à 128±20 µm pour U-87 MG). Par conséquent, les sphéroïdes multicellulaires tumoraux constitués de MCF-7 ont un meilleur rapport surface/volume conduisant à l'augmentation de l'accumulation de NEs. De faibles taux d'accumulation pourraient être expliqués par l'existence de PEG de faible poids moléculaire à la surface des NEs. En conséquence, les NEs adhèrent lentement aux cellules, et leur mouvement dans l'espace intracellulaire a été démontré par vidéo.

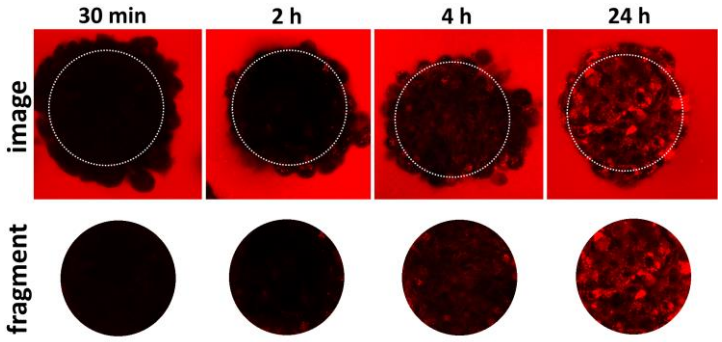

Figure 12. Accumulation de nanoémulsions constituées de vésicules d'une taille de 34 nm dans des sphéroïdes multicellulaires tumoraux (SMT) formés à partir de cellules U-87 MG. Pour la realisation de l'analyse quantitative, la fluorescence moyenne de l'image est divisée par la fluorescence des nanoémulsions. La fluorescence a été mesurée avec un programme image J.

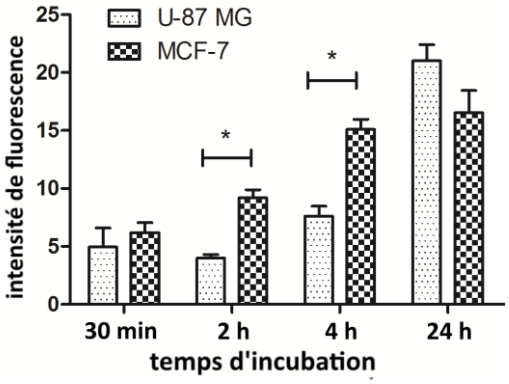

Figure 13. Accumulation de nanoémulsions constituées de vésicules de 34 nm dans des sphéroïdes multicellulaires tumoraux (SMT) formés à partir de cellules U-87 MG et MCF-7. * $p<0.05$ (test U de Mann–Whitney).

Ce processus s'est avéré être dépendant de la concentration en NEs, du temps d'incubation ainsi que du diamètre des sphéroïdes. Selon les observations qui ont pu être réalisées, les NEs s'accumulent dans les membranes cellulaires et non à l'intérieur des cellules. Cette observation a permis d'envisager d'utiliser les NEs non seulement comme vecteurs de médicaments mais également comme agents de visualisation.

- Conclusion générale

L'effet d'auto-assemblage de cellules induit par l'addition d'un peptide cyclique de type RGDfK et de sa modification, à savoir sous la forme cyclo-RGDfK (TPP) directement appliqué sur des cultures de cellules a été découvert et étudié pour 16 lignées cellulaires de diverses origines. Basé sur ce phénomène, une approche nouvelle hautement reproductible en une seule étape a permis le développement et la formation de sphéroïdes multicellulaires. Basé sur cette technique, deux nouveaux modèles 3D *in vitro* ayant une structure de type « cœur-écorce » très prononcée ont été mises à profit pour réaliser de la co-culture tumorale et de cellules normales. Les sphéroïdes tumoraux induits par la présence du peptide RGD ont été utilisés comme modèle *in vitro* 3D pour étudier l'efficacité à la fois de principes actifs de faibles poids molécualires (doxorubicine et ses dérivés, curcumine, témozolomide) et de vecteurs de délivrance de médicaments nano- et micro-métriques (microcapsules, micelles, nanoémulsions). Des méthodes à la fois quantitatives (dosages MTT- et XTT, cytométrie de flux, fluorimétrie) et qualitatives

(analyses d'images par microscopie confocale) ont été utilisées pour étudier les sphéroïdes tumoraux. En résumé, le travail doctoral a contribué au développement d'une technique *in vitro* permettant la formation de sphéroïdes induits par la présence d'un peptide de type RGD et de les utiliser comme outil permettant de « trier » à la fois de nouvelles substances anticancéreuses et des systèmes de délivrance de médicaments.

- Références

[1] A. Narang, D. Desai, Anticancer Drug Development, in: Y. Lu, R.I. Mahato (Eds.), Pharm. Perspect. Cancer Ther. SE - 2, Springer US, 2009: pp. 49–92.

[2] M. Hay, D.W. Thomas, J.L. Craighead, C. Economides, J. Rosenthal, Clinical development success rates for investigational drugs, Nat. Biotechnol. 32 (2014) 40–51.

[3] X. Xu, M.C. Farach-Carson, X. Jia, Three-dimensional in vitro tumor models for cancer research and drug evaluation, Biotechnol. Adv. 32 (2014) 1256–1268.

[4] A.C. Luca, S. Mersch, R. Deenen, S. Schmidt, I. Messner, K.-L. Schäfer, et al., Impact of the 3D microenvironment on phenotype, gene expression, and EGFR inhibition of colorectal cancer cell lines., PLoS One. 8 (2013) e59689.

[5] D. V LaBarbera, B.G. Reid, B.H. Yoo, The multicellular tumor spheroid model for high-throughput cancer drug discovery, Expert Opin. Drug Discovery. 7 (2012)

[6] R.M. Sutherland, J.A. McCredie, W.R. Inch, Growth of multicell spheroids in tissue culture as a model of nodular carcinomas, J. Natl. Cancer Inst. 46 (1971) 113–20.

[7] J. Hickman, R. Graeser, R. de Hoogt, S. Vidic, C. Brito, M. Gutekunst, et al., Three-dimensional models of cancer for pharmacology and cancer cell biology: Capturing tumor complexity in vitro/ex vivo, Biotechnol. J. 9 (2014) 1115–1128.

[8] E.E. Robinson, K.M. Zazzali, S.A. Corbett, R.A. Foty, Alpha5beta1 integrin mediates strong tissue cohesion, J. Cell Sci. 116 (2003) 377–86.

[9] A. Ivascu, M. Kubbies, Rapid Generation of Single-Tumor Spheroids for High-Throughput Cell Function and Toxicity Analysis, J. Biomol. Screening. 11 (2006) 922–932.

[10] P. Salmenperä, E. Kankuri, J. Bizik, V. Sirén, I. Virtanen, S. Takahashi, et al., Formation and activation of fibroblast spheroids depend on fibronectin–integrin interaction, Exp. Cell Res. 314 (2008) 3444–3452.

[11] D. Heckmann, A. Meyer, B. Laufer, G. Zahn, R. Stragies, H. Kessler, Rational Design of Highly Active and Selective Ligands for the α5β1 Integrin Receptor, ChemBioChem. 9 (2008) 1397–1407.

[12] J.M. Caron, M. Bannon, L. Rosshirt, J. Luis, L. Monteagudo, J.M. Caron, et al.,

Methyl Sulfone Induces Loss of Metastatic Properties and Reemergence of Normal Phenotypes in a Metastatic Cloudman S-91 (M3) Murine Melanoma Cell Line, PLoS One. 5 (2010) e11788.

[13] J.M. Gozgit, B.T. Pentecost, S. a Marconi, C.N. Otis, C. Wu, K.F. Arcaro, Use of an aggressive MCF-7 cell line variant, TMX2-28, to study cell invasion in breast cancer., Mol. Cancer Res. 4 (2006) 905–13.

[14] J. Dittmer, B. Leyh, The impact of tumor stroma on drug response in breast cancer, Semin. Cancer Biol. 31 (2015) 3–15.

[15] T.S. Jones, E.C. Holland, Standard of care therapy for malignant glioma and its effect on tumor and stromal cells, Oncogene. 31 (2012) 1995–2006.

[16] E. Markvicheva, L. Bezdetnaya, A. Bartkowiak, A. Marc, J.-L. Gorgen, F. Guillemin, et al., Encapsulated multicellular tumor spheroids as a novel in vitro model to study small size tumors, Hem. Ind. 57 (2003) 585–588.

[17] D.S. Zaytseva-Zotova, O.O. Udartseva, E.R. Andreeva, A. Bartkowiak, L.N. Bezdetnaya, F. Guillemin, et al., Polyelectrolyte microcapsules with entrapped multicellular tumor spheroids as a novel tool to study the effects of photodynamic therapy, J. Biomed. Mater. Res., Part B. 97B (2011) 255–262.

[18] A. Shehzad, Y.S. Lee, Molecular mechanisms of curcumin action: Signal transduction, BioFactors. 39 (2013) 27–36.

[19] S.S. Bansal, M. Goel, F. Aqil, M. V. Vadhanam, R.C. Gupta, Advanced drug delivery systems of curcumin for cancer chemoprevention, Cancer Prev. Res. 4 (2011) 1158–1171.

[20] T. Minko, E. V. Batrakova, S. Li, Y. Li, R.I. Pakunlu, V.Y. Alakhov, et al., Pluronic block copolymers alter apoptotic signal transduction of doxorubicin in drug-resistant cancer cells, J. Controlled Release. 105 (2005) 269–278.

[21] R. Schneider-Stock, I.H. Fakhoury, A.M. Zaki, C.O. El-Baba, H.U. Gali-Muhtasib, Thymoquinone: fifty years of success in the battle against cancer models, Drug Discovery Today. 19 (2014) 18–30.

[22] T.N. Borodina, D.O. Grigoriev, M. a. Carillo, J. Hartmann, H. Moehwald, D.G. Shchukin, Preparation of multifunctional polysaccharide microcontainers for lipophilic bioactive agents, ACS Appl. Mater. Interfaces. 6 (2014) 6570–6578.

[23] A.S. Klymchenko, E. Roger, N. Anton, H. Anton, I. Shulov, J. Vermot, et al., Highly lipophilic fluorescent dyes in nano-emulsions: towards bright non-leaking nano-droplets, RSC Adv. 2 (2012) 11876.

[24] N. Anton, P. Gayet, J.-P. Benoit, P. Saulnier, Nano-emulsions and nanocapsules by the PIT method: An investigation on the role of the temperature cycling on the

emulsion phase inversion, Int. J. Pharm. 344 (2007) 44–52.

LISTE DES PRESENTATIONS

Oral communications :

1) **Akasov R.**, Markvicheva E. Novel 3D *in vitro* models based on multicellular tumor spheroids to test anticancer nanosized formulations // Proceedings of the International conference «Biocatalysis-2015: fundamentals and applications» (Moscow region, Russia). – 21-25 June, 2015. – P. 53.
2) **Akasov R**., Zaytceva E, Borodina T, Markvicheva E. Encapsulation of Lipophilic Antitumor Drugs in Polysaccharide Microcontainers // Proceedings of the XXII International Conference on Bioencapsulation (Bratislava, Slovakia). – 17-20 September 2014. – P. 46-47.
3) **Akasov R**., Drozdova M., Zaytseva-Zotova D., Yuablokova T., Marc A., Chevalot I., Burov S., Markvicheva E. Microencapsulated Tumor Spheroids as a 3D Model to Study Cytotoxicity of Novel Antitumor Preparations // Proceedings of the XX International Conference on Bioencapsulation (Orillia, Canada). – 21-24 September 2012 – P. 70-71.
4) **Akasov R**., Drozdova M., Zaytseva-Zotova D., Marc A., Chevalot I., Burov S., Yuablokova T., Markvicheva E. Alginate-chitosan microcapsules as a 3D Model to Study Cytotoxicity of Doxorubicin Derivatives // Proceedings of the XI International Conference “Modern Perspectives in Chitin and Chitosan Studies (Murmansk, Russia). – 25-29 June 2012. – P. 250-255.

Posters :

5) **Akasov R**., M.Chiper., Burov S., T. Vandamme, Markvicheva E. Development of polymeric micelles for curcumin delivery // Proceedings of the 5th Russian-Hellenic Symposium with International Participation and Young Scientist’s School “Biomaterials and Bionanomaterials: Recent Advances and Safety-Toxicology Issues” (Heraklion, Crete-Greece). – 4-11 May 2014. – P.18.
6) **Akasov R.**, Zaytseva-Zotova D., Burov S., Markvicheva E. A new approach to produce microencapsulated co-culture tumor spheroids by RGD-dependent cell aggregation // Proceedings of the XXI International Conference on Bioencapsulation (Berlin, Germany). - 28-30 August 2013. – P. 70-71.
7) **Akasov R.**, Drozdova M., Zaytseva-Zotova D., Burov S., Marc A., Chevalot I., Markvicheva E. 3-D *in vitro* systems based on polyelectrolyte microcapsules and RGD-peptides for antitumor drug screening // Proceedings of the 4th Russian-

Hellenic Symposium with International Participation and Young Scientist's School "Biomaterials and Bionanomaterials: Recent Advances and Safety-Toxicology Issues" (Heraklion, Crete-Greece). – 6-13 May 2013. – P.29.

LISTE DES PUBLICATIONS

1) **Akasov R**., Haq S., Haxho F., Samuel V., Burov S. V, Markvicheva E., Neufeld R.J., Szewczuk M.R. Sialylation transmogrifies human breast and pancreatic cancer cells into 3D multicellular tumor spheroids using cyclic RGD-peptide induced self-assembly // *Oncotarget*. 2016, DOI: 10.18632/oncotarget.11868
2) **Akasov R**, Gileva A, Zaytseva-Zotova D, Burov S, Chevalot I, Guedon E, Markvicheva E. 3D in vitro co-culture models based on normal cells and tumor spheroids formed by cyclic RGD-peptide induced cell self-assembly // *Biotechnology Letters*, DOI: 10.1007/s10529-016-2218-9
3) **Akasov R**, Zaytseva-Zotova D, Burov S, Leko M, Dontenwill M, Chiper M, Vandamme T, Markvicheva E. Formation of multicellular tumor spheroids induced by cyclic RGD-peptides and use for anticancer drug testing in vitro // *Int J Pharm.* 2016 Jun 15; 506(1-2):148-57.
4) **Akasov R**, Borodina T, Zaytseva E, Sumina A, Bukreeva T, Burov S, Markvicheva E. Ultrasonically Assisted Polysaccharide Microcontainers for Delivery of Lipophilic Antitumor Drugs: Preparation and in Vitro Evaluation // *ACS Appl Mater Interfaces*. 2015 Aug 5; 7(30):16581-9.
5) Attia MF, Anton N, **Akasov R**, Chiper M, Markvicheva E, Vandamme TF. Biodistribution and Toxicity of X-Ray Iodinated Contrast Agent in Nano-emulsions in Function of Their Size // ***Pharm Res***. 2016 Mar; 33(3):603-14.
6) Khan IU, Stolch L, Serra CA, Anton N, **Akasov R**, Vandamme TF. Microfluidic conceived pH sensitive core-shell particles for dual drug delivery // *Int J Pharm*. 2015 Jan 15; 478(1):78-87.
7) Attia MF, Anton N, Chiper M, **Akasov R**, Anton H, Messaddeq N, Fournel S, Klymchenko AS, Mély Y, Vandamme TF. Biodistribution of x-ray iodinated contrast agent in nano-emulsions is controlled by the chemical nature of the oily core // *ACS Nano*. 2014 Oct 28; 8(10):10537-50.
8) Khan IU, Serra CA, Anton N, Li X, **Akasov R**, Messaddeq N, Kraus I, Vandamme TF. Microfluidic conceived drug loaded Janus particles in side-by-side capillaries device // *Int J Pharm*. 2014 Oct 1; 473(1-2):239-49.

CONTENT

ACKNOWLEDGEMENTS

I wish to thank, first, my supervisors, Prof. Elena Markvicheva and Prof. Thierry Vandamme for their support and guidance through my work on this Thesis. Their advices were very valuable and always greatly appreciated.

I would like to acknowledge the financial, academic and technical support of the Institute of bioorganic chemistry (Moscow, Russia) and University of Strasbourg (France). I also thank the Russian Foundation for Basic Research for their financial support of our studies and France Government for the bursary during my residence in France through the program "Bourses d'Excellence Eiffel" in 2013-2014. Many thanks to non-profit scientific association Bioencapsulation Research Group for the continious financial support of young scientists on BRG conferences and training schools.

Grateful thanks to my colleagues, both past and present members of the laboratories both in Russia and France. I would also like to thank Dr. Sergey Burov (Institute of Macromolecular Compounds, Saint-Petersburg, Russia) for the synthesis of RGD-peptides and doxorubicin derivatives; Drs. Tatiana Borodina and Tatiana Bukreeva (Shubnikov Institute of Crystallography, Moscow, Russia) for the obtaining of polysaccharide microcontainers; Dr. Manuela Chiper (University of Strasbourg, France) for the synthesis of curcumin micelles; Drs. Andrey Klymchenko and Nicolas Anton (University of Strasbourg, France) for the obtaining of nanoemulsions; Dr. Monique Dontewill (University of Strasbourg, France) and Drs. Elena Svirshchevskaya and Elena Kovalenko (Institute of bioorganic chemistry, Moscow, Russia) for their help with cell culturing.

My special gratitude to Drs. Ronald Neufeld and Myron Szewczuk (Queens University, Kingston, Canada) for the opportunity to join their laboratory in Canada to study some aspects of RGD-induced cell self-assembly.

Finally, I would like to express many thanks to my dear family and friends. This thesis would not have been possible without the support of all of these people

INTRODUCTION

Development of novel anticancer formulations is a priority challenge in biomedicine. As known, about 10 000 compounds with potential antitumor activity are evaluated in preclinical and clinical tests every year [1]. Additionally, various nano- and micro- particles have been proposed for drug delivery purpose (liposomes, nanoemulsions, polyelectrolyte microcapsules, metal-based particles, etc). These vehicles protect drugs from premature degradation as well as provide targeted drug delivery to tumors due to enhanced permeability and retention (EPR) effect [2]. However, only 6.7% of antitumor preparations which enter to Phase I clinical trials, use to meet FDA approval [3]. It is the worst level among all drug-candidates which is about two-fold lower compared to the relevant rate of other (non-antitumor) drugs [3]. This evidence confirms low prognostic value of current *in vitro* antitumor drug testing techniques. One of the reasons is that routine cytotoxicity tests are performed *in vitro* using conventional monolayer cell cultures. However, the *in vitro* models based on monolayer cultures (2D) leave much to be desired, since they can not well mimic solid tumors, in particular the behavior of cancer cells, in terms of cell interactions with extracellular matrix (ECM) and cell–to-cell communications. For this reason, a number of three-dimensional (3D) models have been recently proposed. The advantages of 3D tumor models for drug screening have been discussed in numerous papers and reviews [4–6]. For example, cells in 2D monolayer culture are exposed to uniform concentrations of oxygen and nutrients, while in solid tumors the cells occur at gradient conditions of vital factors. As a result, it could lead either to enhancement or vice versa inhibitory effects on tumor progression [7]. Moreover, chemotherapeutics can be easily delivered to target cells in monolayer cell culture conditions, while *in vivo* drugs have to penetrate through several layers of stromal cells. Finally, cell growth in 3D cultures leads to a divergent gene expression compared to that in a monolayer [8,9]. All the above mentioned issues result in a reduced sensitivity to chemotherapeutic agents in 3D conditions compared to the monolayer culture.

Multicellular tumor spheroids (MTS) are 3D dense spherical aggregates which could mimic solid small size tumors in terms of simulating cell-cell interactions and microenvironment in tumors. First time, MTS have been proposed by R Sutherland in early 1970s [10], and since those time they have become a useful tool in tumor biology, in particular radiation biology, photodynamic and chemotherapies [11,12]. Several approaches have been proposed to MTS

formation, such as spinner flasks, rotary cell culture systems, hanging drops, liquid overlay, low binding plates, or microencapsulation in polyelectrolyte microcapsules [13,14]. However, despite the encouraging results there is no "an ideal technique" for highthroughput drug screening which could meet all necessary requirements, such as rapidity, reproducibility, simplicity and cost-effectiveness [15]. For example, rotary cell cultivation systems or shakers which are widely used for MTS generation can not provide rather narrow spheroid size distribution, while handing-drop technique is extremely cost- and laborintensive [16]. Nowadays, cell cultivation in ultra-low attachment (ULA) round-bottom plates is one of the most common approaches due to the simple protocol and high reproducibility. However, this technique is also limited with a small MTS number (one spheroid per well) and an occasional formation of loose aggregates instead of dense spheroids.

The aim of the Thesis was to develop a novel highly reproducible technique for MTS formation based on a RGD-induced cell self-aggregation, and to demonstrate the availability of these spheroids as 3D *in vitro* model to test anticancer drugs and drug delivery vehicles.

More specifically, the tasks were as follows :

1. To study RGD-induced cell aggregation using cell lines which differ in characteristics and origin.
2. To evaluate spheroids properties (e.g. shape, size, cell viability) as a function of cell type and RGD-induced cell aggregation conditions.
3. To develop a technique for formation of co-culture spheroids from tumor and normal cells using RGD-induced cell aggregation platform.
4. To fabricate some drug delivery vehicles loaded with various antitumor drugs for their further cytotoxicity evaluation on the spheroids .
5. To demonstrate that the RGD-induced tumor spheroids can be used as 3D *in vitro* model to test anticancer drugs and drug delivery vehicles.

- **Funding and sources**

This work was supported by the Russian Foundation for Basic Research and by the France Government (Bourses d'Excellence Eiffel, 2013-2014).

LITERATURE REVIEW

CHAPTER I. Models for anticancer drugs testing

1.1.1. Classical *in vitro* and *in vivo* models

Monolayer cell cultures are the most common *in vitro* model for anticancer drug testing. However, this two-dimension (2D) culture can not well mimic solid tumors, in particular the behavior of cancer cells in terms of their interactions with ECM network and cell–to-cell communications. Therefore, a prognostic value of this model leaves much to be desired. Thus, in the early 1990s, the National Cancer Institute introduced a "disease-oriented" drug screening approach using a panel of 60 human cancer cell lines derived from nine different types of cancer. This approach was designed to facilitate high-throughput screening of large numbers of drugs for further preclinical assessment in xenograft models [17]. Unfortunately, the results demonstarted the general failure of this approach, since the clear correlation between *in vitro* and *in vivo* efficacy was not found [17,18]. Contrary, animal tumor models are of great prognostic value, since they are complex and allow to study biodistribution and pharmacokinetics. However, animals differ from humans in some physiological aspects, so the therapy outcome might also be different [19,20]. More over, there is a need to develop animal models to test anticancer agents in brain, kidney, cervix, lymphatics, the hematopoietic system, and skin (melanoma) [21]. Additionally, the use of animals for drug testing is limited with strict ethical rules.

In summary, 2D *in vitro* models lack realistic complexity, while animal models are expensive, time consuming, and often fail to reflect human tumor biology. That is why the development of 3D *in vitro* models is of great importance.

1.1.2. Three-dimensional cell cultures *in vitro*

Three-dimensional *in vitro* tumor models could be considered as an intermediate step between classical monolayer cell cultures *in vitro* and animal tumor models *in vivo*. On one hand, these models are quite enough for routine testing. On the other hand, they form in vivo-like structures which are similar to real tumors [4]. The use of these models also allow to specify therapeutic drug concentrations before *in vivo* testing, since cells in 3D conditions are more

resistant to therapy compared to the monolayer cultures. Here, we describe some of the most common 3D *in vitro* models used in tumor biology and anticancer drug screening.

1.1.2.1. Ex vivo cultures

The term *ex vivo* means that the samples to be tested have been extracted from the organism by biopsy. This is the earliest 3D *in vitro* tumor model which was used for drug testing before the appearance of immortalised cell lines [22]. E*x vivo* cultures are very similar to real tumors, since they involve not only tumor cells, but also stroma cells and extracellular matrix proteins. *Ex vivo* cultures recapitulate the structural complexity and heterogeneity of tunors, making them an important adjunct to current cell-line-based and animal-based models. However, obtaining *ex vivo* cultures is labor-intensive, while the obtained cultures are short-lived like any primary culture. Neverheless, they are often used to discover oncomarlers, study cell proliferation and cell migration mechanisms as well as to evaluate the efficacy of antitumor therapy [23]. It is also of great interest to use these *ex vivo* cultures in personalized anti-tumor therapy [24,25].

1.1.2.2. Multilayer cell cultures

Formation of multilayer cell culture (MCC) is the simpliest approach to formation of 3D *in vitro* tumor model. For this purpose, the cells are cultivated in semi-permeable chambers coated with ECM proteins. More cells are in the chamber, the higher cell layer can be obtained (up to 1 mm, ~200 μm generally). The multilayer cell culture from human cancer cells have been successfully used to study tissue pharmacokinetics of anticancer drugs. [26,27]. Additionally, they are used to determine oxygenation and consumption of solid tumors [28]. The MCC is rather simple and easy-to-use model which is very useful in case of cell lines that cannot be grown like other 3D *in vitro* systems. However, MCC is not a true three-dimensional system since oxygen and nutrition gradients are similar to the two-dimentional culture, not to real tumors [28].

1.1.2.3. Three-dimensional matrices

Three-dimensional matrices for cell culture are used in tissue engineering as a tool to provide cell growth in native microenvironment. However, 3D matrices could be used not only for tissue engineering but also for “tumor enginnering” [29,30]. Generally, these are hydrogels fabricated from natural polymers (Matrigel®, collagen, or chitosan) or synthetic materials (for instance, poly(D,L-lactide), poly(D,L-lactide-co-glycolide), or polycaprolactone) [4].

Matrigel® is a trade name of gelatinous protein mixture secreted by Engelbreth-Holm-Swarm (EHS) mouse sarcoma cells produced and marketed by Corning Life Sciences and BD Biosciences. This is the most common matrix for culture of cancer cells [31]. Use of natural biopolymers, like Matrigel® or collagen, allows to recapitulate the complicated extracellular environment which occurs in tumors *in vivo*. However, the use of matrices complicates some experiments, e.g. microscopic observation or cell viability assays. That is why 3D matrices are commonly used in fundamental studies of tumor biology, for example evaluation of cell-matrix interactions, cell adhesion and spreading, or co-culture conditions. Thus, collagen gels were used to evaluate the involvement of primary fibroblasts in drug resistance of human adenocarcinoma MCF-7 cells [32], or to study a role of tissue macrophages in a squamous cellular carcinoma organotypic model [33].

1.1.2.4. Multicellular tumor spheroids

Multicellular tumor spheroids are gaining the increasing popularity as a 3D *in vitro* model for antitumor drugs testing. MTS are dense spherical aggregates (50-1000 μm in diameter) which could mimic solid small size tumors in terms of simulating cell-cell interactions and microenvironment in tumors. This model was adopted to cancer research by Sutherland et al. in the middle of the 1970th [10]. Presently, tumor spheroids are considered as a rational platform to predict *in vivo* drug efficacy. There are some advantages of MTS system over other 3D *in vitro* models. Thus, unlike to *ex vivo* cultures, they are generated from well-established immortalized cell lines. Unlike to multilayer cell cultures, MTS have spherical organization similar to the architecture of tumor *in vivo* . The absence of external 3D hydrogel matrice allows to study them by any cell biology assay [34]. Tumor spheroids are also often called *tumorospheres*, *oncospheres,* or *tumoroids* [35]. Spheroids from brain, breast, or colon cancer cell lines are named as neurospheres, mammospheres, or colonospheres, respectively [35].

Spheroid morphology depends on the cell line and culture conditions. Thus, four types of tumor spheroids could be generated from four various breast adenocarcinoma cell lines [36]. The first type has well-organized round spherical shape with regular nucleuses and strong cell-cell contacts. Spheroids round in shape from S1 cell line are shown in **Figure 1**. Sometimes, round spheroids have a hollow in the center because of to the epithelial nature of cells [37] or cell apoptosis [38]. The other breast adenocarcinoma cell line BT-474 can form so called "mass spheroids" with disorganized nucleuses and strong cell-cell adhesion (Figure 1). Mass

spheroids have higher expression of some keratins that prevents central hollow formation [39]. Two other types of spheroids, namely grape-like and stellate ones, have poor cell-cell contacts and have no well-arranged shape. Stellate morphology is common for spheroids in Matrigel or collagen hydrogel and arises as a result of cell invasion to matrix. The grape-like spheroids from SK-BR-3 cells and stellate spheroids from MDA-MB-231cells are also shown in the Figure 1.

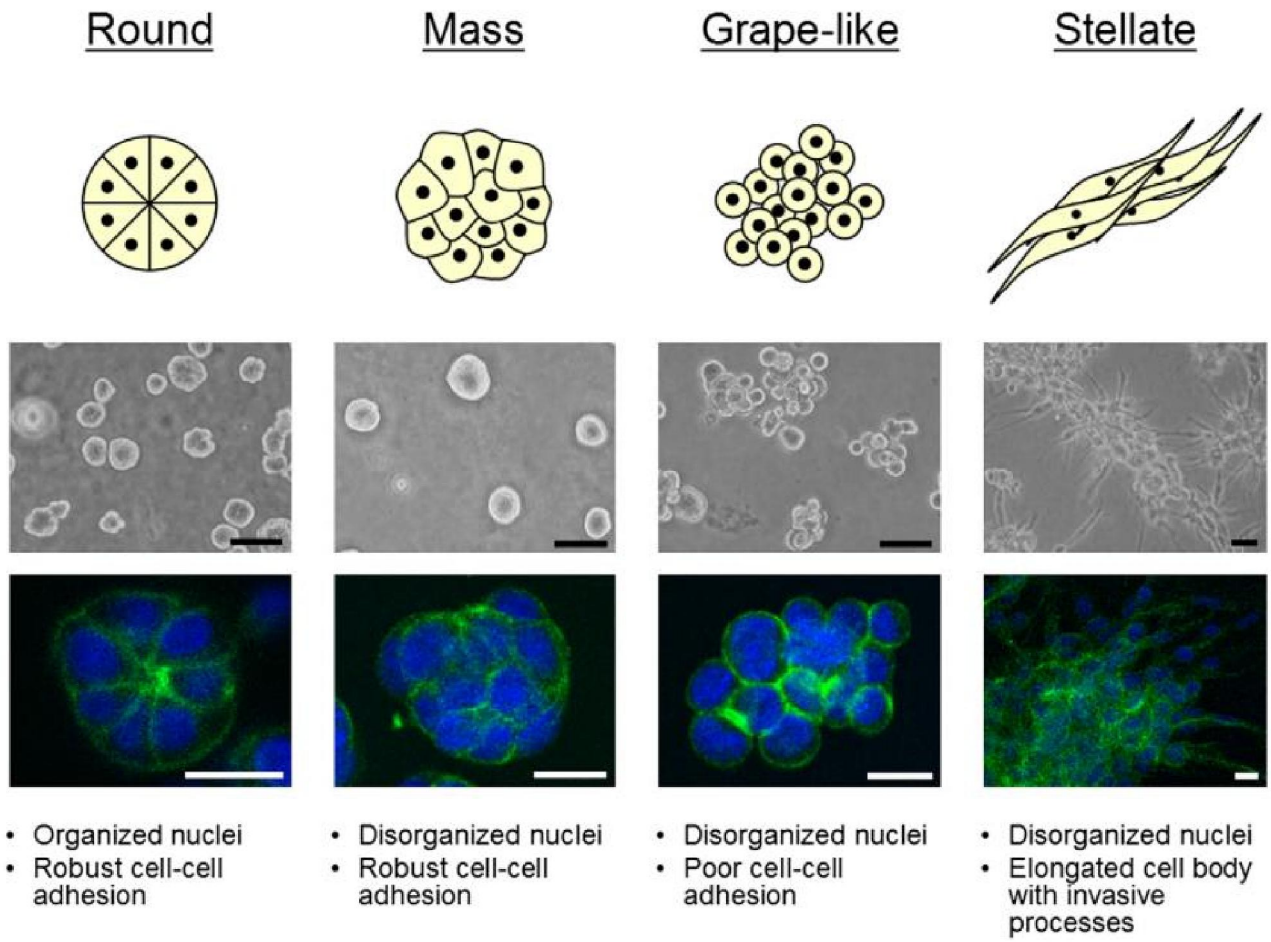

Figure 1. Breast cell line colony morphologies in 3D culture fall into four distinct groups. A schematic and key descriptors of each morphology is shown in addition to phase contrast and F-actin and nuclear fluorescence images of representative cell lines of each morphology: for Round, S1 is shown; Mass, BT-474; Grape-like, SK-BR-3; and Stellate, MDA-MB-231. Scale bars: phase contrast, 50 μm; fluorescence, 20 μm [36].

1.2. Characterization of multicellular tumor spheroids

1.2.1. Tumor spheroids advantages over conventional 2D cell culture

1.2.1.1. Cell morphology is similar to in vivo conditions

Cell cultivation as flat monolayer results in a simple geometry with only one cell surface to adhere (apical-basal polarity). These conditions are good enough for epithelial cells, but most carcinoma cells are known for epithelial-mesenchymal transition [40,41]. Thus, they need more complicated 3D environment. Changes in cell shape and morphology ultimately modify cellular function, e.g. abilities to apoptosis induction or to nanoparticles uptake through the alteration of cell surface/cytoplasm ratio [42]. Therefore, cell cultivation as tumor spheroids allows to mimic physiological conditions and, as a result, to get more adequate results in drug testing.

1.2.1.2. Three-dimensional architecture and cell heterogenity

When cancer cells grow in a flat monolayer, there are no oxygen, nutrient, or waste gradients. As a result, cell proliferation rate is similar everywhere across the surface of the culture plate. However, tumors *in vivo* have 3D architecture, and the conditions inside the tumors greatly differ. Tumor spheroids can reproduce oxygen and nutrient gradients typical for *in vivo* tumors [43]. As a result, cells in the spheroids form differential zones of proliferation with more rapid cell division in the outer layer of the spheroid [12]. Generally, it results in a cell cycle arrest inside spheroids and a mild proliferation rate reduction [38,44]. Moreover, if the spheroid diameter is higher than 400-500 μm, a necrotic core formation usually occurred. The other result of oxygen and nutrient gradients is pH changes inside the spheroids [45]. Therefore, MTS are a promising tool to test pH-dependent drugs or drug delivery vehicles [46,47], or cell-cycle specific drugs [48]. The 3D architecture of MTS is also often used to study the infiltration of drug vehicles into solid tumors.

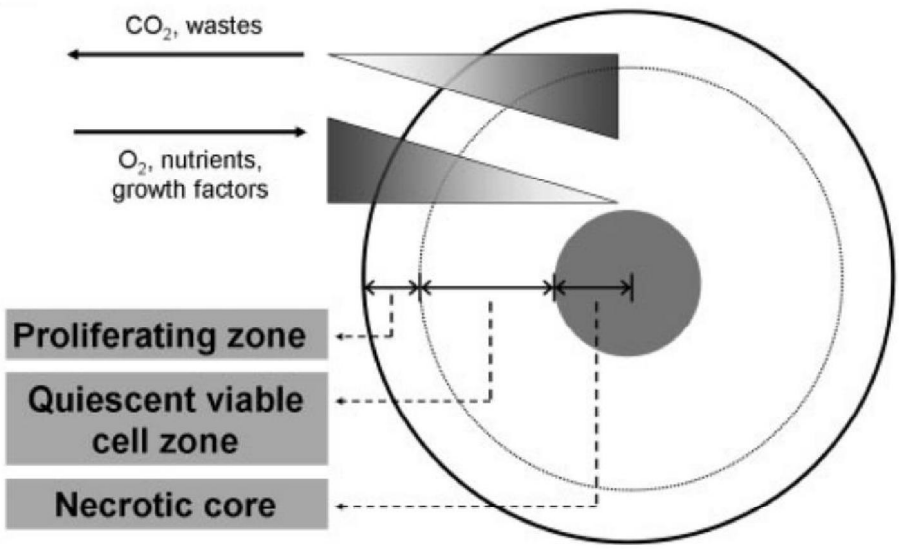

Figure 2. Spherical geometry of the tumor spheroid with a concentric organization of proliferating, quiescent and dead cell zones [12].

1.2.1.3. Tumor-specific gene expression

Cells growth in 3D cultures induces divergent gene expression compared to the expression profile in monolayer culture [49,50]. Thus, in melanoma NA8 spheroids the expression of about 100 genes was found to be three-fold higher compared to the monolayer, while the expression of other 73 genes decreased [51]. In other reports, rather good correlation between caspase-3 protein, E-cadherin, and levels of MIBI proliferation marker was found for ovarian cancer spheroids *in vitro* and ovarian cancer tissue *in vivo* [8]. The protein expression depends also on the spheroid zone, for instance outer proliferation or quiescent internal zones [52]. Generally speaking, alterations in gene expression drive changes in cell morphology, proliferation rates and drug resistance, thereby providing a more representative model of tumor *in vivo*.

1.2.1.4. Mimicing the tumor microenvironment

Upregulation of ECM proteins expression in tumor spheroids (E-cadherin, fibronectin, and collagen) leads to the formation of the microenvironment which is similar to that in tumors *in vivo* [44,53]. Apart from the expression level, cell culture in tumor spheroids results in tumor-related protein phosphorylation, e.g. EGFR or cMET [54]. Additionally, tumor spheroids can be used to co-culture cancer and stromal cells (mesenchimal stem cells, tumor-assosiated fibroblasts, macrophages, etc) [55,56]. Since the tumor spheroids mimic well enough

microenvironment which occurs *in vivo*, they have been used to study immune response of normal cells to the tumor growth [57,58].

1.2.1.5. Development of resistance to therapy

Development of resistance to therapy in tumor spheroids could be explained by all MTS characteristics mentioned above. Thus, penetration of drugs and drug delivery vehicles into tumor spheroids is limited by diffusion. The drugs can lose efficacy due to some biochemical alteration of cells which are growing in the spheroids. For example, mechanism of the action of some antitumor drugs is related to DNA damage and inhibition of cell division. However, quiescent cells are less sensitive to this effect, since their division is inhibited anyway. Additionally, the cells in the tumor spheroids demonstrate higher expression of multiple drug resistant proteins compared to those in monolayer [44]. Co-culture of tumor and normal cells can also lead to changes in cell response to drug therapy [59]. Therefore, we can conclude, that tumor spheroids are more adequate system for drug testing than monolayer culture.

1.2.2. Methods for tumor spheroid formation

The optimal technique has to be relatively inexpensive, amenable to mass spheroid production, and suitable for antitumor drugs testing. Up to date, several approaches to tumor spheroid formation have been reported. Here, we would like to describe and discuss some of these techniques.

1.2.2.1. Spontaneous cell aggregation

Spontaneous cell aggregation is one of the simpliest approaches to form tumor spheroids. It is based on an ability of a few number of human cancerous cell lines (breast adenocarcinoma MDA-MB-231, glioblastoma U-87 MG, some ovarian carcinoma cells) to self-assembly with further formation of tumor spheroids [60]. This technique has some disadvantages, since it could be used only for rather small number of cell lines and does not allow to affect the properties of the spheroids obtained. Nevertheless, this is rather interesting example to demonstrate how tumor cells can spontaneously transfer from monolayer (2D) to spheroids (3D) conditions as well as to be considered as an analogue of metastatic process *in vitro* [61].

1.2.2.2. Spinner flask and gyratory rotation systems

Spinners are widely used to generate large quantities of spheroids. For this purpose, cells are transferred to the culture medium and cultivated as a suspension culture. To prevent cell

adhesion to the surface, an intensive agitation is used (by spinner flasks rotation, or shaking, or magnetic mixing). In these culticvation systems the cells aggregate trying to attach to each other, and as a result, form first aggregates and then rather dense tumor spheroids [62,63]. The main advantage of these systems is generation of a lot of spheroids in well-controlled conditions (pH, nutrition and oxygen supply). However, the spheroids produced in spinner flask/gyratory rotation systems are highly heterogeneous in size and shape. Additionally, the cells in these systems can suffer from hydrodynamic stress. As a result, spinner flask and gyratory rotation systems are rarely used for MTS production despite of the possible automatization of this process [64].

1.2.2.3. Liquid overlay technique

The liquid overlay technique (LOT) is based on self-cell aggregation, since in these systems the adhesive forces between cells are stronger than interactions between cells and flask bottom [60]. To prevent cell adhesion to the bottom of cell culture plate, the latter is coated with agar/agarose (1.5–3%), or poly(2-hydroxymethyl methacrylate) (pHEMA), or Matrigel. To precipitate cells in the well center, round-bottom or conical-bottom plates are used [65]. LOT is widely used due to its simplicity and reproducibility [66]. A number of companies (Corning, InSphero, Essen BioScience) produce low-adhesive round-bottom plates for tumor spheroid generation. Cell cultivation on superhydrophobic surfaces could be considered as a close LOT analogue [67]. Additionally to the merits mentioned above, LOT allows to co-culture tumor and normal cells in well-controlled conditions [56,68]. However, not all cell lines can form MTS in LOT system, and moreover, the number of the spheroids obtained is rather small (one spheroid per well) [14].

1.2.2.4. Hanging-drop technique

Tumor spheroid formation by handing-drop technique is carried out by growing a small drop of suspension cell culture (25-40 µl) which hands onto the underside of the culture dish lid. As a result, spheroids with well-controlled size can be produced rather fast [69]. The method does not require any special equipment and allows to generate spheroids with desired sizes and cell numbers. However, this technique is extremely labor-intensive and generally not adapted to long-term cell cultivation. To simplify it, special 96- and 384-well plates were developed by 3D Biomatrix [70]. A co-culture approach of normal and tumor cells in these plates was

demonstrated [71]. Nevertheless, use of handing-drop technique for mass MTS production and drug testing is still challenging.

1.2.2.5. Microencapsulation technique

Microencapsulation technique was firstly proposed for insulin-producing cells (pantreatic islets) in semi-permeable biocompatible microcapsules by Lim и Sun in the 1980s [72]. Polyelectrolyte complexes of alginate and poly-L-lysine (or poly-L-ornithine) were used for this purpose. Similar approach to generate multicellular tumor spheroids in polyelectrolyte alginate-oligochitosan microcapsules was proposed by Markvicheva et al [73]. Tumor cells entrapped in microcapsules formed MTS in 2-3 weeks of cultivation, and then were successfully used to test cytotoxicity of antitumor drugs [74], drug delivery vehicles [75], as well as to study the effects of photodynamic therapy [76]. The spheroids diameter can be changed by varying microcapsule diameter. The size of the microcapsules depends on the equipment for sodium alginate dispersion in calcium chloride solution (electrostatic bead generator, ultrasound generator, or air-flow device). Moreover, this technique allows to generate co-colture spheroids from tumor and normal cells within the microcapsules.

1.2.2.6. Microfluidic tehnique

Microfluidic technique has been used in cell biology since 1990s but it was proposed for tumor spheroids production rather recently [77]. The use of the microfluidic system facilitates cell-based assays of extremely small sample volumes (10^{-9}-10^{-18} l) due to chips formed from polydimethylsiloxane (PDMS) by soft lithography technique. The cells can be accumulated in special niches and form tumor spheroids in function of chip architecture (channels and cavities). Otherwise, the cells can be embedded in calcium alginate microbeads like in the microencapsulation technique [78]. Drug testing can be carried out inside the chips or in common culture plates. The microfluid technique allows to generate a lot of tumor spheroids, including co-culture spheroids [79]. However, this technique is not widely used until now, since it is rather complicated and expensive due to special equipment needed [80,81]. Nevertheless, a number of studies where it is used is growing rather fast [81].

1.2.2.7. Other techniques

Recently, a novel technique for tumor spheroid formation based on magnetic cell levitation was proposed [82]. For this purpose, human glioblastoma cells were incubated with a hydrogel loaded with gold and magnetite (Fe_3O_4) nanoparticles. Then the cell aggregation was by

spatially controlling the magnetic field. The size and shape of the spheroids was controlled by varying the magnetic field parameters. Protein expression profiles in the magnetically levitated cells were similar to those observed in human tumour xenografts [82]. It should be noted that small ECM proteins amount in the medium promoted cell aggregation. This approach can be also used to carry out co-culture of tumor and normal cells [83].

A novel enzymatically-degradable PEG-peptide conjugate was proposed as cell crosslinker for spheroid formation [84]. The oleyl groups at both ends of the polymer chain were used as anchoring moiety which can penetrate cell membrane bilayer via hydrophobic interaction, while the incorporation of the GGLGPAGGK sequence in the polymer chain rendered cell crosslinker enzymatically degradable. The spheroids from hepatocarcinoma HepG2 cells demonstrating some liver-specific functions were prepared by this technique.

3D bioprinting approach initially proposed for tissue engineering [85] holds also great potential for applications in cancer research [86]. Thus, HeLa cells were entrapped in gelatin/alginate/fibrinogen hydrogels, in order to construct *in vitro* cervical tumor models [87].

1.2.3. Vehicles for antitumor drug delivery

Nanoparticles have unique biological properties given their small size and large surface area-to-volume ratio, which allows them to bind, absorb, and carry compounds, such as small molecule drugs, DNA, RNA, proteins, and probes with high efficiency [87]. Up to date, about ten of nanoparticle-based antitumor drugs have been approved for clinics, while a large amount of nanoparticular-drugs is under laboratory investigation.

1.2.3.1. Albumin complexes

Being the most abundant protein in human blood plasma, human serum protein (HSA) constitutes about half of serum protein. HSA plays an important role in the transport of poorly water soluble compounds, including endogenous metabolites, namely fatty acids, bilirubin, urobilin as well as exogenous drugs. Since HSA accumulates in tumors due to ERP effect [2], it is promising for delivery of antitumor drugs. For this purpose, anticancer agent can be conjugated with HSA through the pH-dependent [88] or antigen-dependent [89] linker. Atternatively, the drug molecule can be modified to form stable non-covalent complex with endogenous albumin in the blood. For example, an albumin-binding prodrug of doxorubicin,

namely (6-maleimidocaproyl)hydrazone derivative of doxorubicin (DOXO-EMCH) entered Phase II of clinical trials [90].

1.2.3.2. Liposomes

Liposomes are spherical vesicles with at least one lipid bilayer. For the first time, liposomes as a model of cell membrane were described by British haematologist A. Bangham in 1964 [91]. Few years later, they were proposed as a drug delivery vehicle [92]. Liposomes are compatible with lipid bilayer cell membrane, since they are commonly fabricated from phospholipids, namely phosphatidylcholine, but can also contain other lipids, such as egg phosphatidylethanolamine etc [93]. Furthermore, many liposomal formulations have been designed to provide drug release in response to specific stimuli, such as pH, temperature, external alternating magnetic field, ultrasound or light [94]. However, liposomes have rather low drug-loading capacity and generally require additional functionalization. For example, polyethylene glycol (PEG) is commonly used to provide long-term stability and to address problems related to short shelf-life, poor solubility and rapid clearance [95]. Recently, hybrid liposomal cerasomes have been proposed to enhance morphological stability compared to conventional liposomes [96]. Cerasomes are composed of lipid-bilayer membrane with internal aqueous compartment like liposomes but are additionally covered with a silicate surface framework.

Presently, there are at least 5 liposomal drugs for cancer therapy among 13 formulations which have been approved by FDA [97]. The first FDA-approved nanodrug Doxil (liposomal doxorubicin) was approved in 1995 [98].

1.2.3.3. Nano-emulsions

Nanoemulsions (NEs), like liposomes, are lipid-based drug delivery systems. A typical nanoemulsion contains oil, water and an emulsifier [99]. NEs can be prepared by different techniques, broadly classified into two primary categories: high-energy and low-energy methods. High energy methods include high pressure homogenization or ultrasonication [100]. Low energy methods exploit specific system properties to produce small droplets without consuming significant energy through spontaneous emulsification or phase-inversion temperature techniques [101]. Since nanoemulsion applications for antitumor drug delivery and tumor visualization look promising, there is a need to continue studies in these areas [102].

1.2.3.4. Solid lipid nanoparticles

Solid lipid nanoparticles (SLN) were developed at the early 1990s as an alternative lipid-based delivery system. Generally, SLN are spherical in shape and consist of a solid lipid core stabilized by a surfactant. A term "lipid" is used here in a broader sense and includes triglycerides, diglycerides, monoglycerides, fatty acids, etc. Since SLN are fabricated from physiological lipids, there is no risk of side-effects. Since SLN are solid at room and body temperature, they have better mechanical properties than emulsions or liposomes. Solid lipids provide also better controlled drug release due to increased mass transfer resistance [103]. The use of SLN as antitumor drug delivery vehicles was reviewed earlier [104]. Pulmonary delivered paclitaxel-loaded SLN nanoparticles successfully passed preclinical trials [105].

1.2.3.5. Carbon and silica nanopartiles

Carbon- (e.g. graphen, grapheme oxide) and silica-based nanoparticles, namely mesoporous silica are also promising for antitumor drug delivery. Graphene and its derivatives are rather novel materials in biomedicine and are attractive due to their two-dimensional planar structure, high specific surface, chemical and mechanical stabilities and rather good biocompatibility [106][107]. Thus, they were reported to deliver doxorubicin [108] as well as some other cargo molecules, including antibodies and RNA/DNA molecules [107]. However, carbon-based nanoparticles are not biodegradable, therefore their use is limited [109].

Unlike grapheme, mesoporous silica nanoparticles (MSN) were proposed as drug delivery system several decades ago [95]. The mesopore structure and high specific surface allow to load MSN with rather big amounts of chemotherapeutics [110]. Additionally, due to active surface groups, MSN could be easily functionalized. Silica is biocompatibile material and can be safely taken up by cells through endocytosis [111].

1.2.3.6. Quantum dots and metal-based nanoparticles

Metal-based NPs are non-biodegradable drug delivery system. Generally, they are obtained from gold, titan, zinc, and ferrum. Metal NPs have been proposed for theranostic (therapy + diagnostic). Diagnostics of tumor localization can be carried out via magnetic resonance imaging in case of iron oxide NPs or computer tomography using gold, tantal, lantanoids NPs. Cytotoxicity of the metal NPs can occur as a result of metal properties (reactive oxygen generation, calcium level influence) or through the conjugation of antitumor drugs [112]. Presently, there are at least two formulations based on iron-oxide nanoparticles which have

been approaved by FDA, namely Resovist for hepatocellular carcinoma visualization [113] and NanoTherm for glioblastoma treatment [114]. A few other prepaprations are under preclinical or clinical trials [115].

Quantum dots (QD) are often used for *in vitro* and *in vivo* imaging [116]. These semiconductor quantum dot nanocrystals have been emerged as an alternative tool to organic dyes and fluorescent proteins. QD are brighter and more stable against photobleaching than standard fluorescent indicators [117,118]. The main disadvantage of QD is their cytotoxicity. That is why efforts of most of the researches are focused on cytotoxicity reduction, and biocompatibility enhancement through surface modification, while targeting is reached by QD conjugation with antibodies, peptides, or small molecules [119].

1.2.3.7. Polymer nanoparticles

Biodegradable polymers offer great potential for controlled drug delivery, since they can be degraded by enzyme cleavage or just resorbed in the body. Polyesters (PLA, PLGA etc) are the most attractive polymers for biomedicine purposes. They exhibit a wide range of erosion times, have tunable mechanical properties, and were approved by FDA in the !980th [120]. Additionally, it is possible to tune the physico-chemical properties of the nanoparticles by controlling some relevant parameters, such as polymer molecular weight, ratio lactide/ glycolide and drug concentration, in order to provide controlled drug release. BIND-014, targeted nanoparticles for doxetaxel delivery to PSMA-expressed cells [121] is one of the numerous PLA- and PLGA-based systems presently used for biomedical applications. The anoother example is poly(alkyl cyanoacrylate) (PACA) which was shown to overcome multidrug resistance in tumor cells [122]. Intracellular drug release rate can be tuned by choosing appropriate monomers from the PACA family or by using hybrid PACA nanoparticles which contain different monomers [123]. To cobclude, polymeric micro- and nanoparticles are promising vehicles for antitumor drug delivery.

1.2.3.8. Polyelectrolyte microcapsules

Polyelectrolyte microcapsules are fabricated by so-called layer-by-layer (L-b-L) technique This technique is based on the consecutive assembly of oppositely charged polyelectrolytes on an inorganic core as a template [124]. Thus, the spherical calcium carbonate core can be dissolved by treatment with chelating agents (EDTA or sodium citrate), in order to obtain hollow capsule loaded with chemotherapeutics or dyes. Presently, this technique is widely

used by a lot of research groups from all over the world for various biomedical applications, namely drug delivery [125] including antitumor drugs [126] and DNA encapsulated vaccines [127]. The size of polyelectrolyte microcapsules depends on the core diameter which could be within a range of 0.5 – 3 μm. As a result, the diameter of polyelectrolyte capsules is usually about 1-5 μm. Recently, a novel heat shrink technique was proposed to minimize the size up to 400-500 nm [128]. The capsule properties can be modified by varying polycations and polyanions. Thus, an antitumor drug doxorubicin was used as a material to fabricate microcapsules together with the modified polysaccharide alginate dialdehyde through self-cross-linking [129]. In this case doxorubicin was used both as a shell material and an active compound. Drug release from the capsules can be realized via pH-dependent [126] or ultrasound-dependent [130] manner.

1.2.3.9. Polymeric micelles

Polymeric micelles are nanosized core-shell structures formed by auto-assembly of amphiphilic block copolymers. If the copolymers are in water solution, the core of the micelles is hydrophobic, and therefore can be used to load hydrophobic drugs [131]. The hydrophilic shell could be coated with PEG or functionalized with ligands to tumor-specific receptors. Pluronic block copolymers (also termed 'Poloxamer' or 'Synperonic') consist of ethylene oxide (EO) and propylene oxide (PO) blocks arranged in a triblock structure: EO_x –PO_y –EO_x. This arrangement results in an amphiphilic copolymer, in which the number of hydrophilic EO (x) and hydrophobic PO (y) units can be altered to vary the size, hydrophilicity and lipophilicity. Pluronic block copolymers have been used extensively in a variety of pharmaceutical formulations, including delivery of low molecular drugs [132]. They can be used not only as inert carrier materials, but also can cause various functional alterations in cells, e.g. overcoming multidrug resistance [133] or passing through blood-brain barrier to target tumors in brain [134]. Up to date, there are several micellar-based preparation approved by FDA, for instance paclitaxel-based formulation Genexol-PM [135]. A lot of formulations are under preclinical and clinical trials [136]. Among disadvantages of micelles, rather low drug loading capacity, poor stability in blood, and insufficient binding and cell uptake in case of solid tumors could be mentioned [137].

1.2.3.10. Dendrimers

Dendrimers are nano-sized, radially symmetric molecules with well-defined, homogeneous, and monodisperse structure that has a typically symmetric core, an inner shell, and an outer shell [138]. Dendrimers are widely employed for various biomedical applications, including drug delivery [95]. Drugs could be loaded in dendrimer based delivery systems by three ways : (a) physical entrapment, (b) electrostatic interactions, and (c) covalent conjugation [139]. For example, the most common polyamidoamine dendrimers can selectively host methotrexate [140]. The branches can be additionally modified with ligands to target tumor cells or to prevent non-specific binding to normal cells. However, the possible toxicity of dendrimers (especially for non-biodegradable materials) are under discussion [141]. For last two decades, a number of dendrimer-based delivery systems were developed, and novel promising studies in this area are expected [142].

1.2.4. Drug testing in tumor spheroid model

1.2.4.1. Cell cycle specific agents

As well known, cancer cells, contrary to normal cells, grow and divide in an uncontrolled manner. Cancer cells often deregulate the cell cycle and undergo unscheduled cell divisions, therefore inhibition of the cell cycle give a chance for effective antitumor therapy [143]. Most anticancer drugs perturb the proliferation cycle of tumor cells by inhibiting/damaging cell cycle events. Therefore, further development of this approach is of great interest [144]. Testing of cell-cycle specific agents in tumor spheroid model might be especially fruitful, since cell cycle in spheroids differs from this one in monolayer culture greatly. Thus, for SKOV3 and IGROV1 spheroids G0/G1 cell cycle arrest was found after 1 and 4 days of incubation, respectively [145]. For Capan-2 spheroids G1 or G2 arrest was shown to depend on epidermal growth factor (EGF) presence and cell localization either in the spheroid outer layer or in the core [146]. Therefore, higher cytotoxicity of agents specific to these cell phases could be expected. Indeed, this effect was demonstrated for some drugs, including etoposide [146], roscovitine [147], or suberanilohydroxamic acid [48].

1.2.4.2. Nanoparticle size

Rather low penetration of nanoparticles (NP) to solid tumors limits the therapeutic efficacy of such formulations for cancer therapy [148]. That is why NP size is one of the most important characteristics of drug delivery system. Since an interstitial space in solid tumors is about 1-2

μm [148], this size can be considered as the upper size limit of the drug vehicles. However, smaller size might be more promising in terms of better penetration through the ECM matrix in tumors. Spheroids already have been proven to be a critical tool to study the penetration of nanoscale materials and intratumoral transport of nanoparticle drugs [149]. Thus, it was demonstrated, that polystyrene nanoparticles with the mean size of 20 and 40 nm were able to accumulate in the core of the spheroids from human cervical carcinoma SiHa cells, while 100 and 200 nm nanoparticles were found at the spheroid rim [150]. This general trend (the less size – the better spheroid infiltration) was found for many delivery systems, namely gold nanoparticles [151], PAMAM-dendrimers [152], or PEG-b-P(Glu) micelles [153]. It is important, that drug loading in the nanoparticles results in the enhancement of drug uptake by tumor cells. Thus, using doxorubicin-loaded PEO-PHB-PEO micelles with the mean size of 37 nm, it was possible to deliver more drug to tumor spheroids then in case of native doxorubicin [154]. As a result, these doxorubicin-loaded PEO-PHB-PEO micelles were more effective against tumors *in vivo*. [154][154][154]

However, tumor spheroids are not able to reproduce EPR effect or uptake of nanoparticles by liver, spleen, or kidney. That is why the use of the smallest NP might be not the best decision for *in vivo* applications. For example, it was found, that 100-200 nm liposomes infiltrated in tumors *in vivo* better, than 63 nm liposomes [155]. Additionally, as well known, nanoparticles with diameter with a range of 5-10 nm rapidly undergo renal clearance [156]. The possible solution is to use a combined delivery system of size-variable nanoparticles. This approach was realized for gelatin nanoparticles with a mean size of 100 nm loaded with quantum dots (10 nm). Gelatin NP were degraded by proteolytic enzymes in tumors, and as a result quantum dots better penetrated into the tumors. The efficacy of this strategy was confirmed by *in vivo* studies [157].

We have discussed the penetration of round-shape nanoparticles above. However, due to the modern techniques like nanoimprint lithography, the particles with various shape and aspect ratio can be generated. Thus, it was shown that disk-like particles (100 nm height, and 325 nm diameter) better infiltrated into tumor spheroids compared to nanorods (400×100×100 nm), but were less effective compared to the round-shape NP of the similar volume [158].

1.2.4.3. Surface modification of nanoparticles

Surface modification of nanoparticles allows to tune their properties, in order to provide better tumor infiltration and accumulation. Thus, nanoparticles are often protected from the cells of immune system by polyethylene glycol (PEG) [159]. As a result, NP can penetrate to the spheroid core through an interstitial space. For example, PLGA NP coated with PEG penetrated two-fold faster into the HeLa spheroid (250 μm) than those covered with cell-penetrating MPG peptide [160]. Surface charge also can play an important role in NP infiltration into tumors. Thus, classical zwitterionic DMPC:chol liposomes with a small negative charge not only associated with the tumor spheroids, but also extensively penetrated almost through-out the interstitial space [161]. Contrary, strongly cationic DMPC:DC-chol vesicles interacted with the tumor cells, inhibiting further liposome infiltration into the tumor spheroids. The opposite trend was found for PAMAM dendrimers. Thus, cationic amine-terminated PAMAM dendrimers exhibited accumulation in the spheroids compared to those which had either neutral or negative charge [152]. In this case, the higher charge led to the higher accumulation level, while a smaller charge resulted in the deeper infiltration.

Tumor-targeting of the nanoparticle surface can promote tumor infiltration and accumulation. Thus, integrin α6β1-targeted PEG-PLA micelles demonstrated more effective penetration into the tumor spheroids compared to non-targeted micelles [162]. In turn, liposomes coated with RGD-peptide and transferrin targeted endothelial and tumor cells, as well as penetrated into the core of the rat glioma C6 tumor spheroids both *in vitro* and *in vivo* conditions [163]. PEGylated poly(trimethylene carbonate) micelles functionalized with c(RGDyK) showed the strongest penetration and accumulation into 3D tumor spheroids as well as into the subcutaneous mice xenografts [164].

Delivery of nanoparticles to solid tumors may be also improved by the incorporation of ECM-modulating enzymes in the delivery formulation. Thus, collagenase-coated, 100 nm carboxylated polystyrene nanoparticles demonstrated a 4-fold higher accumulation in the spheroid core compared to control nanoparticles [150].

Additionally, co-culture spheroids could be considered as a model of blood brain barrier *in vitro* [165]. Permeability of polyether-copolyester (PEPE) dendrimers across the in vitro BBB model and their distribution into avascular human glioma tumor spheroids was studied. It was

found that glucosylation increased the cumulative permeation of dendrimers across BBB as well as accelerated infiltration into tumor spheroids which was found to be 6 h and 12 h for glucosylated and non-glucosylated dendrimers, respectively [166].

1.2.4.4. pH-triggered drugs

Measurement of pH values in tissue has shown that the microenvironment in tumors as well as in tumor spheroids is generally more acidic than this one in normal tissues due to the production of lactic acid and ATP hydrolysis in hypoxic regions of tumors [167]. Thus, acidic pH values as low as 6.3 was shown for the core of BT474 spheroids *in vitro* [46]. For *in vivo* conditions, pH 6.6 was reported for human xenografts in animals at a distance of 200 μm from the nearest blood vessel [168] and the average low value of pH ranges from 6.0 to 6.2 was demonstrated for tumors in human [169]. Low pH values can protect cells in the spheroids in case of treatment with drugs with weak acid properties like antracyclins [170]. Contrary, the cytotoxicity effect could be enhanced in case of weak base drugs like chlorambucil or mitomycin C [167,170,171]. It could be concluded that the intratumoral pH gradient plays an important role in the pH-dependent modulation of cytotoxicity of weak electrolytes.

Low pH values in tumors might be used for development of pH-triggered drug delivery vehicles. For example, pH-sensible doxorubicin-loaded DSPC/cholesterol liposomes were compared with non-pH-sensible liposomes and free doxorubicim using BT474 multicellular spheroids [46]. pH-triggered liposomes were found to release encapsulated doxorubicin intracellularly and intratumorally, and therefore they were more effective compared to conventional liposomes both *in vitro* and *in vivo* studies. It shoud be noted, that pH-triggered drug delivery systems are usually proposed for lysosome delivery [172], since lysosomes are involved in the endocytic pathway and also have acidic pH in a range of 4.5-5.0 [173]. So, it is of great interest to test these lysosome-targeted drugs in a tumor spheroids model.

CHAPTER II. EXPERIMENTAL PART

2.1. Reagents

1. Dulbecco's Modified Eagle Medium (DMEM), PanEko, Russia
2. Fetal bovine serum (FBS), PAA Laboratories, Austria
3. Sodium chloride, cell culture grade, PanEko, Russia
4. Phosphate-buffered saline pH 7,4 (PBS), PanEko, Russia
5. Versene solution, PanEko, Russia
6. Trypsin-EDTA solution, PanEko, Russia
7. L-Glutamine, PanEko, Russia
8. Sodium Piruvate, PanEko, Russia
9. 2-Mercaptoethanol, Loba Feinchemie, Austria
10. Gentamicin, PanEko, Russia
11. Penicillin-Streptomycin, PAN Biotech, Germany.
12. Dimethyl sulfoxide (DMSO), cell culture grade, Helicon, Russia
13. Formaldehyde 37%, AppliChem, USA

Reagents for cell encapsulation

14. Sodium alginate (medium viscosity,~3500 cps at 25°C), Sigma-Aldrich, USA
15. $CaCl_2 \times 2H_2O$., Sigma-Aldrich, USA.
16. EDTA sodium salt, Sigma-Aldrich, USA
17. Oligochitosan (3.5 kDa, deacetylation degree 89 %) was a kind gift from Prof. A. Bartkowiak and was prepared as described ealier [174].

Reagents for RGD-induced cell aggregation:

18. Linear and cyclic RGD-peptides were synthesized at Institute of Macromolecular Compounds, Russian Academy of Sciences, St. Petersburg, Russia
    1) cyclo-RGDfK
    2) cyclo-RGDfK(TPP), cyclo-RGDfK peptide modified with triphenylphosphonium cation (TPP)
    3) RGDF
    4) RGDF(TPP), RGDF peptide modified with TPP.
    5) $KRGDF(TPP)_2$, RGDF peptide modified with two TPP molecules.

19. The K34c ligand is 2-(S)-2,6-dimethylbenzamido)-3-[4-(3-pyridin-2-ylaminoprooxy)-phenyl]propionic acid. It was a kind gift from Prof. Horst Kessler and was synthesized as described earlier [175]
20. Neuraminidase (Neu), Sigma-Aldrich, USA
21. Biotinylated *Maackia Amurensis* Lectin II (MAL II), Vector Laboratories, USA
22. Biotinylated *Sambucus Nigra* Lectin (SNA), Vector Laboratories, USA
23. Peanut Agglutinin (PNA), Vector Laboratories, USA
24. Wheat Germ Agglutinin (WGA), Vector Laboratories, USA
25. Agarose, Sigma-Aldrich, USA
26. DyLight 488 Streptavidin, Vector Laboratories, USA

Cell dyes:

27. Trypan blue, Flow Laboratories Inc., USA
28. MTT reagent (3-(4,5-dimethylthiazol-2-yl)-2,5-diphenyltetrazolium bromide), PanEko, Russia
29. Hoechst 33342, PanEko, Russia
30. Calcein AM, eBioscience, USA
31. Propidium iodide (PI), eBioscience, USA
32. DiO (3,3'-dioctadecyloxacarbocyanine perchlorate), Sigma-Aldrich, USA
33. DiI 1,1′-Dioctadecyl-3,3,3′,3′-tetramethylindocarbocyanine perchlorate), Sigma-Aldrich, USA
34. MitoTracker Orange, Thermo Scientific, USA
35. Nyle Red (NR), Sigma-Aldrich, USA
36. Nyle Red 668 (NR 668) was a kind gift from Prof. Andrey Klymchenko and was synthesized as described earlier [176].

Antitumor drugs:

37. Gemcitabine hydrochloride, Sigma-Aldrich, США.
38. Doxorubicin hydrochloride, Sigma-Aldrich, США.
39. Curcumin, Sigma-Aldrich, США.
40. Oseltamivir phosphate, La Roche Ltd., Канада.
41. Tamoxifen, Sigma-Aldrich, США.
42. Temozolomide, Schering-Plough Corporation, США.

43. Thymoquinone, Sigma-Aldrich, США.
44. 5-Fluorouracil, Sigma-Aldrich, США.
45. Doxorubicin derivatives were synthesized at Institute of Macromolecular Compounds, Russian Academy of Sciences, St. Petersburg, Russia
    1) N-palmitoyl-doxorubicin (N-Palm-DOX);
    2) Palmitoyl-hydrazone of doxorubicin (Palm-N_2H-DOX);
    3) DOX conjugate with the hydrazide of 1-carboxy-5-fluorouracil (DOX-FU5);
    4) DOX conjugate with aminoguanidine (DOX-AMG);
    5) DOX conjugate with (4-carboxybutyl)triphenylphosphonium bromide (DOX-TPP).
46. Curcumin conjugate with Plutonic F68 was synthesized at the University of Srasbourg (France).

Reagents for fabrication of polysaccharide microcontainers:

47. Low molecular weight chitosan [20–300 cps, 1 wt% in 1% acetic acid (25°C), 75–85% deacetylated], Sigma-Aldrich, USA
48. Xanthan gum [from Xanthomonas campestris, 800–1200 cps, 1% in H2O (25°C)],, Sigma-Aldrich, USA
49. Soybean oil, Sigma-Aldrich, USA
50. Poly-L-lysine (PLL), 40 000–60 000 Da, Sigma-Aldrich, USA

Reagents for nano-emulion production:

51. Labrafac WL, Gattefossé, France
52. Cholecalciferoyl 2,3,5-triiodobenzoate was synthesized at the University of Srasbourg (France).
53. Kolliphor ELP (Cremophor ELP), BASF, Germany
54. Solutol HS 15, BASF, Germany

2.2. Methods

2.2.1. Cell culture

A list of cell lines used in this study is shown in **Table 1**. MCF-7/ADR cells were a generous gift of Dr. Akatov (Institute of Theoretical and Experimental Biophysics RAS, Pushchino, Moscow region, Russia). PANC1 were purchased from ATCC collection. Tamoxifen-resistant MCF-7 TMX gemcitabine-resistant PANC1-GemR cells were obtained at Prof. Szewczuk's laboratory (Queen's University, Kingston, Canada). Other cells were kindly provided by Drs. E. Svirchevskaya and E. Kovalenko (Shemyakin-Ovchinnikov Institute of Bioorganic Chemistry RAS, Moscow, Russia). The cells were cultured in DMEM supplemented with 10% FBS, which contained penicillin-streptomycin at 37°C in a 5% CO_2 humidified atmosphere. The medium was replaced every 3–4 days.

Table 1. Cell lines.

Cell line	Origin	Morpholofy
MCF-7	Human, breast adenocarcinoma	epithelioid
MCF-7/ADR	Human, doxorubicin-resistant breast adenocarcinoma	epithelioid
MCF-7/TMX	Human, tamoxifen-resistant breast adenocarcinoma	epithelioid
PANC1	Human, pancreatic carcinoma	epithelioid
PANC1/ GemR	Human, gemcitabine-resistant pancreatic carcinoma	epithelioid
U-87 MG	Human, glioblastoma	epithelioid
HCT-116	Human, colon colorectal carcinoma	epithelioid
HepG2	Human, hepatocellular carcinoma	epithelioid
A-375	Human, melanoma	epithelioid
HeLa	Human, cervical adenocarcinoma	lymphoblastoid
A-172	Human, glioblastoma	fibroblast-like

Cell line	Origin	Morpholofy
HaCaT	Human, keratinocytes	epithelioid
HOS	Human, osteosarcoma	fibroblast-like/ epithelioid
M-3	Mouse, melanoma	epithelioid
L-929	Mouse, transformed fibroblasts	fibroblast-like
BNL-CL2	Mouse, embryotic hepatocytes	epithelioid
RAW 264.7	Mouse, monocytes/macrophages	macrophage-like

2.2.2. Cytotoxicity study of RGD-peptides

Cytotoxicity of RGD-peptides was determined by MTT-assay (P. 2.3.8) and "live-dead" fluorescente assay.

2.2.2.1. "Live-dead" fluorescente assay

2D cell culture: Cells were seeded at a cell culture glass slide (10^4 cells/well) followed by overnight incubation. Then the RGD-peptide solution (1–100 μM) in DMEM (10% FBS) was added. After 24 h of incubation with the peptide, the cells were washed 3 times with PBS (pH 7.4), treated with Hoechst 33342, Calcein AM and PI solutions (5 mM of each dye in PBS), and then incubated for 20 min. Finally, the cells were washed with PBS 3 times, transferred to the CC/Mount fluorophore protector and observed with Leica TCS SP confocal scanning system (Leica, Germany). The excitation wavelengths were 360 nm for Hoechst 33342, 488 nm for Calcein AM, 543 nm for PI, and fluorescence signals were collected in 380– 460 nm for Hoechst 33342, 500–530 nm for Calcein AM and 560–650 nm for PI. The images were processed in Leica software.

3D cell culture: Spheroid formation was performed as described in P. 2.2.4.1 or 2.3.4.2. Incubation time with cell dyes was 30-40 min. The stained spheroids were sedimentated and carefully transferred to the glass slide. The fluorescent measurements were performed at the wavelenghs mentioned above for 2D cell culture.

2.2.3. Methods for tumor spheroid formation for *in vitro* studies

2.2.3.1. RGD-indiced technique

Spheroid formation was performed as described in P. 2.2.2.2. Cyclo-RGDfK(TPP) peptide solutions (25, 50, or 100 μM) were added to monolayer cell cultures. The spheroids were generated in DMEM (10% FBS) after 2-3 days of cell cultivation in CO_2-incubator.

2.2.3.2. Liquid-overlay technique

Tumor spheroid formation on agarose-coated plates was performed as previously described [66]. Briefly, 1.5% wt of agarose in DMEM was heated on water bath for 15 min. Then 50 μL of agarose gel was added to each well of a flat-bottom 96-well plate under sterile conditions. The plates with agarose were cooled down to room temperature for 15 min. Cells were seeded on the agarose-coated plates (5,000-10,000 cells/well, 100 μL of medium in each well) and incubated at 37°C. The spheroid formation was found after 1-2 days of incubation.

2.2.3.3. Microencapsulation technique

Cell microencapsulation was carried out as described earlier [76]. Briefly, the cells were added to a sterile sodium alginate solution (1.5% w/v, 10^6 cells per ml), and the mixture was dropped into a $CaCl_2$ solution (0.5% w/v) using an electrostatic bead generator. To form an alginate-oligochitosan membrane, the obtained Ca-alginate microbeads were incubated in an oligochitosan solution (0.2% w/v) for 10 min. Then the beads were washed with a 0.9% NaCl solution, and treated with a 50 mM EDTA solution for 10 min, in order to dissolve a Ca-alginate core. Finally, the obtained microcapsules were washed 3 times with 0.9% NaCl solution, transferred to culture flasks with DMEM (10% FBS) and placed into a CO_2-incubator. All solutions for cell microencapsulation were prepared in the 0.9% NaCl solution. Cell growth in the microcapsules was observed using light microscopy (Reichert Microstar 1820E, Germany). Spheroid formation was found after 10-14 days of incubation.

2.2.4. Methods for RGD-induced cell self-assembly study

2.2.4.1. Preparation of RGD-peptides solutions

Peptides were dissolved in DMEM to get final concentration of 400 μM and sterilized through a 0.22 μm syringe filter. Peptides stock solutions were stored at -20°C.

2.2.4.2. Qualitive study of RGD-induced aggregation

The cells were seeded in DMEM supplemented with 10% FBS in 96-well plate (10^4

cells/well). After cell attachment, the medium was replaced in each well with 100 ml of DMEM supplemented with FBS (2.5; 5; 10 % v/v) or with serum free DMEM which contained RGD-peptides. Peptide concentration in the medium was in a range of 1–100 μM. Cell aggregation with subsequent spheroid formation was observed using light microscope (Zeiss Axiovert 25, Germany) equipped with the CCD camera (Axiocam, Germany) after 24, 48, and 72 h of incubation. Spheroid diameters were measured using ImageJ software and mean values were calculated (at least 200 measurements for each sample).

2.2.4.3. Quantative measurement of RGD-induced aggregation

The cells were seeded in DMEM supplemented with 10% FBS in 96-well plate (10^4 cells/well). After cell attachment, the medium was replaced in each well with 100 μl of DMEM supplemented with 10% FBS which contained 1-100 μM of cyclo-RGDfK(TPP). After 2-4 days of incubation, the spheroids were transferred to 1.5 ml Eppendorf tubes, while the non-aggregated cells were still attached to the plate bottom. To measure cell viability, WST-1 assay based on the reduction of a tetrazolium compound to a soluble derivative was used. The absorbance at 420 nm is directly proportional to a number of living cells. The absorbance readings were taken after adding WST-1 reagent to each well (10% v/v of WST-1 in DMEM), followed by incubation at 37°C for 2 h before reading at the indicated time point. To determine cell viability as a percentage of control for each peptide concentration, the following formula was used:

[(Absorbance of cells with peptide in the medium)−(Absorbance of medium without peptide)] / [(Absorbance of cells alone on day 0)−(Absorbance of medium)] × 100,

where day 0 is a time point when the peptide was added.

2.2.4.4. Inhibition of RGD-induced cell aggregation

The cells were seeded in DMEM supplemented with 10% FBS in 96-well plate (10^4 cells/well). After cell attachment, the medium was replaced in each well with 100 μl of DMEM supplemented with 10% FBS which contained 25 μM (for M-3 cells) or 50 μM (for MCF-7 cells) of cyclo-RGDfK(TPP)-peptide. Then, one of the following reagents was added: ligand K34c (0.1-250 μM), or MAL II lectin (0.05-50 μg/ml), or SNA lectin (0.05-50 μg/ml), or PNA agglutinin (0.05-50 μg/ml), or WGA agglutinin (0.05-50 μg/ml), or neuraminidase (0.025-25U). Cell aggregation was observed using light microscope (Zeiss Axiovert 25, Germany) equipped with the CCD camera (Axiocam, Germany).

2.2.4.5. Flow cytometry of cell surface sialic acids

Flow cytometry analysis of biotinylated MAL II or SNA was conducted through staining membranes of live cells. Live cells (MCF-7 and MCF-7/TMX, PANC1 and PANC1/GemR) were stained with biotinylated lectins after incubation on ice for 1 h and followed with DyLight 488 conjugated strept-avidin for additional 30 min on ice. Then the cells were fixed. Control cells were stained with DyLight488 conjugated streptavidin for 30 min on ice. The cells were analyzed by Beckman Coulter Cytomics FC500 flow cytometer. The median fluorescence was calculated for 500,000 acquired cells (100% gated). The data represent one of two experiments with similar results..

2.2.4.6. Study of disaggregation of RGD-inducedspherois

To study spheroid stability after the RGD-peptide removal, the spheroids were transferred to Eppendorf tubes and washed three times with a completed DMEM (10% FBS). Then they were transferred to 96-well plates and observed by light microscope (Zeiss Axiovert 25 (Zeiss, Germany) or Reichert Microstar 1820E (Reichert Technologies, Germany) after 24–72 h of incubation.

2.2.5. Co-culture of tumor spheroids and single stromal cells in mixed spheroids

2.2.5.1. Cell staining

Lipophilic DiO and DiI dyes were dissolved in DMSO at 10 mM, and stored at -20°C. Cells were seeded in 25 cm^2 T-flasks (2×10^6 cells per flask) and incubated in the CO_2-incubator overnight. The medium was removed and the cells were washed twice with PBS (pH 7.4). Mouse melanoma M-3 cells and mouse fibroblast L-929 cells were incubated in serum free DMEM containing DiO (10 μM) or DiI (5 μM), respectively, at 37°C for 30 min. To remove the unbounded dyes, supernatants were drained off, and the cells were washed with DMEM.

2.2.5.2. Co-culture of tumor and stromal cells in mixed spheroids

Mouse melanoma M-3 cells stained with DiO and mouse fibroblasts L-929 stained with DiI were harvested and seeded in 96-well plate in various cell count ratios. The percentage ratio of M-3/L-929 cells was varied as 25/75, 50/50 and 75/25 %. Total cell count was 10^4 per well. After 2–3 h, the medium was replaced with 100 μl fresh DMEM (10 % FBS) containing 50 μM cyclo-RGDfK(TPP)-peptide. Finally, the plate was transferred to the CO_2-incubator, and spheroid formation was observed in 2–3 days. Then the spheroids were stained with Hoechst 33342 dye (50 μM, 30 min) and observed by confocal microscopy (Nikon TE-2000, Japan).

2.2.5.3. Co-culture of tumor spheroids and single stromal cells in liquid overlay system

Agarose (1.5 % w/v) in DMEM was sterilized in a water bath for 15 min, and then 250 µl of it was added to each well of a flat-bottom 24-well plate. The plate was cooled to room temperature and used for cell cultivation. Mouse melanoma M-3 cells were stained with DiO, and MTS were generated by addition of DMEM containing 25 µM cyclo-RGDfK(TPP) peptide as described above. The obtained tumor spheroids were collected in 72 h, added to previously DiI-stained L-929 cells (M-3 cells/L-929 cells count ratio was 1:1), and the cell mixture was transferred to 24-well agarose-coated plates. Then 400 µl DMEM [10 % FBS, 25 µM cyclo-RGDfK(TPP)] was added to each well. The plates were incubated in the CO_2-incubator for 2 days. The co-culture spheroid formation was monitored by confocal microscopy (Nikon TE-2000, Japan) (P. 2.2.5.2).

2.2.5.4. Co-culture of tumor spheroids and single stromal cells in alginate–chitosan microcapsules

Mouse melanoma M-3 cells were stained with DiO, and MTS were generated by addition of DMEM (10 % FBS) containing 25 µM cyclo-RGDfK(TPP) as described above. The obtained spheroids were collected in 72 h, mixed with previously DiI-stained L-929 cells (M-3 cells/L-929 cells ratio was 1:1). The cell mixture was then entrapped in the alginate/chitosan microcapsules as described above, and cultivated for 14 days. The generation of co-culture spheroids within microcapsules was observed by confocal microscopy (Nikon TE-2000, Japan).

2.2.6. Development of novel antitumor preparations

2.2.6.1. Doxorubicine derivatives

All DOX derivatives and conventional DOX were dissolved in DMSO to get final concentration of 10 mM, except HSA complexes that were dissolved in serum free DMEM. The stock solutions were stored at -20°C. All appropriate working dilutions in cell culture medium were prepared immediately prior to testing.

2.2.6.2. Curcumin-loaded micelles

Conjugate CUR-F68 (MC-17 sample) was dissolved in MilliQ-water, PBS (pH 7.4), or DMEM at room or physiological (37°C) temperature to get solutions with concentrations in a range of 0.01-10 mg/ml. For *in vitro* testing, the MC-17 sample was dissolved in PBS (pH 7.4)

at room temperature to get final concentration of 10 mg/ml and sterilized through a 0.22 μm syringe filter. The stock solutions were stored at +4°C no more then 2 weeks. All appropriate working dilutions in cell culture medium were prepared immediately prior to testing experiments.

2.2.6.3. Thymoquinone-loaded polysaccharide microcontainers

For preparation of polysaccharide microcontainers (MC), chitosan was dissolved at 0.25% w/v in 0.1 M HCl, whereas xanthan gum solution was prepared by dissolving 0.25% (w/v) in deionized water. In both cases, the pH was adjusted to 2 with 0.1 M HCl (the acidic pH of the solutions is prerequisite to avoid electrostatic interaction between the polysaccharides in the mixture). Chitosan/xanthan gum MCs were obtained as described earlier [177]. Briefly, equal volumes (2 mL) of chitosan and xanthan gum solutions (0.25% w/v, pH 2) were mixed, and then soybean oil containing TQ (100 mg/mL) or NR (10 mg/mL) was added, and the mixture was exposed to high-intensity ultrasound using a 7 mm diameter titanium sonotrode (56 $W \cdot cm^{-2}$, 20 kHz, 5 min) (Ultrasonic Processor UP400S, Hielscher Ultrasonics GmbH). An oil/water ratio of 1:150 or 1:30 was used to generate MCs 0.5 and 2 μm in diameter, respectively. The obtained MCs were separated from the reaction mixture by centrifugation (6.708g, 5 min) and washed three times with Milli-Q water. The encapsulated TQ content was estimated by determining the difference in drug concentration in the solution before and after MC synthesis using UV−vis spectroscopy at 257 nm (PerkinElmer Lambda 650). The encapsulation efficiency was up to 95%. To modify the MC surface with poly-L-lysine, 100 μL of the MC solution was added to 1 mL of a 0.2% (w/v) PLL solution in 0.15 N NaCl, and the mixture was shaken for 15 min (IKA MS3 basic, IKA Works Inc.)

2.2.6.4. NR 668-loaded nano-emulsions

Nanoparticle emulsions (NR 668-loaded nano-emulsions) were formulated using a modified method based on spontaneous nano-emulsification as previously described [178]. Briefly, the oil phase was mixed with non-ionic surfactant and this mixture was heated to ensure its homogenization. Then, this phase was suddenly mixed with warm water, generating the stable nano-emulsions within seconds. In the case of iodinated cholecalciferol, the protocol had been adapted due to the crystalline nature of this compound. Iodinated cholecalciferol was solubilized in another oil (medium chain triglyceride, Labrafac® WL), and then this mixture

was added to the non-ionic surfactant (Kolliphor ELP or Solutol HS 15). The size of the nano-emulsion was in function of the oil and oil-to-surfactant ratio as decribed ealier [101].

2.2.7. Characterization of size and surface charge of the nanoparticles

The hydrodynamic sizes and polydispersity indexes (PDI) of the particles were measured using dynamic light scattering (DLS) (Malvern Instruments, Orsay, 752 France). The helium/neon laser, 4 mW, was operated at 633 nm with the scatter angle fixed at 173° and the temperature maintained at 25°C. The sizes of the nano-emulsions were determined directly after their formulation at room (+25 °C) or physiological temperature (+37 °C). All experiments were performed in triplicate.

2.2.8. Study of nanoparticles surface morphology

Microcontainer morphology was studied by cryo-scanning electron microscopy (cryo-SEM) as decribed earlier [177]. Briefly, each sample was frozen by plunging it into a nitrogen slush at atmospheric pressure. Samples were freeze-fractured at -150°C, etched for 60 s at -98°C, sputtered with platinum in a GATAN Alto 2500 Cryo preparation chamber, and then transferred into a cryo-SEM system Zeiss Gemini 1530 (Zeiss, Germany).

2.2.9. Cytotoxicity studies

Cell viability was studied by MTT-assay.

For 2D conditions, cells were seeded in a 96-well plate (10^4 cells/well) followed by overnight incubation. Then the cells were exposed to RGD-peptides or drugs treatment. Appropriate working dilutions in DMEM (10% FBS or without FBS) were prepared immediately prior to the experiments. After 24, 48, and 72 h of incubation the cells were treated with 100 ml of a MTT solution (0.5 mg/ml in DMEM). After 4 h incubation, the medium was replaced with 100 ml of DMSO, in order to dissolve formazan crystals formed. To keep alive floating cells, a supernatant after MTT treatment was transferred to Eppendorf tubes, and the cells were precipitated by centrifugation (125g, 5 min). The optical density (OD) at 570 nm was measured using Varioskan Flash reader (Thermo Scientific, USA). The viability of cells after peptides treatment was expressed in% compared to the control according to the equation: (OD sample - OD background)/(OD control - OD background)*100%.

For 3D conditions, MTS were generated with cyclo-RGDfK(TPP) or in chitosan mirocapsules as described above. Aliquots of the microencapsulated spheroids (25 µl of slurry) were added

into each well of 96-well plates. Then the spheroids were exposed drugs treatment. The other steps were the same as for 2D conditions.

2.2.10. Assessment of the intracellular drug distribution

Assessment of the intracellular drug distribution was conducted by confocal microscopy.

For 2D conditions, the cells were seeded on a cell culture 8-well glass slide (50000 cells per well) followed by an overnight incubation. Then the cells were incubated with the 250 µl of drug solution/NP suspension solutions in serum free medium in the CO_2-incubator. The cells were additionally stained with Hoechst 33342 (50 µM, 10 min) and Calcein AM (25 µM, 15 min) for nuclei and cytoplasm visualization, respectively. In some experiments, in order to visualize mitochondria, the cells were stained with MitoTracker Orange (500 nM, 30 min). Finally, the cells were washed three times with PBS (pH 7.4), mounted in the CC/Mount fluorophor protector, and observed using Leica CTR 6500 confocal microscope (Leica, Germany). The excitation wavelengths were 360 nm for Hoechst and CUR, 488 nm for Calcein AM, and 543 nm for DOX, NR, NR 668, and MitoTracker Orange. Fluorescence signals were collected at 380-460 nm for Hoechst, 500-530 nm for Calcein AM, and 560-650 nm for DOX, NR, NR 668, and MitoTracker Orange. The images were processed in Image J software.

For 3D conditions, MTS were generated with cyclo-RGDfK(TPP) or in chitosan mirocapsules as described above. Then the spheroids were exposed to drugs treatment. The cells in spheroids were additionally stained with Hoechst 33342 (50 µM, 30 min) and Calcein AM (25 µM, 30 min) for nuclei and cytoplasm visualization, respectively. Then the spheroids were transferred to 1.5 ml Eppendorf tubes and washed 3 times with cold PBS (pH 7.4). Finally, the the spheroids were carefully transferred to the glass slide and observed using Leica CTR 6500 confocal microscope (Leica, Germany).

2.2.11. Assessment of cellular drug uptake

2.2.11.1. Flow cytometry

For 2D conditions, cells were seeded in a 24-well plate (10^5 cells/well) followed by overnight incubation. Then the cells were exposed to drugs or nanoparticles treatment. After washing cells three times with PBS (pH 7.4), they were treated with trypsin-EDTA solution for 5 min to detach the cells from the surface. The obtained cells were washed with cold PBS (pH 7.4) and

studied by BD FACSCalibur (BD Biosciences, USA). The median fluorescence was calculated for 50,000 acquired cells using WinMDI 2.9 and Flowing Software 2.5.1 software. The data are a representation of one out of two experiments showing similar results.

For 3D conditions, MTS were generated with cyclo-RGDfK(TPP) peptide as described above. To quantify drug accumulation inside the tumor spheroids, the drugs were resuspended in DMEM and added to the MTS in the plates. Then the plates were transferred to the CO_2-incubator. To disrupt the spheroids, they were washed with PBS (pH 7.4) and treated with trypsin-EDTA solution for 30 min. The obtained single cells were washed with PBS (pH 7.4), filtered through the 100 µm membrane to remove cell aggregates, and then studied using BD FACSCalibur (BD Biosciences, USA). The median fluorescence is calculated for 50,000 acquired cells. The data are a representation of one out of two experiments showing similar results.

2.2.11.2. Fluorimetry

For 2D conditions, cells were seeded in a 24-well plate (10^5 cells/well) followed by overnight incubation. Then the cells were exposed to nanoparticles treatment. Then the MTS were washed with PBS (pH 7.4) and treated with 250 µl of DMSO to extract Nile Red (NR) dye, and fluorescence was measured using a Varioskan Flash detection system (Thermo Scientific, USA) with an excitation wavelength of 550 nm and an emission wavelength of 630 nm. Uptake data were expressed as a percentage of fluorescence associated with the cells versus fluorescence of the feed solution.

For 3D conditions, Tumor spheroids were generated with cyclo-RGDfK(TPP) peptide as described above. To quantify the nano-particles accumulation inside the tumor spheroids, the NR-loaded NP were resuspended in DMEM and added to the spheroids in the plates. Then the plates were transferred to the CO_2-incubator. After 0.5-8 h incubation, the MTS were washed with PBS (pH 7.4) and treated with 250 µl of DMSO to extract NR. Fluorescence was measured using a Promega GloMax-Multi detection system at 525 nm for excitation and 580−640 nm for emission. Uptake data were expressed as a percentage of fluorescence associated with the cells versus fluorescence of the feed solution.

.

CHAPTER III. RESULTS AND DISCUSSION

3.1. Novel technique for tumor spheroid formation using synthetic RGD-peptides

3.1.1. Formation of tumor spheroids using synthetic RGD-peptides

3.1.1.1. Publication 1

"Formation of multicellular tumor spheroids induced by cyclic RGD-peptides and use for anticancer drug testing in vitro"

Akasov R, Zaytseva-Zotova D, Burov S, Leko M, Dontenwill M, Chiper M, Vandamme T, Markvicheva E. // Int J Pharm. 2016. Vol. 506, № 1–2, P. 148–157.

3.1.1.2. Update to Publication 1

The role of α5β1 integrin in self-cell assembly was also studied using the K34c ligand. The K34c ligand was found to inhibit RGD-induced aggregation of mouse melanoma M-3 cells at concentrations of 10 μM and higher ones **(Figure 3)**. It can be explained as a result of competitive binding K34c ligand with integrins which prevented binding cyclo-RGDfK(TPP).

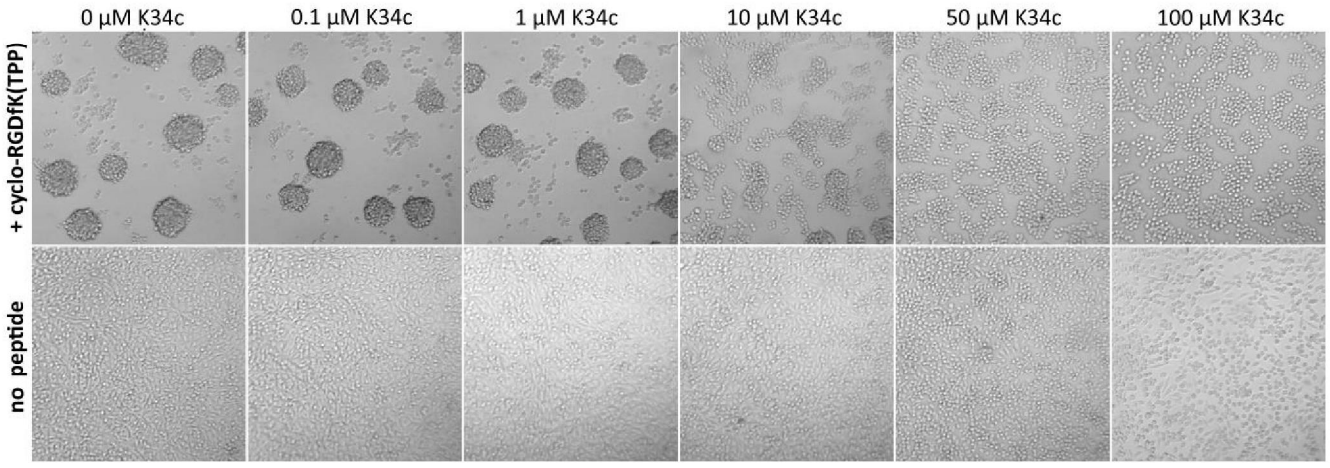

Figure 3.. Upper row: inhibition of RGD-induced cell aggregation of mouse melanoma M-3 cells in the presence of the K34c ligand (0.1-100 μM). Lower row: the influence of the K34c ligand on M-3 monolayer cell culture. DMEM+10% FBS, 25 μM cyclo-RGDfK(TPP), 72 h incubation.

Since the size is one of the main spheroids characteristics, we have studied the influence of some RGD-induced aggregation conditions to MTS size. Thus, the relationship between the

initial amount of cells in each well and the spheroid size was shown. There was no spheroid formation for M-3 cells in case when cell densities were less then 5,000 cells per well in the 96-well plate **(Figure 4).** Contrary, if there was more then 50,000 cells per well, a huge irregular cell aggregate was obtained instead of the spheroids. We assume that amounts in a range of 10,000-25,000 cells per well were crucial for MTS generation. The spheroid sizes were found to slightly vary, in particular the mean MTS size was 113±27 μm in case of 10,000 cells per well and 125±28 μm when cell density of 25,000 cells per well was used.

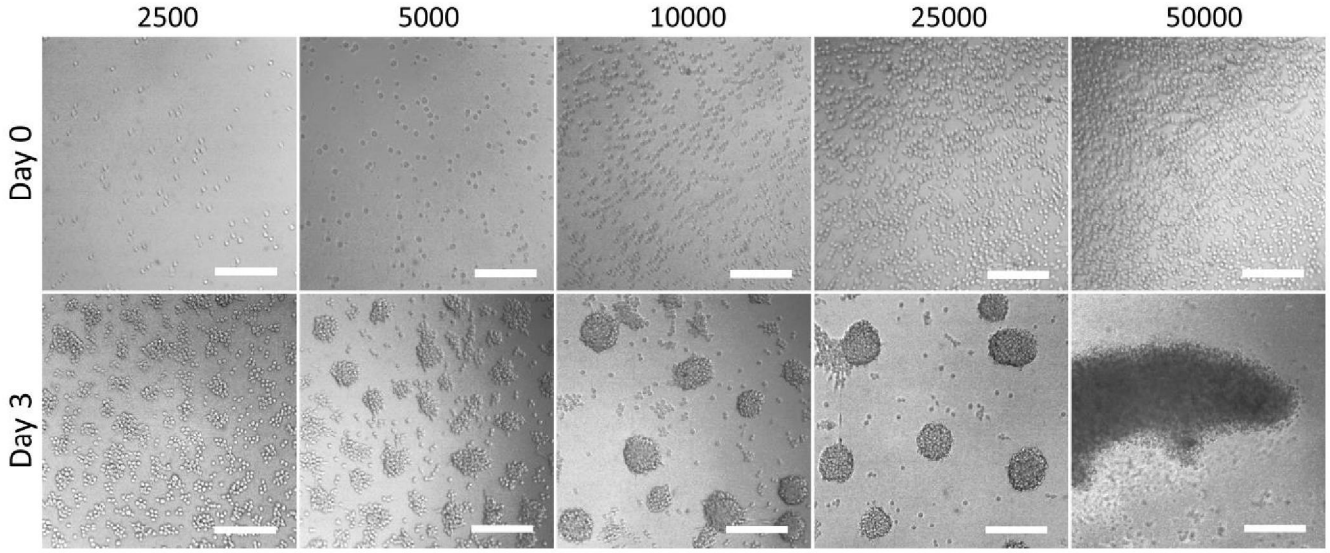

Figure 4. Micrographs of mouse melanoma M-3 cells (2,500-50,000 cells per well) in the presence of 25 μM cyclo-RGDfK(TPP) peptide. DMEM+10% FBS, scale-bar is 200 μm.

Long-term cultivation for more than 4 days allowed to enlarge the spheroids size **(Figure 5)**. Thus, the mean size of MCF-7-based spheroids increased from 103±21 μM (day 2) to 293±66 μM (day 8). However, this size enhancement occured not only due to cell growth in the spheroids but also because of spheroid aggregation. As a result, spheroid size distribution increased, while a total spheroid number decreased. Therefore, incubation for 3 days was chosen for further research.

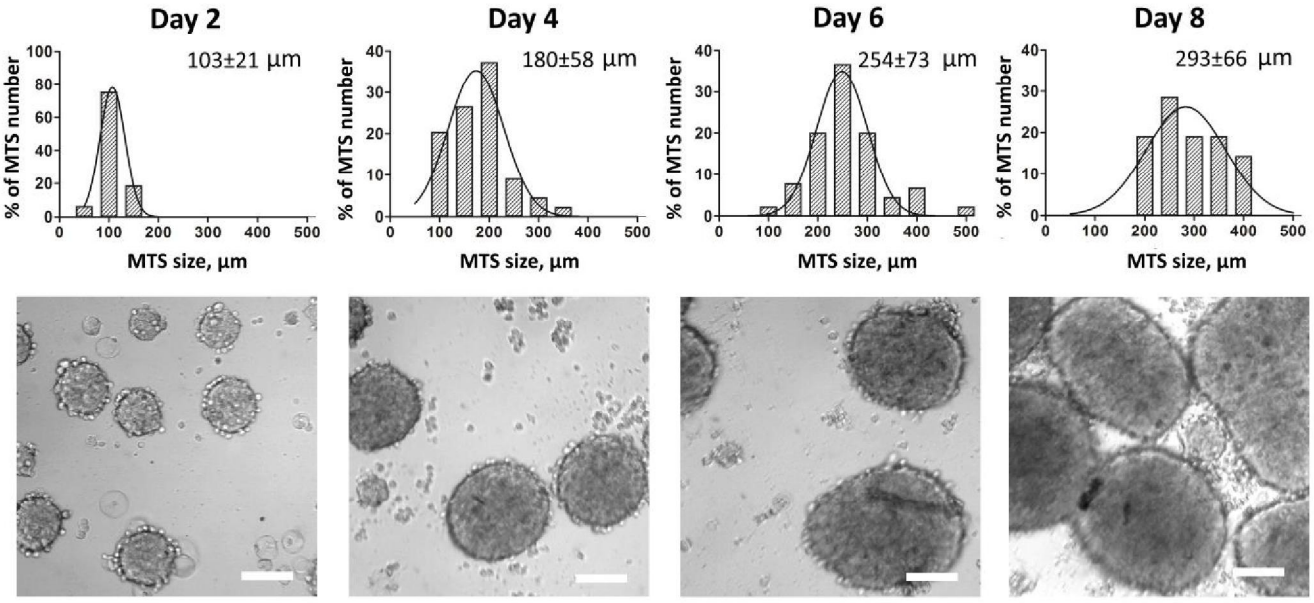

Figure 5. Spheroid size distribution and micrographs of the spheroids generated from human breast adenocarcinoma MCF-7 cells after 2, 4, 6, and 8 days of cell cultivation in DMEM (10% FBS) which contained 50 µM cyclo-RGDfK(TPP). Scale bar is 100 µm.

3.1.2. Involvment of syalic acids to RGD-induced cell aggregation

3.1.2.1. Publication 2

"Sialylation transmogrifies human breast and pancreatic cancer cells into 3D multicellular tumor spheroids using cyclic RGD-peptide induced self-assembly"

Akasov R., Haq S., Haxho F., Samuel V., Burov S. V, Markvicheva E., Neufeld R.J., Szewczuk M.R. // Oncotarget 2016. Vol. 7, № 40, P. 66119–66134.

3.1.3. Formation of co-culture spheroids using RGD-induced cell aggregation

3.1.3.1. Publication 3

"3D in vitro co-culture models based on normal cells and tumor spheroids formed by cyclic RGD-peptide induced cell self-assembly"

Akasov R, Gileva A, Zaytseva-Zotova D, Burov S, Chevalot I, Guedon E, Markvicheva E. // Biotechnol. Lett. 2017. Vol. 39, № 1, P. 45–53.

3.2. Novel antitumor drugs and drug delivery vehicles for testing in tumor spheroids

3.2.1. Testing of novel doxorubicin derivatives

3.2.1.1. Publication 4

"Novel doxorubicin derivatives: synthesis and cytotoxicity study in 2D and 3D in vitro models"

Roman Akasov, Maria Drozdova, Daria Zaytseva-Zotova, Maria Leko, Pavel Chelushkin, Annie Marc, Isabelle Chevalot, Sergey Burov, Thierry Vandamme, Elena Markvicheva. Manuscript submitted.

3.2.2. Testing of curcumin-loaded micelles

Curcumin (CUR), a main active component of turmeric (*Curcuma longa*), is a natural low molecular weight polyphenolic compound with pronounced anticancer activity. CUR inhibits proliferation, invasion, angiogenesis, and metastasis of tumors through interaction with multiple cells signaling proteins [179]. However, the use of CUR is limited because of its low bioavailability and poor water solubility [180]. Therefore development of novel formulations for CUR delivery is of great importance. Immobilization of CUR in various nano-sized drug delivery systems allows to overcome these limitations [181]. However, most of the proposed delivery systems are based on physical CUR entrapment in drug carriers, while covalent conjugation is a new promising approach. In the current research, CUR conjugates with biodegradable pluronic block copolymers have been developed and proposed for drug delivery.

3.2.2.1. Preparation and characterization of curcumin-loaded micelles

Totally, four CUR conjugates with biodegradable pluronic block copolymers have been synthesized. However, almost all of them were characterized with low CUR entrapment (<2 wt %). Only one conjugate of CUR with Pluronic F-68 (MC-17 micelles) was found to contain 4 wt % of CUR while 9 wt % was the theoretical maximum. Therefore, only MC-17 conjugate has been chosen for further *in vitro* study. MC-17 sample easily soluble in different water solutions (deionized water, PBS, DMEM) at the concentrations up to at least 600 μM, and formed micelles with the mean sizes in a range of 100-600 nm in function of MC-17 concentration and medium temperature **(Table 2)**. It is interesting that MC-17 micelles were

formed at concentration of 0.01 mg/ml, whereas critical micelle concentration (CMC) for initial Pluronic F68 was found to be 0.3-0.4 mg/ml [182]. This might be explained with the hydrophobic properties of curcumin. Micelles with the mean size of 107 nm (1 mg/ml, 25°C) were chosen for futher testing using 2D and 3D cell cultures.

Table 2. Mean size of MC-17 micelles in function of MC-17 concentration and PBS (pH 7.4) temperature.

MC-17 concentration, mg/ml	Temperature (°C)	Mean size, nm	PDI
0.01	25	273	0.46
0.1	25	255	0.31
1	25	107	0.57
0.01	37	604	0.50
0.1	37	402	0.37
1	37	293	0.37

3.2.2.2. In vitro testing of curcumin-loaded micelles

The cytotoxicity of free CUR and the MC-17 micelles loaded with CUR *in vitro* was measured by MTT-assay **(Table 3).** The MC-17 micelles were found to be less cytotoxic against wild-type MCF-7 and U-87 MG cells but more toxic for drug-resistant MCF-7/ADR cells compared to free CUR. Thus, IC_{50} values of the MC-17 micelles and free CUR for MCF-7/ADR cells after 72 h incubation were 16.4 μM and 59.8 μM, respectively. Therefore, it could be concluded that the MC-17 micelles did overcome multiple multiple drug resistance in case of MCF-7/ADR cells. Initial pluronic F68 did not reveal any cytotoxicity at the concentrations up to 250 μM.

Table 3. IC_{50} values of MC-17 micelles and free CUR in monolayer cell culture.

Cells	IC_{50}, μM					
	Free CUR			MC-17 CUR-loaded micelles		
	24 h	48 h	72 h	24 h	48 h	72 h
U-87 MG	38.1	36.3	30.2	159.0	141.5	55.0
MCF-7	29.1	9.2	5.4	110	48	21.5
MCF-7/ADR	90.6	52.3	59.8	33.7	18	16.4

As it was expected, the tumor spheroids were more resistant to drug treatment compared to monolayer culture. Thus, the IC_{50} values of free CUR for 2D and 3D culture of U-87 MG cells after 72 h incubation were 30.2 μM and 94.1 μM, respectively. Contrary to the resistance in

MCF-7/ADR cells, the MC-17 micelles could not overcome drug resistance in the tumor spheroids. They were 2-3 fold less effective in case of the tumor spheroids than free CUR in terms of IC_{50} values **(Table 4).**

Table 4. IC50 values of free CUR and the MC-17 micelles loaded with CUR in the tumor spheroids from U-87 MG and MCF-7 cells.

Cells	IC_{50}, μM					
	Free CUR			MC-17 CUR-loaded micelles		
	24 h	48 h	72 h	24 h	48 h	72 h
U-87 MG	157.5	123.0	94.1	454.7	360.0	197.4
MCF-7	167.8	135.3	126.1	494.2	339.8	224.3

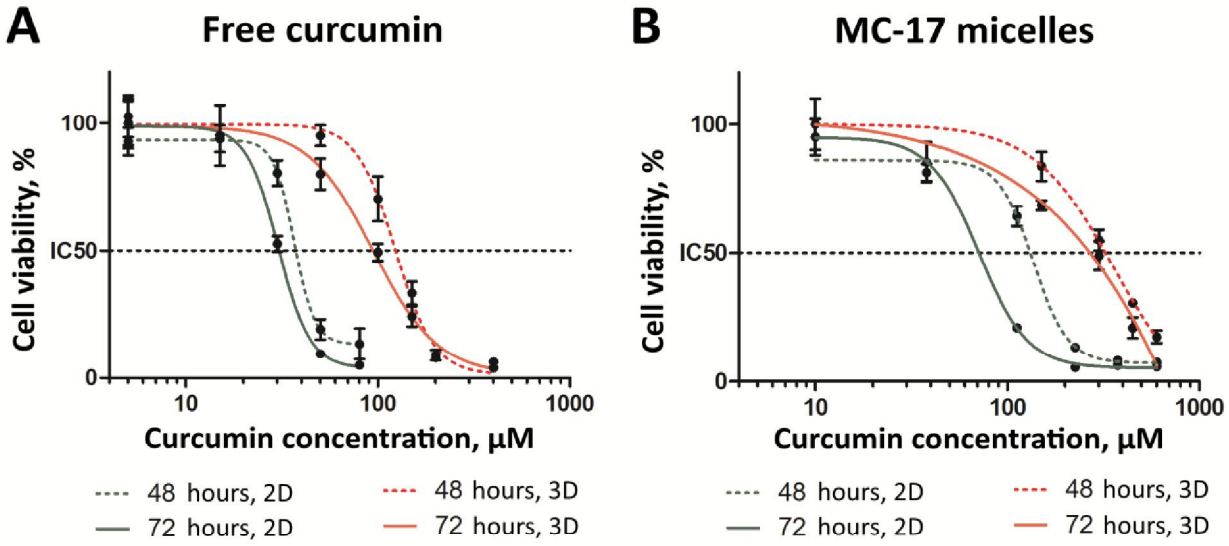

Figure 6. Cytotoxicity of free curcumin (A) and the MC-17 micelles loaded with curcumin (B) for U-87 MG cells. 2D monolayer culture (black curves) and 3D spheroids (red curves). MTT-assay results. Non-treated cells of monolayer cell culture are taken as a control (100 %).

Besides the IC_{50} values, the differences in the shape of cytotoxicity curves for 2D monolayer culture and 3D spheroids could be discussed. Thus, all the S-shaped curves in case of the 3D tumor spheroids were more flat due to the irregular drug distribution in 3D environment **(Figure 6).** The similar trend was observed in case of the MC-17 CUR-loaded micelles compared to free CUR.

Higher efficacy of the MC-17 CUR-loaded micelles against MCF-7/ADR cells could be explained by higher micelle accumulation in the cells due to overcoming MDR proteins effect. Indeed, flow cytometry data demonstrated better accumulation of the MC-17 micelles

compared to free CUR in monolayer culture but this difference was probably too small to increase cytotoxicity **(Figure 7 A, B)**. Contrary, the accumulation level of the MC-17 micelles in the tumor spheroids was lower than that of free CUR. It could be explained by better penetration of free CUR than the micelles into the MTS (Figure 7 C). Nevertheless, the MC-17 micelles could be considered as a promising model due to the possible prolonged bloodstream circulation and EPR-induced passive tumor targeting *in vivo*.

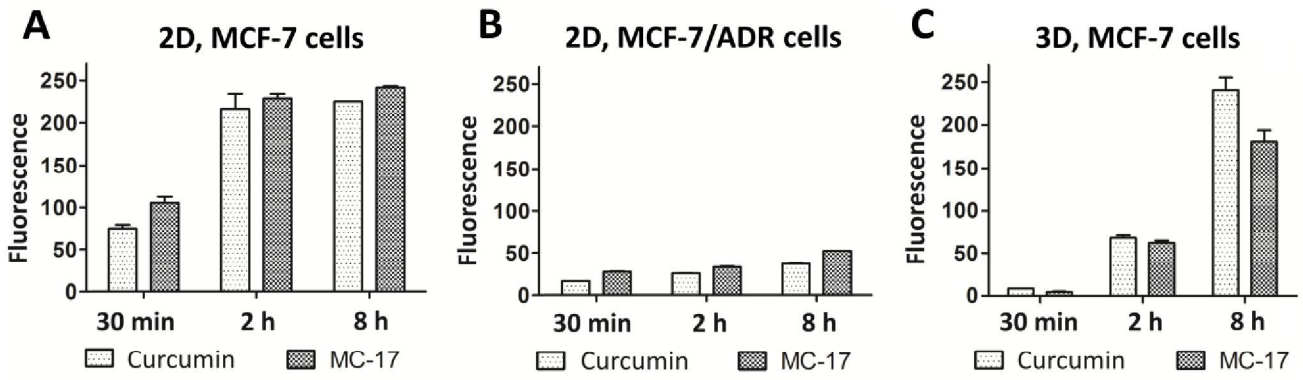

Figure 7. Accumulation of free CUR and CUR-loaded MC-17 micelles in MCF-7 and MCF-7 ADR cells: 2D (A,B) and 3D (C) culture. Flow cytometry data.

On the other hand, a clear difference in intracellular localization of free CUR and the MC-17 micelles was found by confocal microscopy. Thus, fluorescence of free CUR was homogenious in the entire cytoplasm, while MC-17 micelles formed single fluorescent dots **(Figure 8)**. This was found for both MCF-7 and MCF-7/ADR cells but was more pronounced for MCF-7/ADR cells. Since low molecular weight drugs penetrated through the cell membrane while nanoparticles are generally internalized by endocytosis, we could suggest that the MC-17 micelles were localized in lysosomes. Contrary, there is a literature evidence that DOX-Pluronic P85 micelles did overcome MDR in MCF-7/ADR cells through mitochondria localization [183]. Probably, a similar mechanism can lead to the higher cytotoxicity of the MC-17 CUR-loaded micelles to MCF-7/ADR cells.

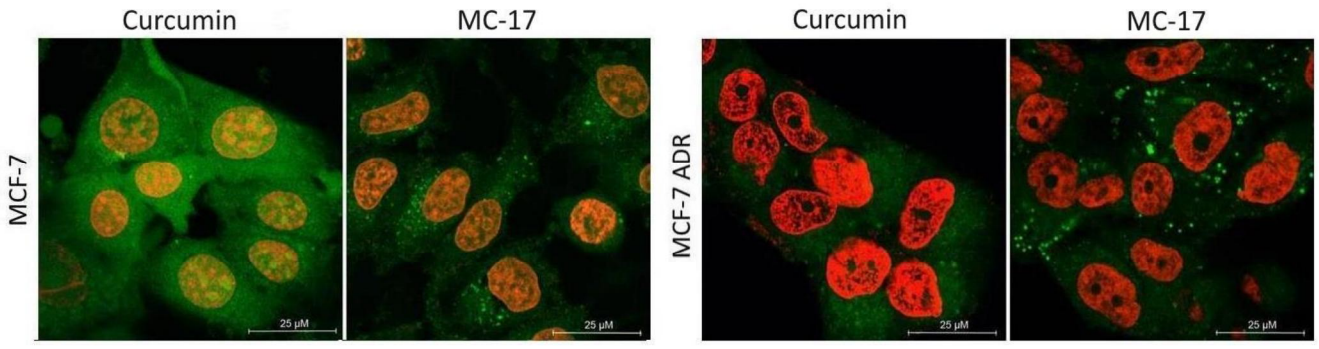

Figure 8. Accumulation of free CUR and CUR-loaded MC-17 micelles in MCF-7 and MCF-7/ADR cells. Confocal microscopy images. Curcumin is green, cell nucleuses are red. Scale bar is 20 μm.

Curcumin and MC-17 micelles distribution in the tumor spheroids was also studied by confocal microscopy. Free CUR was found to penetrate into the center of the tumor spheroids, while the MC-17 micelles were found generally in the outer spheroid layer **(Figure 9).** The fluorescence of free CUR was higher compared to the fluorescence of the MC-17 micelles, and was generally associated with cytoplasm like in the case of monolayer culture.

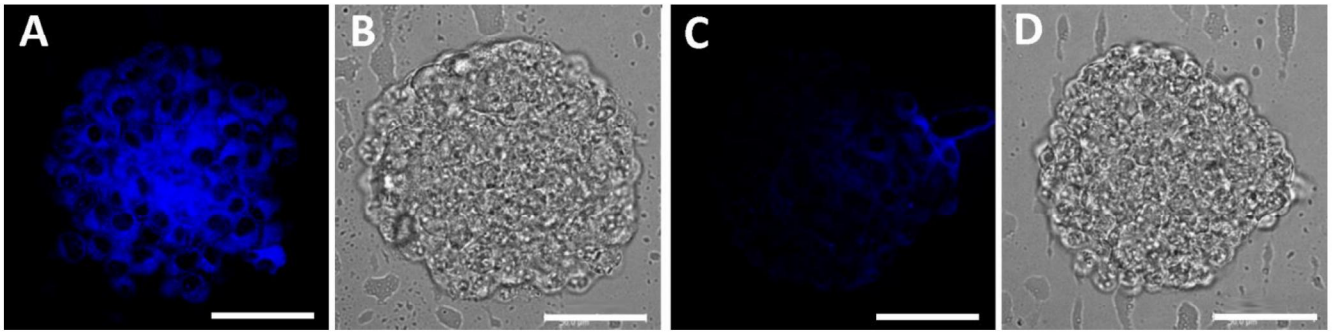

Figure 9. Accumulation of free CUR (A, B) and CUR-loaded MC-17 micelles (C, D) in the MCF-7-based tumor spheroids. Confocal microscopy data, fluorescent and transparent modes. Curcumin is blue, scale bar is 50 μm.

In summary, a novel biodegradable delivery system based on the CUR-Pluronic F68 conjugate was developed. This conjugate formed micelles with the mean size in a range of 100-600 nm which allowed to enhance CUR solubility in water solutions. The 100 nm curcumin-loaded micelles were developed for overcoming drug resistance in 2D and 3D cell cultures. The MC-17 micelles were able to inhibit cell growth of the multidrug resistant MCF-7/ADR cells more effectively than free curcumin. Thus, IC_{50} values of MC-17 micelles and free CUR after 72 h incubation were 16.4 μM and 59.8 μM, respectively. However, the MC-17 micelles loaded with CUR could not overcome drug resistance in the tumor spheroids. The IC_{50} values in case of the MC-17 micelles and free CUR after 72 h incubation with MTS from MCF-7 cells were 224.2 μM and 126.1 μM, respectively. Nevertheless, the MC-17 micelles could be considered as a promising model due to the possible prolonged bloodstream circulation and EPR-induced passive tumor targeting *in vivo*.

3.2.3. Testing of thymoquinone-loaded microcontainers

3.2.3.1. Publication 5

"Ultrasonically assisted polysaccharide microcontainers for delivery of lipophilic antitumor drugs: preparation and in vitro evaluation"

Akasov R, Borodina T, Zaytseva E, Sumina A, Bukreeva T, Burov S, Markvicheva E. // ACS Appl Mater Interfaces. 2015 Vol. 7, № 30, P. 16581–16589.

3.2.4. Testing of NR-668-loaded nano-emulsions

Besides antitumor drug delivery, nano- and micro- vehicles could be used for diagnosis and visualization tumors *in vivo*. Fluorescent dyes as well as iodinated contrast agents might be used for this purpose. In the current research modified dye Nile Red 668, was used which is more bright and stable compare to the initial Nile Red [176]. This dye was encapsulated in nanoparticle emulsions formulated using a modified method based on spontaneous nanoemulsification as previously described [101]. The aim was to study the ability of nano-emulsions to infiltrate into tumor spheroids in function of their size and cell line.

3.2.4.1. Preparation , characterization, and study of NR-668 loaded nanoemulsions in monolayer culture

Publication 6

"Biodistribution and Toxicity of X-Ray Iodinated Contrast Agent in Nano-emulsions in Function of Their Size"

Attia MF, Anton N, Akasov R, Chiper M, Markvicheva E, Vandamme TF. // Pharm Res. 2016 Vol. 33, № 3, P. 603–614.

3.2.4.2. The in vitro testing of NR-668-loaded nano-emulsions in tumor spheroids

Tumor spheroids were generated from MCF-7 and U-87 MG cells by RGD-induced cell aggregation technique. Infiltration of NR-668-loaded nano-emulsions of different size in the range of 20-200 nm was studied by confocal microscopy.

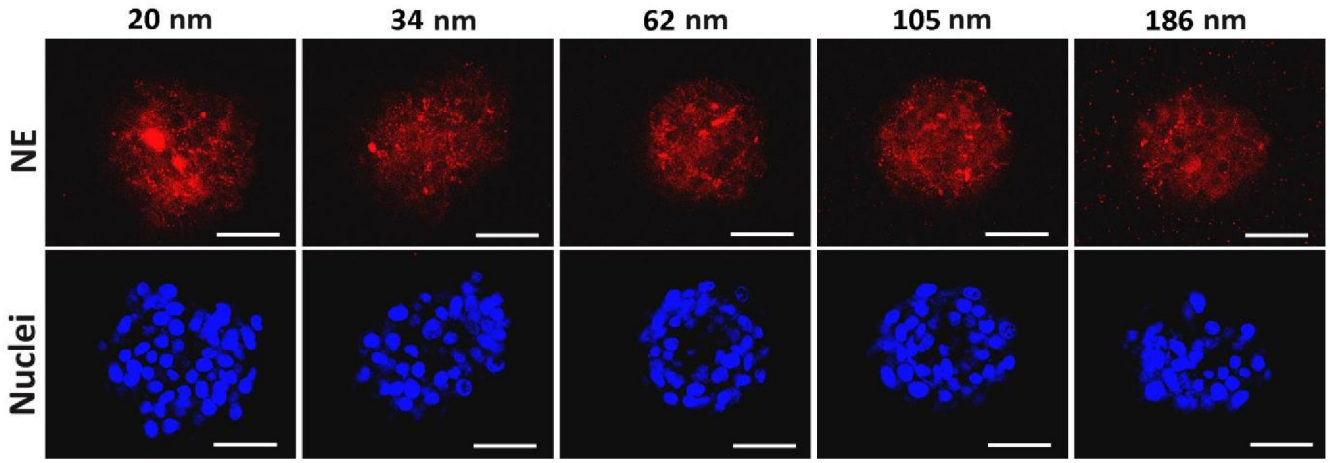

Figure 10. Accumulation of NR 668-loaded nano-emulsions of different size in the tumor spheroids from MCF-7 cells after 4 h incubation. Cell nucleuses are blue (Hoechst 33342), scale bar is 50 μm.

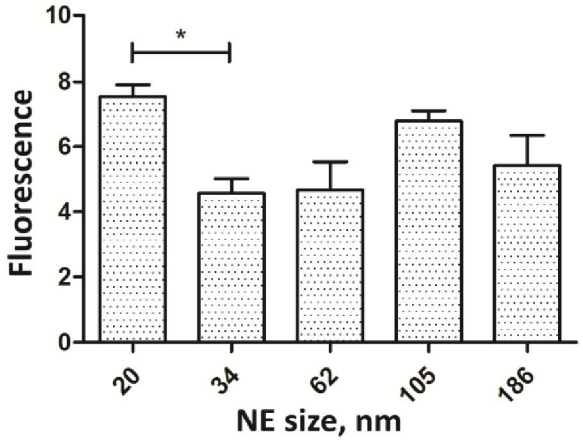

Figure 11. NE accumulation in the spheroids from MCF-7 cells after 4 h of incubation. Fluorescence level was evaluated using confocal images with ImageJ software. U=0.0571 (Mann–Whitney U test).

Despite no clear significant difference between the samples was found **(Figure 10)**, the preferred accumulation of 20 nm NE after 4 h incubation could be noticed **(Figure 11)**. Use of Cremophor instead of Kolliphor for nano-emulsion (NE) production also slightly influenced on the accumulation level (7.6±1.4 vs 4.6±0.5, respectively, 34 nm NE, 4 h of incubation).

Nano-emulsions were found to easily penetrate through the whole spheroid volume regardless of NE size. However, after 2 h incubation the 32 nm NE better accumulated within 10-20 μm layer from U-87 MG spheroids surface, while after 4 h incubation they were found within 40-50 μm layer **(Figure 12)**. Contrary, this phenomenon was not found for the nano-emulsions with the mean size of 105 nm.

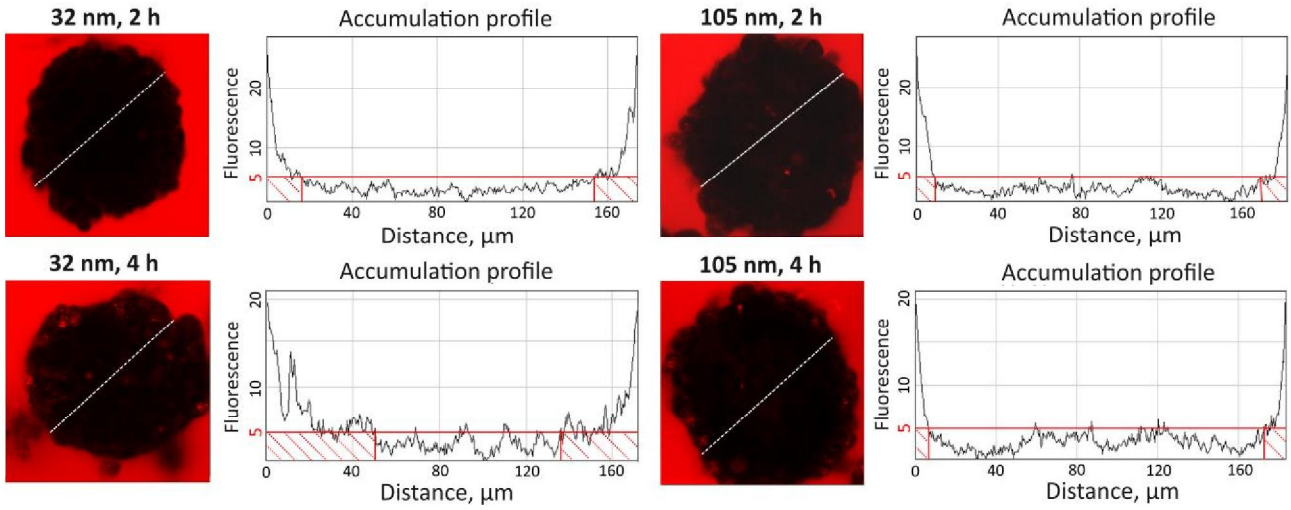

Figure 12. Accumulation profiles of NR 668-loaded nano-emulsions in the tumor spheroids from U-87 MG cells in function of their size after 2 and 4 h incubation. The images were obtained with ImageJ program (Plot Profile plugin).

On the other hand, a clear correlation between nano-emulsion accumulation and incubation time was revealed **(Figure 13).** Moreover, during the first 4 hours the NE accumulation in MTS from MCF-7 cells was higher than that in case of U-87 MG cells-based ones **(Figure 14).** However, this difference could be explained by the differences in MTS sizes of two cell lines (98±24 µm for MCF-7 cells vs 128±20 µm for U-87 MG cells). As a result, MTS from MCF-7 cells had higher surface/volume ratio which leaded to the enhanced NE accumulation. Low accumulation rates might be explained by the presence of low-molecular weight PEG on the NE surface. As a result, NE slowly attached to cells, and their movement into an intracellular space was demonstrated with time-laps video.

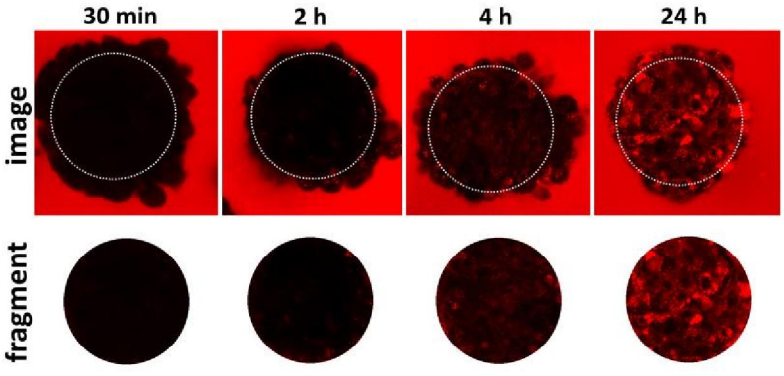

Figure 13. Accumulation of 34 nm NE in the spheroids from U-87 MG cells. The mean fluorescence of the image divided to the mean fluorescence of the NE suspension. Fluorescence was measured with ImageJ.

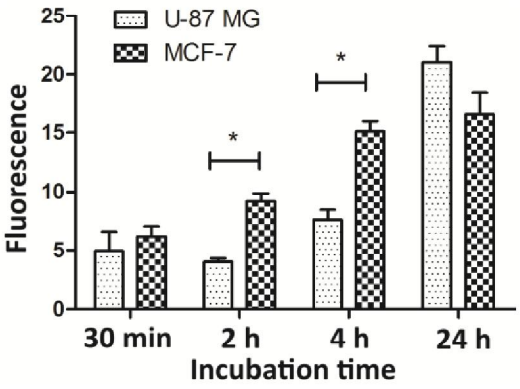

Figure 14. Accumulation of 34 nm NE in MTS from U-87 MG and MCF-7 cells. * $p<0.05$ (Mann–Whitney U test).

In summary, the NR 668-loaded nano-emulsions were proposed in this research for tumor visualization *in vivo*. The cytotoxicity of the nano-emulsions was determined using normal cells, namely murine macrophages RAW 264.7 and murine hepatocytes BNL.CL2. The ability of the nano-emulsions to accumulate in tumors in function of their mean size (20-200 nm) was studied *in vitro* using tumor spheroids from human breast adenocarcinoma MCF-7 and glioblastoma U-87 MG cells. The nano-emulsions with the mean size of 20 nm were the most effective in terms of spheroid infiltration. The rate of NE accumulation in the spheroids from MCF-7 cells was higher compared to that of U-87 MG cells .

CONCLUSIONS

The cell self-assembly effect induced by the addition of cyclic RGDfK peptide and its modification, namely cyclo-RGDfK(TPP) peptide directly to the monolayer cultures was discovered and studied for 16 cell lines of various origin. Based on this phenomenon, a novel one-step highly reproducible approach to multicellular spheroid formation was developed. Based on this technique, two novel 3D *in vitro* models with well pronounced core–shell structure have been developed to generate co-culture spheroids from tumor and normal cells. The RGD-induced tumor spheroids were used as a 3D *in vitro* model to study efficacy of both low-molecular drugs (doxorubicin and its derivatives, curcumin, temozolomide) and nano-sized drug delivery vehicles (microcontainers, micells, nanoemulsions). Both quantitative (MTT- and XTT-assays, flow cytometry, fluorimetry) and qualitative (imaging analysis by confocal microscopy) methods were successfully applied to tumor spheroids. In summary, the developed technique for RGD-induced multicellular spheroid formation was demonstrated as a promising tool to test both novel antitumor drugs and drug delivery systems *in vitro*.

ABBREVIATIONS

MTS – multicellular tumor spheroids

RGD – amino-acid sequence arginine (R) – glycine(G) – aspartic acid (D)

TPP – triphenylphosphonium

MTT – 3-(4,5-dimethylthiazol-2-yl)-2,5-diphenyltetrazolium bromide

EDTA – ethylenediaminetetraacetic acid

DMEM – Dulbecco's Modified Eagle Medium

FBS – fetal bovine serum

2D and 3D – two-dimensional and three-dimensional

EPR - enhanced permeability and retention

MDR – hultiple drug resistance

HSA – human serum albumin

MC – microcontainers

PEG - polyethylene glycol

NE – nanoemulsions

DOX – doxorubicin

CUR – curcumin

TQ – thymoquinone

TMX - tamoxifen

NR (NR 668) - Nyle Red (Nyle Red 668)

REFERENCES

1. Narang A., Desai D. Anticancer Drug Development // Pharmaceutical Perspectives of Cancer Therapeutics SE - 2 / ed. Lu Y., Mahato R.I. Springer US, 2009. P. 49–92.
2. Maeda H., Nakamura H., Fang J. The EPR effect for macromolecular drug delivery to solid tumors: Improvement of tumor uptake, lowering of systemic toxicity, and distinct tumor imaging in vivo // Adv. Drug Delivery Rev. 2013. Vol. 65 № 1. P. 71–79.
3. Hay M., Thomas D.W., Craighead J.L. et al. Clinical development success rates for investigational drugs // Nat. Biotechnol. 2014. Vol. 32 № 1. P. 40–51.
4. Xu X., Farach-Carson M.C., Jia X. Three-dimensional in vitro tumor models for cancer research and drug evaluation // Biotechnol. Adv. 2014. Vol. 32 № 7. P. 1256–1268.
5. Thoma C.R., Zimmermann M., Agarkova I. et al. 3D cell culture systems modeling tumor growth determinants in cancer target discovery ☆ // Adv. Drug Delivery Rev. Elsevier B.V., 2014. Vol. 69–70. P. 29–41.
6. Weigelt B., Ghajar C.M., Bissell M.J. The need for complex 3D culture models to unravel novel pathways and identify accurate biomarkers in breast cancer // Adv. Drug Delivery Rev. Elsevier B.V., 2014. Vol. 69–70. P. 42–51.
7. Mehta G., Hsiao A.Y., Ingram M. et al. Opportunities and challenges for use of tumor spheroids as models to test drug delivery and efficacy // J. Controlled Release. 2012. Vol. 164 № 2. P. 192–204.
8. Myungjin Lee J., Mhawech-Fauceglia P., Lee N. et al. A three-dimensional microenvironment alters protein expression and chemosensitivity of epithelial ovarian cancer cells in vitro // Lab. Investig. 2013. Vol. 93 № 5. P. 528–542.
9. Luca A.C., Mersch S., Deenen R. et al. Impact of the 3D microenvironment on phenotype, gene expression, and EGFR inhibition of colorectal cancer cell lines. // PLoS One. 2013. Vol. 8 № 3. P. e59689.
10. Sutherland R.M., McCredie J.A., Inch W.R. Growth of multicell spheroids in tissue culture as a model of nodular carcinomas // J. Natl. Cancer Inst. 1971. Vol. 46 № 1. P. 113–120.
11. Benien P., Swami A. 3D tumor models: history, advances and future perspectives // Futur. Oncol. 2014. Vol. 10 № 7. P. 1311–1327.
12. Lin R.Z., Chang H.Y. Recent advances in three-dimensional multicellular spheroid culture for biomedical research // Biotechnology journal. 2008. Vol. 3 № 9–10. P. 1172–1184.
13. Hickman J., Graeser R., de Hoogt R. et al. Three-dimensional models of cancer for pharmacology and cancer cell biology: Capturing tumor complexity in vitro/ex vivo // Biotechnol. J. 2014. Vol. 9 № 9. P. 1115–1128.
14. Vinci M., Gowan S., Boxall F. et al. Advances in establishment and analysis of three-dimensional tumor spheroid-based functional assays for target validation and drug evaluation // BMC Biol. 2012. Vol. 10 № 1. P. 29.
15. Ivanov D.P., Parker T.L., Walker D. a et al. Multiplexing spheroid volume, resazurin

and acid phosphatase viability assays for high-throughput screening of tumour spheroids and stem cell neurospheres. // PLoS One. 2014. Vol. 9 № 8. P. e103817.

16. Breslin S., O'Driscoll L. Three-dimensional cell culture: the missing link in drug discovery // Drug Discovery Today. 2013. Vol. 18 № 5–6. P. 240–249.
17. Wilding J.L., Bodmer W.F. Cancer cell lines for drug discovery and development // Cancer Res. 2014. Vol. 74 № 9. P. 2377–2384.
18. Johnson J.I., Decker S., Zaharevitz D. et al. Relationships between drug activity in NCI preclinical in vitro and in vivo models and early clinical trials // Br. J. Cancer. 2001. Vol. 84 № 10. P. 1424–1431.
19. Aggarwal B.B., Danda D., Gupta S. et al. Models for prevention and treatment of cancer: Problems vs promises // Biochem. Pharmacol. 2009. Vol. 78 № 9. P. 1083–1094.
20. van der Worp H.B., Howells D.W., Sena E.S. et al. Can Animal Models of Disease Reliably Inform Human Studies? // PLoS Med. 2010. Vol. 7 № 3. P. e1000245.
21. Steele V.E., Lubet R.A. The Use of Animal Models for Cancer Chemoprevention Drug Development // Semin. Oncol. 2010. Vol. 37 № 4. P. 327–338.
22. Hurley J.D., Yount L.J. Selection of Anticancer Drug for Palliation Using Tissue Culture Sensitivity Studies // Am. J. Surg. 1965. Vol. 109 № 1. P. 39–42.
23. Centenera M.M., Raj G. V, Knudsen K.E. et al. Ex vivo culture of human prostate tissue and drug development // Nat. Rev. Urol. 2013. Vol. 10 № 8. P. 483–487.
24. Kondo J., Endo H., Okuyama H. et al. Retaining cell-cell contact enables preparation and culture of spheroids composed of pure primary cancer cells from colorectal cancer. // Proc. Natl. Acad. Sci. USA. 2011. Vol. 108 № 15. P. 6235–6240.
25. Fong E.L.S., Martinez M., Yang J. et al. Hydrogel-based 3D model of patient-derived prostate xenograft tumors suitable for drug screening // Mol. Pharmaceutics. 2014. Vol. 11 № 7. P. 2040–2050.
26. Al-Abd A.M., Lee J.H., Kim S.Y. et al. Novel application of multicellular layers culture for in situ evaluation of cytotoxicity and penetration of paclitaxel // Cancer Sci. 2008. Vol. 99 № 2. P. 423–431.
27. Pruijn F.B., Sturman J.R., Liyanage H.D.S. et al. Extravascular Transport of Drugs in Tumor Tissue: Effect of Lipophilicity on Diffusion of Tirapazamine Analogues in Multicellular Layer Cultures // J. Med. Chem. 2005. Vol. 48 № 4. P. 1079–1087.
28. Braun R.D., Beatty A.L. Modeling of oxygen transport across tumor multicellular layers // Microvasc. Res. 2007. Vol. 73 № 2. P. 113–123.
29. Ghajar C.M., Bissell M.J. Tumor engineering: the other face of tissue engineering. // Tissue Eng. Part A. 2010. Vol. 16 № 7. P. 2153–2156.
30. Burdett E., Kasper F.K., Mikos A.G. et al. Engineering Tumors: A Tissue Engineering Perspective in Cancer Biology // Tissue Eng. Part B Rev. 2010. Vol. 16 № 3. P. 351–359.
31. Kleinman H.K., Martin G.R. Matrigel: Basement membrane matrix with biological activity // Semin. Cancer Biol. 2005. Vol. 15 № 5. P. 378–386.

32. Krause S., Maffini M. V, Soto A.M. et al. The microenvironment determines the breast cancer cells' phenotype: organization of MCF7 cells in 3D cultures // BMC Cancer. 2010. Vol. 10 № 1. P. 263.

33. Linde N., Gutschalk C.M., Hoffmann C. et al. Integrating Macrophages into Organotypic Co-Cultures: A 3D In Vitro Model to Study Tumor-Associated Macrophages // PLoS One. 2012. Vol. 7 № 7. P. e40058.

34. Jamieson L.E., Harrison D.J., Campbell C.J. Chemical analysis of multicellular tumour spheroids // Analyst. 2015. Vol. 140 № 12. P. 3910–3920.

35. Weiswald L.-B., Bellet D., Dangles-Marie V. Spherical Cancer Models in Tumor Biology // Neoplasia. 2015. Vol. 17 № 1. P. 1–15.

36. Kenny P.A., Lee G.Y., Myers C.A. et al. The morphologies of breast cancer cell lines in three-dimensional assays correlate with their profiles of gene expression // Mol. Oncol. 2007. Vol. 1 № 1. P. 84–96.

37. Sodunke T.R., Turner K.K., Caldwell S.A. et al. Micropatterns of Matrigel for three-dimensional epithelial cultures // Biomaterials. 2007. Vol. 28 № 27. P. 4006–4016.

38. Chitcholtan K., Asselin E., Parent S. et al. Differences in growth properties of endometrial cancer in three dimensional (3D) culture and 2D cell monolayer // Exp. Cell Res. 2013. Vol. 319 № 1. P. 75–87.

39. Edmondson R., Broglie J.J., Adcock A.F. et al. Three-Dimensional Cell Culture Systems and Their Applications in Drug Discovery and Cell-Based Biosensors // Assay Drug Dev. Technol. 2014. Vol. 12 № 4. P. 207–218.

40. Voulgari A., Pintzas A. Epithelial–mesenchymal transition in cancer metastasis: Mechanisms, markers and strategies to overcome drug resistance in the clinic // Biochim. Biophys. Acta - Rev. Cancer. 2009. Vol. 1796 № 2. P. 75–90.

41. Tsai J.H., Yang J. Epithelial-mesenchymal plasticity in carcinoma metastasis // Genes Dev. 2013. Vol. 27 № 20. P. 2192–2206.

42. Baker B.M., Chen C.S. Deconstructing the third dimension - how 3D culture microenvironments alter cellular cues // J. Cell Sci. 2012. Vol. 125 № 13. P. 3015–3024.

43. Kasinskas R.W., Venkatasubramanian R., Forbes N.S. Rapid uptake of glucose and lactate, and not hypoxia, induces apoptosis in three-dimensional tumor tissue culture // Integr. Biol. 2014. Vol. 6 № 4. P. 399.

44. Longati P., Jia X., Eimer J. et al. 3D pancreatic carcinoma spheroids induce a matrix-rich, chemoresistant phenotype offering a better model for drug testing // BMC Cancer. 2013. Vol. 13 № 1. P. 95.

45. Shirmanova M. V., Druzhkova I.N., Lukina M.M. et al. Intracellular pH imaging in cancer cells in vitro and tumors in vivo using the new genetically encoded sensor SypHer2 // Biochim. Biophys. Acta - Gen. Subj. 2015. Vol. 1850 № 9. P. 1905–1911.

46. Bandekar A., Karve S., Chang M.-Y. et al. Antitumor efficacy following the intracellular and interstitial release of liposomal doxorubicin // Biomaterials. 2012. Vol. 33 № 17. P. 4345–4352.

47. Ruan S., Zhang L., Chen J. et al. Targeting delivery and deep penetration using

multistage nanoparticles for triple-negative breast cancer // RSC Adv. 2015. Vol. 5. P. 64303–64317.

48. Lobjois V., Frongia C., Jozan S. et al. Cell cycle and apoptotic effects of SAHA are regulated by the cellular microenvironment in HCT116 multicellular tumour spheroids // Eur. J. Cancer. 2009. Vol. 45 № 13. P. 2402–2411.

49. Bellis A.D., Bernabé B.P., Weiss M.S. et al. Dynamic transcription factor activity profiling in 2D and 3D cell cultures // Biotechnol. Bioeng. 2013. Vol. 110 № 2. P. 563–572.

50. Dardousis K., Voolstra C., Roengvoraphoj M. et al. Identification of Differentially Expressed Genes Involved in the Formation of Multicellular Tumor Spheroids by HT-29 Colon Carcinoma Cells // Mol. Ther. 2007. Vol. 15 № 1. P. 94–102.

51. Ghosh S., Spagnoli G.C., Martin I. et al. Three-dimensional culture of melanoma cells profoundly affects gene expression profile: A high density oligonucleotide array study // J. Cell. Physiol. 2005. Vol. 204 № 2. P. 522–531.

52. McMahon K.M., Volpato M., Chi H.Y. et al. Characterization of changes in the proteome in different regions of 3D multicell tumor spheroids // J. Proteome Res. 2012. Vol. 11 № 5. P. 2863–2875.

53. Mischiati C., Ura B., Roncoroni L. et al. Changes in Protein Expression in Two Cholangiocarcinoma Cell Lines Undergoing Formation of Multicellular Tumor Spheroids In Vitro // PLoS One. 2015. Vol. 10 № 3. P. e0118906.

54. Ekert J.E., Johnson K., Strake B. et al. Three-dimensional lung tumor microenvironment modulates therapeutic compound responsiveness in vitro - Implication for drug development // PLoS One. 2014. Vol. 9 № 3. P. 1–14.

55. Kim S.-A., Lee E.K., Kuh H.-J. Co-culture of 3D tumor spheroids with fibroblasts as a model for epithelial–mesenchymal transition in vitro // Exp. Cell Res. 2015. Vol. 335 № 2. P. 187–196.

56. Ivanov D.P., Parker T.L., Walker D.A. et al. In vitro co-culture model of medulloblastoma and human neural stem cells for drug delivery assessment // J. Biotechnol. 2015. Vol. 205. P. 3–13.

57. Klöss S., Chambron N., Gardlowski T. et al. Cetuximab Reconstitutes Pro-Inflammatory Cytokine Secretions and Tumor-Infiltrating Capabilities of sMICA-Inhibited NK Cells in HNSCC Tumor Spheroids // Front. Immunol. 2015. Vol. 6. P. 1–18.

58. Giannattasio A., Weil S., Kloess S. et al. Cytotoxicity and infiltration of human NK cells in in vivo-like tumor spheroids // BMC Cancer. 2015. Vol. 15 № 1. P. 351.

59. Aljitawi O.S., Li D., Xiao Y. et al. A novel three-dimensional stromal-based model for in vitro chemotherapy sensitivity testing of leukemia cells // Leuk. Lymphoma. 2014. Vol. 55 № 2. P. 378–391.

60. Page H., Flood P., Reynaud E.G. Three-dimensional tissue cultures: Current trends and beyond // Cell Tissue Res. 2013. Vol. 352 № 1. P. 123–131.

61. Pease J.C., Brewer M., Tirnauer J.S. Spontaneous spheroid budding from monolayers: a potential contribution to ovarian cancer dissemination // Biol. Open. 2012. Vol. 1 № 7.

P. 622–628.

62. Santini M.T., Rainaldi G., Indovina P.L. Multicellular tumour spheroids in radiation biology // Int. J. Radiat. Biol. Taylor & Francis, 1999. Vol. 75 № 7. P. 787–799.

63. Sutherland R.M. Cell and environment interactions in tumor microregions: the multicell spheroid model // Sci. . 1988. Vol. 240 № 4849. P. 177–184.

64. Rodday B., Hirschhaeuser F., Walenta S. et al. Semiautomatic Growth Analysis of Multicellular Tumor Spheroids // J. Biomol. Screening. 2011. Vol. 16 № 9. P. 1119–1124.

65. Ivascu A., Kubbies M. Rapid Generation of Single-Tumor Spheroids for High-Throughput Cell Function and Toxicity Analysis // J. Biomol. Screening. 2006. Vol. 11 № 8. P. 922–932.

66. Friedrich J., Seidel C., Ebner R. et al. Spheroid-based drug screen: considerations and practical approach // Nat. Protoc. 2009. Vol. 4 № 3. P. 309–324.

67. Neto a. I., Correia C.R., Oliveira M.B. et al. A novel hanging spherical drop system for the generation of cellular spheroids and high throughput combinatorial drug screening // Biomater. Sci. 2015. Vol. 3 № 4. P. 581–585.

68. Costa E.C., Gaspar V.M., Coutinho P. et al. Optimization of liquid overlay technique to formulate heterogenic 3D co-cultures models // Biotechnol. Bioeng. 2014. Vol. 111 № 8. P. 1672–1685.

69. Kelm J.M., Timmins N.E., Brown C.J. et al. Method for generation of homogeneous multicellular tumor spheroids applicable to a wide variety of cell types // Biotechnol. Bioeng. 2003. Vol. 83 № 2. P. 173–180.

70. Tung Y.-C., Hsiao A.Y., Allen S.G. et al. High-throughput 3D spheroid culture and drug testing using a 384 hanging drop array // Analyst. 2011. Vol. 136 № 3. P. 473–478.

71. Hsiao A.Y., Tung Y.-C., Qu X. et al. 384 hanging drop arrays give excellent Z-factors and allow versatile formation of co-culture spheroids // Biotechnol. Bioeng. 2012. Vol. 109 № 5. P. 1293–1304.

72. Lim F., Sun A.M. Microencapsulated islets as bioartificial endocrine pancreas // Sci. . 1980. Vol. 210 № 4472. P. 908–910.

73. Markvicheva E., Bezdetnaya L., Bartkowiak A. et al. Encapsulated multicellular tumor spheroids as a novel in vitro model to study small size tumors // Hem. Ind. 2003. Vol. 57 № 12. P. 585–588.

74. Tsoy A.M., Zaytseva-Zotova D.S., Edelweiss E.F. et al. Microencapsulated multicellular tumor spheroids as a novel in vitro model for drug screening // Biochem. Suppl. Ser. B Biomed. Chem. 2010. Vol. 4 № 3. P. 243–250.

75. Privalova A.M., Uglanova S. V, Kuznetsova N.R. et al. Microencapsulated Multicellular Tumor Spheroids as a Tool to Test Novel Anticancer Nanosized Drug Delivery Systems In Vitro // J. Nanosci. Nanotechnol. 2015. Vol. 15 № 7. P. 4806–4814.

76. Zaytseva-Zotova D.S., Udartseva O.O., Andreeva E.R. et al. Polyelectrolyte microcapsules with entrapped multicellular tumor spheroids as a novel tool to study the effects of photodynamic therapy // J. Biomed. Mater. Res., Part B. 2011. Vol. 97B № 2.

P. 255–262.

77. Torisawa Y.S., Takagi A., Nashimoto Y. et al. A multicellular spheroid array to realize spheroid formation, culture, and viability assay on a chip // Biomaterials. 2007. Vol. 28 № 3. P. 559–566.

78. Chen M.C.W., Gupta M., Cheung K.C. Alginate-based microfluidic system for tumor spheroid formation and anticancer agent screening // Biomed. Microdevices. 2010. Vol. 12 № 4. P. 647–654.

79. Hsiao A.Y., Torisawa Y., Tung Y.-C. et al. Microfluidic system for formation of PC-3 prostate cancer co-culture spheroids // Biomaterials. 2009. Vol. 30 № 16. P. 3020–3027.

80. Yu L., Grist S.M., Nasseri S.S. et al. Core-shell hydrogel beads with extracellular matrix for tumor spheroid formation // Biomicrofluidics. 2015. Vol. 9 № 2. P. 24118.

81. Sung K.E., Beebe D.J. Microfluidic 3D models of cancer // Adv. Drug Delivery Rev. 2014. Vol. 79–80 № 0. P. 68–78.

82. Souza G.R., Molina J.R., Raphael R.M. et al. Three-dimensional tissue culture based on magnetic cell levitation // Nat. Nanotechnol. 2010. Vol. 5 № 4. P. 291–296.

83. Jaganathan H., Gage J., Leonard F. et al. Three-Dimensional In Vitro Co-Culture Model of Breast Tumor using Magnetic Levitation // Sci. Rep. 2014. Vol. 4. P. 6468.

84. Rao Z., Sasaki M., Taguchi T. Development of amphiphilic, enzymatically-degradable PEG-peptide conjugate as cell crosslinker for spheroid formation // Colloids Surf., B. 2013. Vol. 101. P. 223–227.

85. Norotte C., Marga F.S., Niklason L.E. et al. Scaffold-free vascular tissue engineering using bioprinting // Biomaterials. 2009. Vol. 30 № 30. P. 5910–5917.

86. Knowlton S., Onal S., Yu C.H. et al. Bioprinting for cancer research // Trends Biotechnol. 2015. Vol. 33 № 9. P. 504–513.

87. Zhao Y., Yao R., Ouyang L. et al. Three-dimensional printing of Hela cells for cervical tumor model in vitro // Biofabrication. 2014. Vol. 6 № 3. P. 35001.

88. Du C., Deng D., Shan L. et al. A pH-sensitive doxorubicin prodrug based on folate-conjugated BSA for tumor-targeted drug delivery // Biomaterials. 2013. Vol. 34 № 12. P. 3087–3097.

89. Elsadek B., Graeser R., Warnecke A. et al. Optimization of an Albumin-Binding Prodrug of Doxorubicin That Is Cleaved by Prostate-Specific Antigen // ACS Med. Chem. Lett. 2010. Vol. 1 № 5. P. 234–238.

90. Kratz F. DOXO-EMCH (INNO-206): the first albumin-binding prodrug of doxorubicin to enter clinical trials // Expert Opin. Invest. Drugs. 2007. Vol. 16 № 6. P. 855–866.

91. Bangham A.D., Horne R.W. Negative staining of phospholipids and their structural modification by surface-active agents as observed in the electron microscope // J. Mol. Biol. 1964. Vol. 8 № 5. P. 660–IN10.

92. Gregoriadis G., Ryman B.E. Liposomes as carriers of enzymes or drugs: a new approach to the treatment of storage diseases. // Biochem. J. 1971. Vol. 124 № 5. P. 58–63.

93. Bozzuto G., Molinari A. Liposomes as nanomedical devices // Int. J. Nanomed. 2015.

Vol. 10. P. 975.

94. Eloy J.O., Claro de Souza M., Petrilli R. et al. Liposomes as carriers of hydrophilic small molecule drugs: Strategies to enhance encapsulation and delivery // Colloids Surf., B. Elsevier B.V., 2014. Vol. 123. P. 345–363.

95. Kwon S., Singh R.K., Perez R.A. et al. Silica-based mesoporous nanoparticles for controlled drug delivery // J. Tissue Eng. 2013. Vol. 4. P. 2041731413503357.

96. Yue X., Dai Z. Recent advances in liposomal nanohybrid cerasomes as promising drug nanocarriers // Adv. Colloid Interface Sci. 2014. Vol. 207 № 1. P. 32–42.

97. Allen T.M., Cullis P.R. Liposomal drug delivery systems: From concept to clinical applications // Adv. Drug Delivery Rev. 2013. Vol. 65 № 1. P. 36–48.

98. Barenholz Y. (Chezy). Doxil® — The first FDA-approved nano-drug: Lessons learned // J. Controlled Release. 2012. Vol. 160 № 2. P. 117–134.

99. Gupta A., Eral H.B., Hatton T.A. et al. Nanoemulsions: formation, properties and applications // Soft Matter. Royal Society of Chemistry, 2016. Vol. 12 № 11. P. 2826–2841.

100. Hippalgaonkar K., Majumdar S., Kansara V. Injectable Lipid Emulsions—Advancements, Opportunities and Challenges // AAPS PharmSciTech. 2010. Vol. 11 № 4. P. 1526–1540.

101. Vandamme T., Anton. Low energy nanoemulsification to design veterinary controlled drug delivery devices // Int. J. Nanomed. 2010. Vol. 5 № 1. P. 867.

102. Ganta S., Talekar M., Singh A. et al. Nanoemulsions in Translational Research—Opportunities and Challenges in Targeted Cancer Therapy // AAPS PharmSciTech. 2014. Vol. 15 № 3. P. 694–708.

103. Müller R.H., Radtke M., Wissing S.A. Solid lipid nanoparticles (SLN) and nanostructured lipid carriers (NLC) in cosmetic and dermatological preparations // Adv. Drug Delivery Rev. 2002. Vol. 54 № SUPPL. P. S131–S155.

104. Wong H.L., Bendayan R., Rauth A.M. et al. Chemotherapy with anticancer drugs encapsulated in solid lipid nanoparticles // Adv. Drug Delivery Rev. 2007. Vol. 59 № 6. P. 491–504.

105. Videira M., Almeida A.J., Fabra À. Preclinical evaluation of a pulmonary delivered paclitaxel-loaded lipid nanocarrier antitumor effect // Nanomedicine Nanotechnology, Biol. Med. 2012. Vol. 8 № 7. P. 1208–1215.

106. Cheng R., Xue Y. Carbon Nanomaterials for Drug Delivery // Carbon Nanomaterials for Biomedical Applications / ed. Zhang M., Naik R.R., Dai L. Springer US, 2016. P. 31–80.

107. Liu J., Cui L., Losic D. Graphene and graphene oxide as new nanocarriers for drug delivery applications // Acta Biomater. 2013. Vol. 9 № 12. P. 9243–9257.

108. Yang X., Zhang X., Liu Z. et al. High-Efficiency Loading and Controlled Release of Doxorubicin Hydrochloride on Graphene Oxide // J. Phys. Chem. C. 2008. Vol. 112 № 45. P. 17554–17558.

109. Liu Z., Robinson J.T., Tabakman S.M. et al. Carbon materials for drug delivery & cancer therapy // Mater. Today. 2011. Vol. 14 № 7–8. P. 316–323.

110. Wang Y., Zhao Q., Han N. et al. Mesoporous silica nanoparticles in drug delivery and biomedical applications // Nanomedicine Nanotechnology, Biol. Med. 2015. Vol. 11 № 2. P. 313–327.

111. Hudson S.P., Padera R.F., Langer R. et al. The biocompatibility of mesoporous silicates // Biomaterials. 2008. Vol. 29 № 30. P. 4045–4055.

112. Sharma H., Mishra P.K., Talegaonkar S. et al. Metal nanoparticles: a theranostic nanotool against cancer // Drug Discovery Today. 2015. Vol. 20 № 9. P. 1143–1151.

113. Yoshida T., Enpuku K., Ludwig F. et al. Characterization of Resovist® Nanoparticles for Magnetic Particle Imaging / ed. Buzug M.T., Borgert J. Berlin, Heidelberg: Springe, 2012. P. 3–7.

114. Maier-Hauff K., Ulrich F., Nestler D. et al. Efficacy and safety of intratumoral thermotherapy using magnetic iron-oxide nanoparticles combined with external beam radiotherapy on patients with recurrent glioblastoma multiforme // J. Neurooncol. 2011. Vol. 103 № 2. P. 317–324.

115. Thakor A.S., Gambhir S.S. Nanooncology: The future of cancer diagnosis and therapy // CA. Cancer J. Clin. 2013. Vol. 63 № 6. P. 395–418.

116. Nabiev I., Sukhanova A., Artemyev M. et al. Fluorescent Colloidal Particles as Detection Tools in Biotechnology Systems // Colloidal Nanoparticles in Biotechnology. Hoboken, NJ, USA, 2008. P. 133–168.

117. Sukhanova A., Devy J., Venteo L. et al. Biocompatible fluorescent nanocrystals for immunolabeling of membrane proteins and cells // Anal. Biochem. 2004. Vol. 324 № 1. P. 60–67.

118. Walling M.A., Novak J.A., Shepard J.R.E. Quantum Dots for Live Cell and In Vivo Imaging // Int. J. Mol. Sci. 2009. Vol. 10 № 2. P. 441–491.

119. Rosenthal S.J., Chang J.C., Kovtun O. et al. Biocompatible Quantum Dots for Biological Applications // Chem. Biol. 2011. Vol. 18 № 1. P. 10–24.

120. Makadia H.K., Siegel S.J. Poly Lactic-co-Glycolic Acid (PLGA) as Biodegradable Controlled Drug Delivery Carrier // Polymers. 2011. Vol. 3 № 4. P. 1377–1397.

121. Hrkach J., Von Hoff D., Ali M.M. et al. Preclinical Development and Clinical Translation of a PSMA-Targeted Docetaxel Nanoparticle with a Differentiated Pharmacological Profile // Sci. Transl. Med. 2012. Vol. 4 № 128. P. 128ra39-128ra39.

122. Vauthier C. Drug delivery to resistant tumors: the potential of poly(alkyl cyanoacrylate) nanoparticles // J. Controlled Release. 2003. Vol. 93 № 2. P. 151–160.

123. Sulheim E., Baghirov H., von Haartman E. et al. Cellular uptake and intracellular degradation of poly(alkyl cyanoacrylate) nanoparticles // J. Nanobiotechnology. 2016. Vol. 14 № 1. P. 1.

124. Gil P.R., del Mercato L.L., del_Pino P. et al. Nanoparticle-modified polyelectrolyte capsules // Nano Today. 2008. Vol. 3 № 3–4. P. 12–21.

125. Sukhorukov G.B., Möhwald H. Multifunctional cargo systems for biotechnology // Trends Biotechnol. 2007. Vol. 25 № 3. P. 93–98.

126. Timin A.S., Lepik K. V, Muslimov A.R. et al. Intracellular redox induced drug release in cancerous and mesenchymal stem cells // Colloids Surf., B. 2016. Vol. 147. P. 450–458.

127. Selina O.E., Belov S.I., Vlasova N.N. et al. [Biodegradable microcapsules containing DNA for the new DNA vaccine design]. // Bioorg. Khim. 2009. Vol. 35 № 1. P. 113–121.

128. Trushina D.B., Bukreeva T. V, Antipina M.N. Size-Controlled Synthesis of Vaterite Calcium Carbonate by the Mixing Method: Aiming for Nanosized Particles // Cryst. Growth Des. American Chemical Society, 2016. Vol. 16 № 3. P. 1311–1319.

129. Du C., Zhao J., Fei J. et al. Assembled Microcapsules by Doxorubicin and Polysaccharide as High Effective Anticancer Drug Carriers // Adv. Healthc. Mater. 2013. Vol. 2 № 9. P. 1246–1251.

130. Shchukin D.G., Gorin D.A., Möhwald H. Ultrasonically Induced Opening of Polyelectrolyte Microcontainers // Langmuir. 2006. Vol. 22 № 17. P. 7400–7404.

131. Bontha S., Kabanov A. V, Bronich T.K. Polymer micelles with cross-linked ionic cores for delivery of anticancer drugs // J. Controlled Release. 2006. Vol. 114 № 2. P. 163–174.

132. Batrakova E. V., Kabanov A. V. Pluronic block copolymers: Evolution of drug delivery concept from inert nanocarriers to biological response modifiers // J. Controlled Release. 2008. Vol. 130 № 2. P. 98–106.

133. Kabanov A. V., Batrakova E. V., Alakhov V.Y. Pluronic® block copolymers for overcoming drug resistance in cancer // Adv. Drug Delivery Rev. 2002. Vol. 54 № 5. P. 759–779.

134. Kabanov A. V., Batrakova E. V., Miller D.W. Pluronic® block copolymers as modulators of drug efflux transporter activity in the blood-brain barrier // Adv. Drug Delivery Rev. 2003. Vol. 55 № 1. P. 151–164.

135. Kim D.W., Kim S.Y., Kim H.K. et al. Multicenter phase II trial of Genexol-PM, a novel Cremophor-free, polymeric micelle formulation of paclitaxel, with cisplatin in patients with advanced non-small-cell lung cancer // Ann. Oncol. 2007. Vol. 18 № 12. P. 2009–2014.

136. Tan C., Wang Y., Fan W. Exploring polymeric micelles for improved delivery of anticancer agents: Recent developments in preclinical studies // Pharmaceutics. 2013. Vol. 5 № 1. P. 201–219.

137. Deng C., Jiang Y., Cheng R. et al. Biodegradable polymeric micelles for targeted and controlled anticancer drug delivery: Promises, progress and prospects // Nano Today. 2012. Vol. 7 № 5. P. 467–480.

138. Abbasi E., Aval S., Akbarzadeh A. et al. Dendrimers: synthesis, applications, and properties // Nanoscale Res. Lett. 2014. Vol. 9 № 1. P. 247.

139. Singh J., Jain K., Mehra N.K. et al. Dendrimers in anticancer drug delivery: mechanism of interaction of drug and dendrimers // Artif. Cells, Nanomedicine, Biotechnol. 2016.

Vol. 1401 № January. P. 1–9.

140. Majoros I.J., Williams C.R., Becker A. et al. Methotrexate delivery via folate targeted dendrimer-based nanotherapeutic platform // Wiley Interdiscip. Rev. Nanomedicine Nanobiotechnology. 2009. Vol. 1 № 5. P. 502–510.

141. McNerny D.Q., Leroueil P.R., Baker J.R. Understanding specific and nonspecific toxicities: a requirement for the development of dendrimer-based pharmaceuticals // Wiley Interdiscip. Rev. Nanomedicine Nanobiotechnology. 2010. Vol. 2 № 3. P. 249–259.

142. Markowicz-Piasecka M., Mikiciuk-Olasik E. Dendrimers in drug delivery // Nanobiomaterials in Drug Delivery / ed. Grumezescu A. 2016. P. 39–74.

143. Williams G.H., Stoeber K. The cell cycle and cancer // J. Pathol. 2012. Vol. 226 № 2. P. 352–364.

144. Senese S., Lo Y.C., Huang D. et al. Chemical dissection of the cell cycle: probes for cell biology and anti-cancer drug development // Cell Death Dis. 2014. Vol. 5. P. e1462.

145. Carduner L., Picot C.R., Leroy-Dudal J. et al. Cell cycle arrest or survival signaling through αv integrins, activation of PKC and ERK1/2 lead to anoikis resistance of ovarian cancer spheroids // Exp. Cell Res. 2014. Vol. 320 № 2. P. 329–342.

146. Laurent J., Frongia C., Cazales M. et al. Multicellular tumor spheroid models to explore cell cycle checkpoints in 3D // BMC Cancer. 2013. Vol. 13 № 1. P. 73.

147. Wartenberg M., Fischer K., Hescheler J. et al. Modulation of intrinsic P-glycoprotein expression in multicellular prostate tumor spheroids by cell cycle inhibitors // Biochim. Biophys. Acta - Mol. Cell Res. 2002. Vol. 1589 № 1. P. 49–62.

148. Goodman T.T., Chen J., Matveev K. et al. Spatio-temporal modeling of nanoparticle delivery to multicellular tumor spheroids // Biotechnol. Bioeng. 2008. Vol. 101 № 2. P. 388–399.

149. Waite C.L., Roth C.M. Nanoscale Drug Delivery Systems for Enhanced Drug Penetration into Solid Tumors: Current Progress and Opportunities // Crit. Rev. Biomed. Eng. 2012. Vol. 40 № 1. P. 21–41.

150. Goodman T.T., Olive P.L., Pun S.H. Increased nanoparticle penetration in collagenase-treated multicellular spheroids // Int. J. Nanomed. 2007. Vol. 2 № 2. P. 265–274.

151. Huang K., Ma H., Liu J. et al. Size-Dependent Localization and Penetration of Ultrasmall Gold Nanoparticles in Cancer Cells, Multicellular Spheroids, and Tumors in Vivo // ACS Nano. 2012. Vol. 6 № 5. P. 4483–4493.

152. Bugno J., Hsu H.-J., Pearson R.M. et al. Size and Surface Charge of Engineered Poly(amidoamine) Dendrimers Modulate Tumor Accumulation and Penetration: A Model Study Using Multicellular Tumor Spheroids // Mol. Pharmaceutics. 2016. Vol. 13 № 7. P. 2155–2163.

153. Cabral H., Matsumoto Y., Mizuno K. et al. Accumulation of sub-100 nm polymeric micelles in poorly permeable tumours depends on size // Nat. Nanotechnol. 2011. Vol. 6 № 12. P. 815–823.

154. Kim T.-H., Mount C.W., Gombotz W.R. et al. The delivery of doxorubicin to 3-D

multicellular spheroids and tumors in a murine xenograft model using tumor-penetrating triblock polymeric micelles // Biomaterials. 2010. Vol. 31 № 28. P. 7386–7397.

155. Unezaki S., Maruyama K., Hosoda J.-I. et al. Direct measurement of the extravasation of polyethyleneglycol-coated liposomes into solid tumor tissue by in vivo fluorescence microscopy // Int. J. Pharm. 1996. Vol. 144 № 1. P. 11–17.

156. Blanco E., Shen H., Ferrari M. Principles of nanoparticle design for overcoming biological barriers to drug delivery // Nat. Biotechnol. 2015. Vol. 33 № 9. P. 941–951.

157. Wong C., Stylianopoulos T., Cui J. et al. Multistage nanoparticle delivery system for deep penetration into tumor tissue // Proc. Natl. Acad. Sci. 2011. Vol. 108 № 6. P. 2426–2431.

158. Agarwal R., Jurney P., Raythatha M. et al. Effect of Shape, Size, and Aspect Ratio on Nanoparticle Penetration and Distribution inside Solid Tissues Using 3D Spheroid Models // Adv. Healthc. Mater. 2015. Vol. 4 № 15. P. 2269–2280.

159. Jokerst J. V, Lobovkina T., Zare R.N. et al. Nanoparticle PEGylation for imaging and therapy // Nanomedicine. 2011. Vol. 6 № 4. P. 715–728.

160. Sims L.B., Curtis L.T., Frieboes H.B. et al. Enhanced uptake and transport of PLGA-modified nanoparticles in cervical cancer // J. Nanobiotechnology. 2016. Vol. 14 № 1. P. 33.

161. Kostarelos K., Emfietzoglou D., Papakostas A. et al. Binding and interstitial penetration of liposomes within avascular tumor spheroids // Int. J. Cancer. 2004. Vol. 112 № 4. P. 713–721.

162. Ren Y., Mu Y., Song Y. et al. A new peptide ligand for colon cancer targeted delivery of micelles // Drug Delivery. 2016. Vol. 23 № 5. P. 1763–1772.

163. Qin L., Wang C., Fan H. et al. A dual-targeting liposome conjugated with transferrin and arginine-glycine-aspartic acid peptide for glioma-targeting therapy // Oncol. Lett. 2014. Vol. 8 № 5. P. 2000–2006.

164. Jiang X., Xin H., Gu J. et al. Solid tumor penetration by integrin-mediated pegylated poly(trimethylene carbonate) nanoparticles loaded with paclitaxel // Biomaterials. 2013. Vol. 34 № 6. P. 1739–1746.

165. Urich E., Patsch C., Aigner S. et al. Multicellular Self-Assembled Spheroidal Model of the Blood Brain Barrier // Sci. Rep. 2013. Vol. 3. P. 1500.

166. Dhanikula R.S., Argaw A., Bouchard J.-F. et al. Methotrexate Loaded Polyether-Copolyester Dendrimers for the Treatment of Gliomas: Enhanced Efficacy and Intratumoral Transport Capability // Mol. Pharmaceutics. 2008. Vol. 5 № 1. P. 105–116.

167. Tannock I.F., Rotin D. Acid pH in Tumors and Its Potential for Therapeutic Exploitation // Cancer Res. 1989. Vol. 49 № 16. P. 4373–4384.

168. Helmlinger G., Yuan F., Dellian M. et al. Interstitial pH and pO2 gradients in solid tumors in vivo: high-resolution measurements reveal a lack of correlation. // Nat. Med. 1997. Vol. 3 № 2. P. 177–182.

169. Vaupel P., Kallinowski F., Okunieff P. Blood Flow, Oxygen and Nutrient Supply, and Metabolic Microenvironment of Human Tumors: A Review // Cancer Res. 1989. Vol. 49

№ 23. P. 6449 LP-6465.

170. Kozin S. V, Gerweck L.E. Cytotoxicity of weak electrolytes after the adaptation of cells to low pH: role of the transmembrane pH gradient // Br. J. Cancer. 1998. Vol. 77 № 10. P. 1580–1585.

171. Knuchel R., Hofstadter F., Jenkins W.E.A. et al. Sensitivities of Monolayers and Spheroids of the Human Bladder Cancer Cell Line MGH-U1 to the Drugs Used for Intravesical Chemotherapy // Cancer Res. 1989. Vol. 49 № 6. P. 1397 LP-1401.

172. Kanamala M., Wilson W.R., Yang M. et al. Mechanisms and biomaterials in pH-responsive tumour targeted drug delivery: A review // Biomaterials. 2016. Vol. 85. P. 152–167.

173. Mindell J.A. Lysosomal Acidification Mechanisms // Annu. Rev. Physiol. 2012. Vol. 74 № 1. P. 69–86.

174. Bartkowiak A., Brylak W. Hydrogel microcapsules containing natural and chemically modified oligochitosans – mechanical properties and porosity // Polimery/Polymers. 2006. Vol. 51 № 7–8. P. 547–554.

175. Heckmann D., Meyer A., Laufer B. et al. Rational Design of Highly Active and Selective Ligands for the α5β1 Integrin Receptor // ChemBioChem. 2008. Vol. 9 № 9. P. 1397–1407.

176. Klymchenko A.S., Roger E., Anton N. et al. Highly lipophilic fluorescent dyes in nano-emulsions: towards bright non-leaking nano-droplets // RSC Adv. 2012. Vol. 2 № 31. P. 11876.

177. Borodina T.N., Grigoriev D.O., Carillo M. a. et al. Preparation of multifunctional polysaccharide microcontainers for lipophilic bioactive agents // ACS Appl. Mater. Interfaces. 2014. Vol. 6. P. 6570–6578.

178. Anton N., Gayet P., Benoit J.-P. et al. Nano-emulsions and nanocapsules by the PIT method: An investigation on the role of the temperature cycling on the emulsion phase inversion // Int. J. Pharm. 2007. Vol. 344 № 1–2. P. 44–52.

179. Shehzad A., Lee Y.S. Molecular mechanisms of curcumin action: Signal transduction // BioFactors. 2013. Vol. 39 № 1. P. 27–36.

180. Kurien B.T., Singh A., Matsumoto H. et al. Improving the Solubility and Pharmacological Efficacy of Curcumin by Heat Treatment // Assay Drug Dev. Technol. 2007. Vol. 5 № 4. P. 567–576.

181. Lee W.-H., Loo C.-Y., Young P.M. et al. Recent advances in curcumin nanoformulation for cancer therapy // Expert Opin. Drug Deliv. 2014. Vol. 11 № 8. P. 1183–1201.

182. Samith V.D., Miño G., Ramos-Moore E. et al. Effects of pluronic F68 micellization on the viability of neuronal cells in culture // J. Appl. Polym. Sci. 2013. Vol. 130 № 3. P. 2159–2164.

183. Minko T., Batrakova E. V., Li S. et al. Pluronic block copolymers alter apoptotic signal transduction of doxorubicin in drug-resistant cancer cells // J. Controlled Release. 2005. Vol. 105 № 3. P. 269–278.

Articles removed because subjected to copyrights.

Formation of multicellular tumor spheroids induced by cyclic RGD-peptides and use for anticancer drug testing in vitro

Roman Akasov, Daria Zaytseva-Zotova, Sergey Burov, Maria Lekov, Monique Dontenwill, Manuela Chiper, Thierry Vandamme, Elena Markvichevaa

International Journal of Pharmaceutics, Volumes 506, Issues 1–2, 15 June 2016, Pages 148-157

http://dx.doi.org/10.1016/j.ijpharm.2016.04.005

Sialylation transmogrifies human breast and pancreatic cancer cells into 30 multicellular tumor spheroids using cyclic RGDpeptide induced self-assembly

Roman Akasov, Sabah Haq, Fiona Haxho, Vanessa Samuel, Sergey V. Burov, Elena Markvicheva, Ronald J. Neufeld, Myron R. Szewczuk

Oncotarget. 2016 Oct 4;7(40):66119-66134

http://dx.doi.org/10.18632/oncotarget.11868

3D in vitro co-culture models based on normal cells and tumor spheroids formed by cyclic RGD-peptide induced cell self-assembly

Roman Akasov, Anastasia Gileva, Daria Zaytseva-Zotova, Sergey Burov, Isabelle Chevalot, Emmanuel Guedon, Elena Markvicheva

Biotechnology Letters, January 2017, Volume 39, Issue 1, pp 45–53

http://dx.doi.org/10.1007/s10529-016-2218-9

Novel Doxorubicin Derivatives: Synthesis and Cytotoxicity Study in 2D and 3D in Vitro Models

Roman Akasov, Maria Drozdova, Daria Zaytseva-Zotova, Maria Leko, Pavel Chelushkin, Annie Marc, Isabelle Chevalot, Sergey Burov, Natalia Klyachko, Thierry Vandamme, Elena Markvicheva

Adv Pharm Bull. 2017;7(4):593-601.

http://dx.doi.org/10.15171/apb.2017.071

Ultrasonically Assisted Polysaccharide Microcontainers for Delivery of Lipophilic Antitumor Drugs: Preparation and in Vitro Evaluation

Roman Akasov, Anastasia Gileva, Daria Zaytseva-Zotova, Sergey Burov, Isabelle Chevalot, Emmanuel Guedon, Elena Markvicheva,

ACS Appl. Mater. Interfaces, 2015, 7 (30), pp 16581–16589

http://dx.doi.org/10.1021/acsami.5b04141

Biodistribution and Toxicity of X-Ray Iodinated Contrast Agent in Nano-emulsions in Function of Their Size

Mohamed F. Attia, Nicolas Anton, Roman Akasov, Manuela Chiper, Elena Markvicheva, Thierry F. Vandamme

Pharmaceutical Research, March 2016, Volume 33, Issue 3, pp 603–614

http://dx.doi.org/10.1007/s11095-015-1813-0

Roman AKASOV

Novel 3D *in vitro* models based on multicellular tumor spheroids to test anticancer drugs and drug delivery vehicles

Résumé

Les sphéroïdes multicellulaires tumoraux (SMT) constituent un outil prometteur dans le domaine de l'étude biologique des tumeurs. Le but de la thèse était de développer une technique de la formation de SMT et de démontrer la disponibilité de ces sphéroïdes comme modèle in vitro 3D pour tester l'efficacité de principes actifs anticancéreux ainsi que celle de formulations de délivrance de médicaments. L'effet d'auto-assemblage de cellules induit par une addition des peptides RGD cycliques a été étudié pour 16 lignées cellulaires de différentes origines. Le peptide cyclique RGDfK et sa modification avec le cation triphenylphosphonium (TPP) ont permis de mettre en évidence l'induction de formation de sphéroïdes. Les sphéroïdes ont été employés comme modèles pour évaluer la cytotoxicité de principes actifs antitumoraux (doxorubicine, curcumine, temozolomide) et un certain nombre de formulations nano- et micrométriques (microréservoirs, nano-émulsions et micelles).

Résumé en anglais

Multicellular tumor spheroids (MTS) are a promising tool in tumor biology. The aim of the Thesis was to develop a novel highly reproducible technique for MTS formation, and to demonstrate the availability of these spheroids as 3D in vitro model to test anticancer drugs and drug delivery vehicles. Cell self-assembly effect induced by an addition of cyclic RGD-peptides directly to monolayer cultures was studied for 16 cell lines of various origin. Cyclo-RGDfK peptide and its modification with triphenylphosphonium cation (TPP) were found to induce spheroid formation. The spheroids were used as a model to evaluate the cytotoxicity of antitumor drugs (doxorubicin, curcumin, temozolomide) and a number of nano- and micro- formulations (microcontainers, nano-emulsions and micelles).